Mutation Based Resistance to Antiandrogens in Prostate Cancer

by

Minna Delarae Balbas

A Dissertation

Presented to the Faculty of the Louis V. Gerstner, Jr.
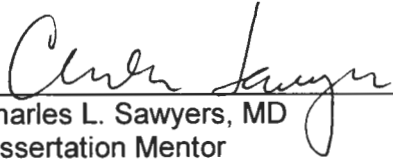
Graduate School of Biomedical Sciences,

Memorial Sloan-Kettering Cancer Center

in Partial Fulfillment of the Requirements for the Degree of

Doctor of Philosophy

New York, NY

May, 2013

_____   _____
Charles L. Sawyers, MD   Date 5/8/13
Dissertation Mentor

Abstract

Androgen receptor (AR) signaling plays a crucial role in the growth and progression of prostate cancer. Current therapies for prostate cancer rely on this dependence and aim to disrupt AR signaling through androgen deprivation and the use of AR antagonists (antiandrogens). While this is usually an effective treatment initially, most prostate tumors eventually regain the ability to grow. Reactivation of AR signaling has been implicated in resistance, often through overexpression or mutation of the androgen receptor. Several AR mutations have been described that broaden ligand specificity or convert AR antagonists into agonists of the mutant receptor. These mutations alter the conformation of antiandrogen-bound AR, such that the antiandrogen now activates the receptor.

The second-generation antiandrogen enzalutamide (formerly MDV3100) recently received FDA approval for patients with castration resistant prostate cancer. Despite its success, the duration of patient response is often limited. To prospectively identify AR mutations that might confer resistance to enzalutamide, we developed and performed a reporter-based mutagenesis screen using an AR-regulated EGFP reporter and randomly mutagenized AR cDNA library. After several rounds of enzalutamide exposure and FACS-sorting, we enriched a population of cells that maintain EGFP expression in the presence of drug. Sequencing of the androgen receptor in these cells revealed a novel mutation (AR F876L) that converts enzalutamide into an agonist. Ectopic expression of AR F876L induces expression of AR target genes and rescues growth inhibition of enzalutamide treatment. This mutation also confers agonism to the antiandrogen ARN-509, which shares the same bisaryl-thiohydantoin core motif as enzalutamide.

Molecular dynamics simulations on antiandrogen-AR complexes suggested a mechanism by which the F876L substitution alleviates antagonism, by repositioning the co-activator recruiting helix 12 of AR. This model then provided the rationale for a focused

chemical screen which, based on existing antiandrogen scaffolds, identified three novel compounds that effectively antagonized AR F876L (and AR WT) to suppress the growth of prostate cancer cells resistant to enzalutamide.

Employing recent advances in isolation of circulating tumor DNA and next generation sequencing, we have begun to address the question of whether this mutation occurs in patients who develop acquired resistance to enzalutamide or ARN-509 therapy. Preliminary results show that the AR F876L mutation emerged in a single patient, upon relapse with ARN-509 therapy. Further sequencing efforts are needed to determine the frequency of this mutation in a larger patient population.

Acknowledgments

I would like to thank my mentor, Dr. Charles Sawyers, for his support, guidance, and encouragement over the past several years. My experience in his lab has been life altering and I am extremely grateful to him for the opportunity to be a part of his lab. He has taught me how to be a good scientist, and to have confidence in my work. His passion for science is contagious. He has been supportive of my personal and professional decisions over the years. For all of this, I am deeply grateful.

I would also like to thank the members of my thesis advisory committee, Dr. David Solit and Dr. Hans-Guido Wendel, and my first year mentor Dr. Ingo Mellinghoff, for their guidance and helpful suggestions.

I am grateful to all of the members of the Sawyers lab; many of them have become close friends and are like a second family to me. In particular I would like to thank John Wongvipat, whose support I appreciate so much, and without whom the lab would fall apart. I am grateful to Karin Hepner, Kate Yen, Michael Burgess, and Brian Skaggs, who taught me so much and encouraged my curiosity during my early years in the lab. My deepest thanks go to Michael Evans, who has been a source of immeasurable support. Finally, I would like to thank my family for their love and encouragement, and for their patience during this journey.

I want to thank everyone who helped establish our graduate program and make it a success, and all the GSK students and administrative staff, especially Iwona Abramek for her help in formatting my dissertation.

Table of Contents

List of Figures

Figure Supplements

List of Tables

List of Abbreviations

ADT: androgen-deprivation therapy

AF: activation function

AIS: androgen insensitivity syndrome

AR: androgen receptor

ARE: androgen response element

CAIS: complete androgen insensitivity syndrome

cDNA: complementary DNA

cfNA: cell-free nucleic acids

ChIP: chromatin immunoprecipitation

CML: chronic myeloid leukemia

CRPC: castration-resistant prostate cancer

CTC: circulating tumor cells

ctDNA: circulating tumor DNA

DBD: DNA-binding domain

DES: diethylstilbestrol (ER agonist)

DHEA: dihydroepiandrosterone

DHT: dihydrotestosterone

EGFP: enhanced green fluorescent protein

EMT: epithelial-mesenchymal transition

ER: estrogen receptor

EYFP: enhanced yellow fluorescent protein

FSH: follicle stimulating hormone

FACS: fluorescence-activated cell sorting

gDNA: genomic DNA

GnRH: gonadotropin-releasing hormone

HSP: heat shock protein

LBD: ligand-binding domain

LH: luteinizing hormone

LHRH: luteinizing hormone-releasing hormone

MAIS: mild androgen insensitivity syndrome

N/C: amino-terminal and carboxyl-terminal

NLS: nuclear localization signal

NTD: N-terminal domain

OHT: 4-hydroxytamoxifen (ER antagonist)

PAIS: partial androgen insensitivity syndrome

Pb.PSE: probasin promoter and PSA enhancer

PCR: polymerase chain reaction

PCa: prostate cancer

PIN: prostatic intraepithelial neoplasia

PSA: prostate specific antigen

qRT-PCR: quantitative reverse transcriptase PCR

R1881: methyltrienolone (synthetic androgen)

SAR: structure-activity relationship

SBMA: spinal and bulbar muscular atrophy

siRNA: small interfering RNA

TAU: transactivation unit

WT: wild-type

Chapter 1 – Introduction

Prostate cancer is the most common cancer for men in the United States, with approximately 200,000 new cases diagnosed every year. Although mortality rates from prostate cancer have been declining for the past decade, it remains one of the leading causes of cancer-related deaths (*1*). The dependence of prostate cancer on androgens has been recognized since the seminal observations of Huggins and Hodges over seventy years ago, that prostate tumors regress in response to castration (*2*). We now know much more about prostate tumorigenesis, but androgen depletion therapy remains the foundation of treatment (*3, 4*). Tumors regress and patients receive benefit, but unfortunately this treatment is only effective for a short time and the cancer regains the ability to grow in low androgen conditions. This stage of the disease is referred to as castration-resistant prostate cancer (CRPC) and until recently there have been no durable therapies available (*4*). The majority of CRPCs maintain dependence on androgen signaling and many novel therapies attempt to more effectively shut this down. Novel antiandrogens have shown encouraging results, and one has recently received FDA approval (*5*), however like with most targeted therapies, resistance develops.

In my dissertation, I have identified and characterized one mechanism of resistance to these second-generation antiandrogens, a novel mutation of the androgen receptor. This discovery led to molecular modeling studies, which provided insight into the binding mode of these antiandrogens, and subsequently led to the design of novel antiandrogens to effectively overcome this mutation-based resistance.

Androgens and the Androgen Receptor

Androgens are the main male sex hormones, and are essential for male development and the maturation and maintenance of male reproductive function (*6*). They elicit their activity through binding and activation of the androgen receptor (AR), a nuclear hormone receptor and transcription factor. The primary androgen, testosterone, is synthesized by the testes and comprises roughly 90% of all androgens in circulation. Testosterone synthesis is predominantly regulated by the hypothalamic-pituitary-gonadal signaling axis, in which gonadotropin-releasing hormone (GnRH) from the hypothalamus stimulates the secretion of luteinizing hormone (LH) by the pituitary gland, which in turn activates production of testosterone by the Leydig cells of the testes. In order to maintain normal levels, testosterone acts via a negative feedback loop to regulate the production and activity of GnRH. (*6, 7*) Other circulating androgens, which include dihydroepiandrosterone (DHEA), androstenediol, and androstenedione, are primarily produced by the adrenal gland and can be converted to testosterone in peripheral tissues by a variety of enzymes involved in steroidogenesis. Most testosterone in circulation is bound to carrier proteins, and only the unbound form is able to diffuse into target tissues, where it is rapidly and irreversibly converted to the more potent androgen, dihydrotestosterone (DHT). In the prostate, the enzyme 5-alpha reductase catalyzes this conversion.

The androgen receptor (AR) is a nuclear hormone receptor and transcription factor that is activated by androgen binding. Both testosterone and DHT can bind to and activate AR, but DHT does so with a much higher affinity and produces greater AR transcriptional activity (*6, 8*). In its unbound state, AR is located in the cytoplasm where it resides in complex with chaperone heat shock proteins (HSP), including HSP90, that stabilize it and maintain its proper folding. Binding of ligand to the androgen receptor

induces a series of conformational changes and its dissociation from the HSP complex. This results in receptor N/C transactivation, dimerization and translocation to the nucleus where it binds to specific recognition sequences, androgen response elements (AREs), in the promoters and enhancers of target genes (*9, 10*). (**Figure 1**) AR activity depends upon its interaction with other proteins, including AR coregulators, other transcription factors, and general transcription machinery. AR coregulators have diverse functions, including chromatin remodeling, histone modifications, DNA repair, and cell cycle regulation. Some nuclear receptor coregulators modify AR transcritptional activity, either positively (coactivators, CoA) or negatively (corepressors, CoR) regulating ligand-dependent transcription of target genes (*11*).
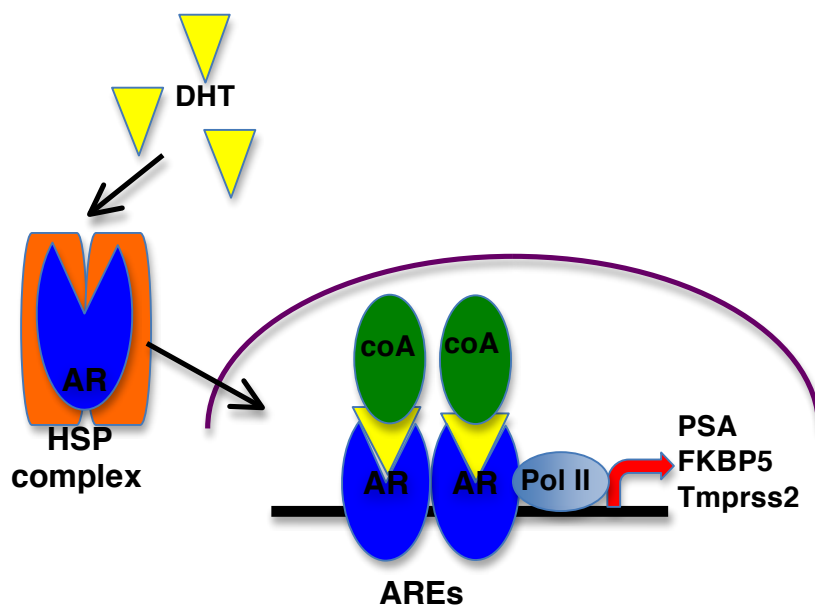
Figure 1. Cartoon depicting androgen receptor (AR) signaling

DHT binds to the androgen receptor, causing it to dissociate from the chaperonin heat-shock protein (HSP) complex, dimerize and translocate into the nucleus. There it associates with coactivator proteins (coA) and binds to androgen responsive elements (AREs) on the DNA, activating or repressing AR target gene transcription.

Androgen Receptor Domain Structure and Activation

The androgen receptor is a member of the nuclear receptor subfamily 3 group C (NR3C), along with the glucocorticoid, progesterone, and mineralocorticoid receptors. The human androgen receptor consists of 919 amino acids, but its length can vary due to stretches of poly-glutamine and poly-glycine repeats. Like all nuclear hormone receptors, AR contains four functional domains: an N-terminal domain (NTD), a hinge region, a DNA-binding domain (DBD), and a ligand-binding domain (LBD) (*8, 12*) (**Figure 2**).
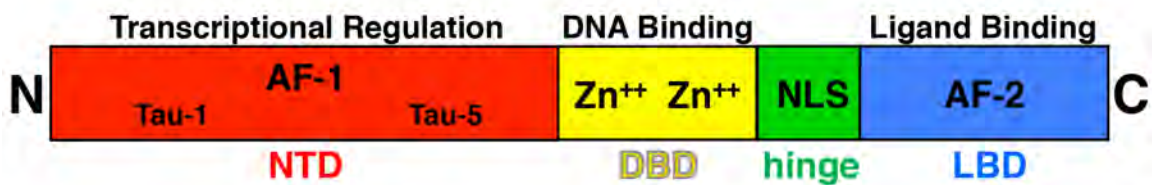
Figure 2. Cartoon depicting the domain organization of the androgen receptor

The N-terminal domain (NTD) is poorly conserved in sequence and function among different nuclear receptors, and in the case of AR, is extremely important for receptor transactivation. The NTD contains the major activation function region (AF-1) of the androgen receptor and contains two transactivation units (TAUs) that participate in transcriptional activation, Tau-1 and Tau-5. Both TAUs are necessary and sufficient for full activity of the androgen receptor, although Tau-1 is more dependent on the LBD. When basal transcription factors contact this domain, the AF-1 folds into a more compact and active conformation, resulting in CoA recruitment and transcription. Tau-5 strongly interacts with the glutamine-rich domain of the AR coactivators, SRC/p160. The

FQNLF motif in the amino-terminal domain is highly conserved between AR of different species, and is required for N/C interaction (*12*).

The DNA-binding domain (DBD) is the most evolutionarily conserved region for all nuclear hormone receptors. The DBD of AR contains several cysteine residues that help form two zinc-fingers and a C-terminal extension. The first zinc-finger helps determine DNA recognition specificity and the second is important for AR dimerization (*6, 12*). Steroid receptors bind to DNA elements comprised of inverted repeats of hexameric binding sites separated by three nucleotide spacers. The androgen receptor shares the same DNA consensus motif (TGTTCT) with the other NR3C family members, but there are also several AR specific binding motifs.

The DBD and LBD of the protein are connected via a flexible linker referred to as the hinge region. The sequence of the hinge region is poorly conserved among steroid receptors, but always contains the nuclear localization signal (NLS) for the receptor. It may also play a role in DNA selectivity and affinity, as well as AR dimerization.

Androgens bind to the ligand-binding domain (LBD) at the carboxyl-terminal end of the protein, which triggers AR transcriptional activity. The LBD of the androgen receptor is structured as a twelve alpha-helical sandwich with a central ligand-binding pocket. Androgen binding induces the repositioning of helix 12, which results in the closing of the pocket and generates a hydrophobic cleft, referred to as activation function region 2 (AF-2). This hydrophobic AF-2 pocket can bind to the FQNLF motif in the AF-1 activation domain in the NTD of the protein. This facilitates binding of coactivator proteins through their LxxLL motifs, to helix 12 of the LBD (*8*). This N/C-terminal transactivation allows dimerization of the receptor to occur, and translocation into the nucleus.

5

Androgen Receptor Alterations

The gene that encodes the androgen receptor lies on the X chromosome at Xq11-12. Alterations in AR are implicated in several disorders, including androgen insensitivity syndrome (AIS), spinal and bulbar muscular atrophy (SBMA), and prostate cancer (*13*).

Androgen insensitivity syndrome is an X-linked disease of individuals with a 46, XY karyotype, characterized by variable defects in male development. AIS results from loss-of-function mutations in the androgen receptor, resulting in peripheral androgen resistance, and can be classified into three clinical subtypes based on the degree of the clinical phenotype: complete (CAIS), partial (PAIS), and mild (MAIS) (*14*). AIS is associated with a wide array of molecular defects in AR which include, point mutations that result in amino acid substitutions or lead to premature termination, insertions or deletions that lead to a frameshift and premature stop codon, complete or partial loss of the gene, and intronic mutations that alter AR mRNA splicing. Over 400 AR mutations have been described that results in AIS, with most being single point mutations that occur in the LBD. The phenotype of AIS individuals depends on the remaining functionality of AR, with truncation mutants that lack transactivation capacity leading to CAIS, and point mutations that only modestly affect AR activity resulting in MAIS (*14*).

In exon 1 of the AR gene, a CAG repeat region codes for a poly-glutamine (polyQ) repeat in the NTD of the protein. This normally consists of 21 ± 2 repeats, but a great deal of polymorphism exists. In cases with a large degree of glutamine variation, this CAG polymorphism is associated with neurological and endocrine disorders, and may play a role in cancer susceptibility (*15*). AR transcriptional activity inversely correlates with polyQ repeat length, with a high number of repeats leading to lower

functionality and fewer repeats leading to a super-active receptor (*13, 15*). Spinal and bulbar muscular atrophy (SBMA) is a rare, chronic, and progressive neuromuscular disorder caused by expansion of the CAG repeat (35 or more). Affected males may display signs of androgen insensitivity, but the main signs of disease are muscle weakness and atrophy of motor neurons in the spinal cord and brainstem (*15*). It has been proposed that polyQ size may play a role in male infertility and excess hair in females. Studies in both prostate and breast cancers, have shown that CAG repeat length correlates with age of diagnosis, total risk, recurrence, and tumor aggressiveness. In the prostate, the risk goes up with a lower repeat length, while in breast tumors longer CAG repeats have higher risk (*13*).

Amplification, point mutation and truncation of the androgen receptor have been described in patients with prostate cancer. These alterations typically occur in patients with advanced disease, who have received several cycles of hormonal therapy. Details of these alterations will be discussed in the section regarding mechanisms of resistance in CRPC.

Crystal Structures of Nuclear Receptors

Crystal structures have been solved of DHT bound to wild-type and mutant AR LBD. Because of the vast difference in steroidal vs. non-steroidal ligands, these structures offer limited insight into how non-steroidal antiandrogens bind and antagonize the receptor. No crystal structure exists of AR in complex with antiandrogens in an antagonist conformation, however several antiandrogen/AR complexes have been solved in the agonist conformation. This has been accomplished using specific AR LBD mutants, in which the activity of the antiandrogen is altered by the mutation into acting as an agonist. The LBD of the AR T877A mutant was co-crystallized with cyproterone

acetate, a steroidal antiandrogen (*16*). Crystal studies of the nonsteroidal androgens S-1 and R-3, that bear structural similarity to nonsteroidal AR antagonists, bicalutamide and flutamide, have further provided insight into the binding of nonsteroidal ligands in the AR LBD (*17*). The crystal structure of the nonsteroidal antiandrogen R-bicalutamide bound to AR W741L LBD was solved and found to have a similar overall folding structure to that of DHT-bound to wild-type AR LBD complex (*18*). (**Figure 3**) These structures provide rational explanations for why the antiandrogen may lose antagonism in the context of specific mutations, and this often is explained by a mutation resulting in the loss of bulk (Trp to Leu or Cys) which allows the helix to adopt a tighter more closed conformation, enabling coactivator recruitment.
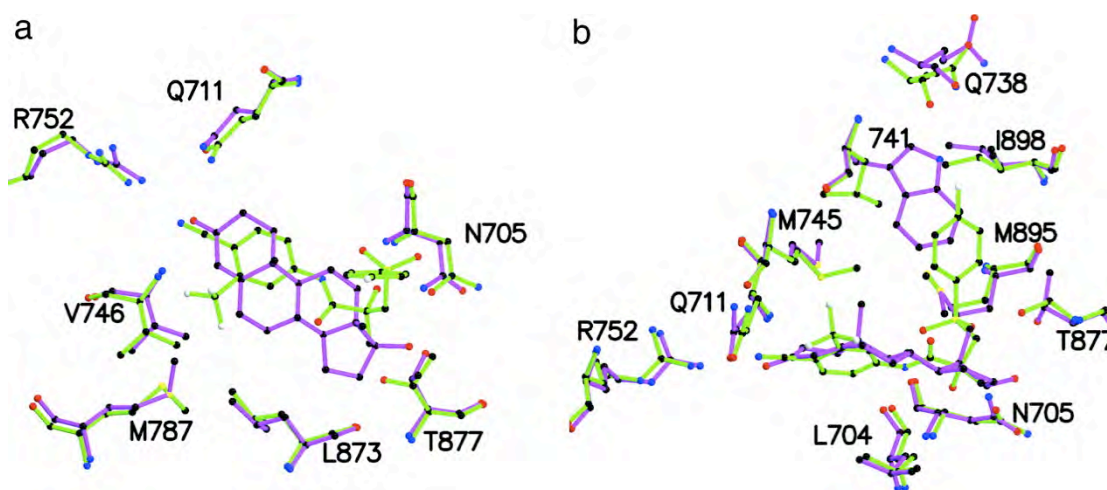
Figure 3. Overlay of AR agonist crystal structures

AR W741L/bicalutamide (green) and AR WT/DHT (purple) highlighting the similar structural alignment. (**a**) Overview of the steroidal plane. Notice the similar positioning of the cyano group of R-bicalutamide to the 3-keto group of DHT and the differences in the location of bulk from these ligands. (**b**) Side view of the steroidal plane. The R-bicalutamide B ring in the W741L AR binds in the region occupied by the Trp-741 indole ring in the WT AR bound to DHT. (*18*)

Proc Natl Acad Sci US A. 2005 Apr 26;102(17):6201- 6.

Many insights into AR antagonist structure/ function have been inferred from X-ray crystallography studies of other nuclear hormone receptors, particularly the estrogen receptor (ER). Crystal structures have been solved of the LBD of the human ER-alpha bound to two chemically related compounds with distinct activity: an ER agonist, diethylstilbestrol (DES), and an ER antagonist, 4-hydroxytamoxifen (OHT) (*19*) (**Figure 4**). In the case of the DES bound ER-alpha LBD, the complex was crystallized along with a short peptide derived from the coactivator GRIP1. This peptide bound as a short alpha-helix in a hydrophobic groove on the surface of the estrogen receptor LBD. In the case of the antagonist OHT structure, this coactivator recognition site is blocked by helix 12 of the ER-alpha LBD. The drastic difference in activity of the agonist and antagonist bound estrogen receptor can be explained by the subtle difference in the orientation of helix 12 of the LBD, which in the case of OHT, mimics the binding of the coactivator GRIP1 and precludes activation of the receptor (*19*).
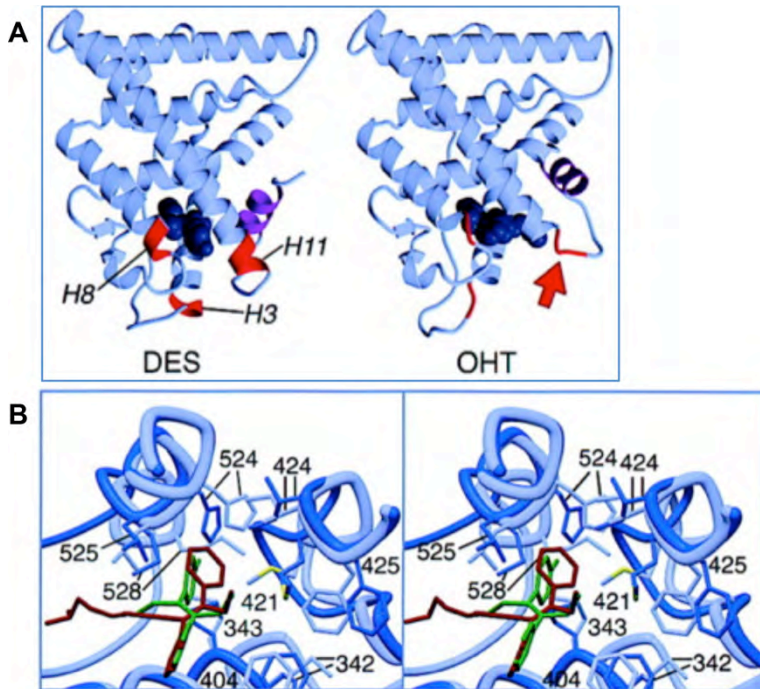
Figure 4. The binding of agonists and antagonists promote different LBD conformations in the estrogen receptor (ER)

(**A**) Ribbon representations of the DES complex (without the coactivator peptide) and the OHT complex. The hormones are shown in space-filling representation. In each complex, helix 12 is colored purple, and the main chain of residues 339 to 341, 421 to 423, and 527 to 530 is colored red. Helices 3, 8, and 11 (H3, H8, and H11, respectively) are labeled in the DES complex. (**B**) The structures of the OHT complex and DES complex were overlapped, OHT is colored red and DES is colored green. The LBD bound to OHT is colored dark blue, and the LBD bound to DES is colored light blue. The side chains of some of the residues whose conformations are dramatically different between the two complexes are drawn.

Prostate Cancer

In addition to being critical for proper development of the prostate, AR signaling is also essential for the growth and survival of prostate tumors, adenocarcinomas derived from the epithelial cells of the prostate gland (*20*). Early detection of prostate cancer occurs through measurement of serum prostate specific antigen (PSA) levels. PSA is an androgen regulated protein, produced and secreted by the prostate, and elevated levels may indicate the presence of a prostate tumor. While PSA levels may suggest the presence of prostate cancer, the only way to confirm diagnosis is through biopsy and histology (*21*).

Early changes in the morphology of the prostate are referred to as prostatic intraepithelial neoplasia (PIN) and can be classified as low or high-grade. PIN is characterized by abnormalities in the nuclei and chromatin content of cells. Epithelia with evidence of low-grade PIN may have some enlarged cells and nuclei, a slight increase in chromatin content, and small nucleoli. High-grade PIN glands have enlarged cells with large nuclei, increased chromatin content with prominent nucleoli, and some disruption of the basal-cell layer. High-grade PIN is the only recognized premalignant lesion for prostate cancer. The diagnosis of prostate cancer includes the features of high grade PIN, but also the presence of mitotic figures, loss of the basal cell layer, infiltrative or cribiform glands, glandular secretions, and stromal invasion (*22*).

The Gleason grading system was introduced over 40 years ago to help evaluate prostate cancer, classifying tumors based on their architecture. This system is still used today, with some modifications, to grade prostate tumors. Pathologists evaluate the tumor pattern on a scale of 1-5 (where 1 is the least, and 5 is the most aggressive/ advanced), and the tumor grade is a sum of the two most common tumor grade patterns

observed (*23*). A patient's Gleason score helps determine the course of treatment that should be taken.

Prostate Cancer Therapy

Current treatment for localized, early-stage prostate cancer is surgery or radiation. This treatment is highly effective, but when there is progression to more advanced or metastatic disease, androgen deprivation therapy (ADT) and other methods of turning off AR signaling are employed (**Figure 5**). This typically involves administration of a GnRH analogue (chemical castration), which aims to turn off androgen biosynthesis, and in some cases combined with an antiandrogen (*24*). Antiandrogens are androgen receptor antagonists that inhibit AR signaling by competing with endogenous androgens for binding to the ligand-binding domain of AR. Non-steroidal antiandrogens are preferred for clinical use because of less cross-reactivity with other nuclear hormone receptors. Three non-steroidal antiandrogens have been used clinically for over a decade for prostate cancer patient care: flutamide, nilutamide, and bicalutamide. Both nilutamide and bicalutamide are derivations of flutamide, improving pharmacokinetic properties and efficacy of the drug, and reducing toxicity. These antiandrogens are often taken in combination with androgen depletion therapies, such as GnRH agonists (e.g., lupron), in cases of metastatic and castration-resistant disease (*25*).

Most patients initially respond to ADT, but this response is limited and most patients experience disease progression within a few years. (**Figure 6**) Though these patients stop responding to ADT, their tumors often still depend on AR signaling. This stage of the disease is referred to as castration-resistant prostate cancer (CRPC) and there is usually some degree of benefit from secondary hormonal manipulations (*25*).

12

Subsequent therapy options include second line antiandrogens, glucocorticoids or corticosteroids to decrease adrenal androgen synthesis, estrogens to inhibit LH production, or nonspecific steroidogenesis inhibitors. Ketoconazole, which inhibits enzymes involved in steroidogenesis, has shown moderate antitumor activity in CRPC, but its use has been limited by toxicity.
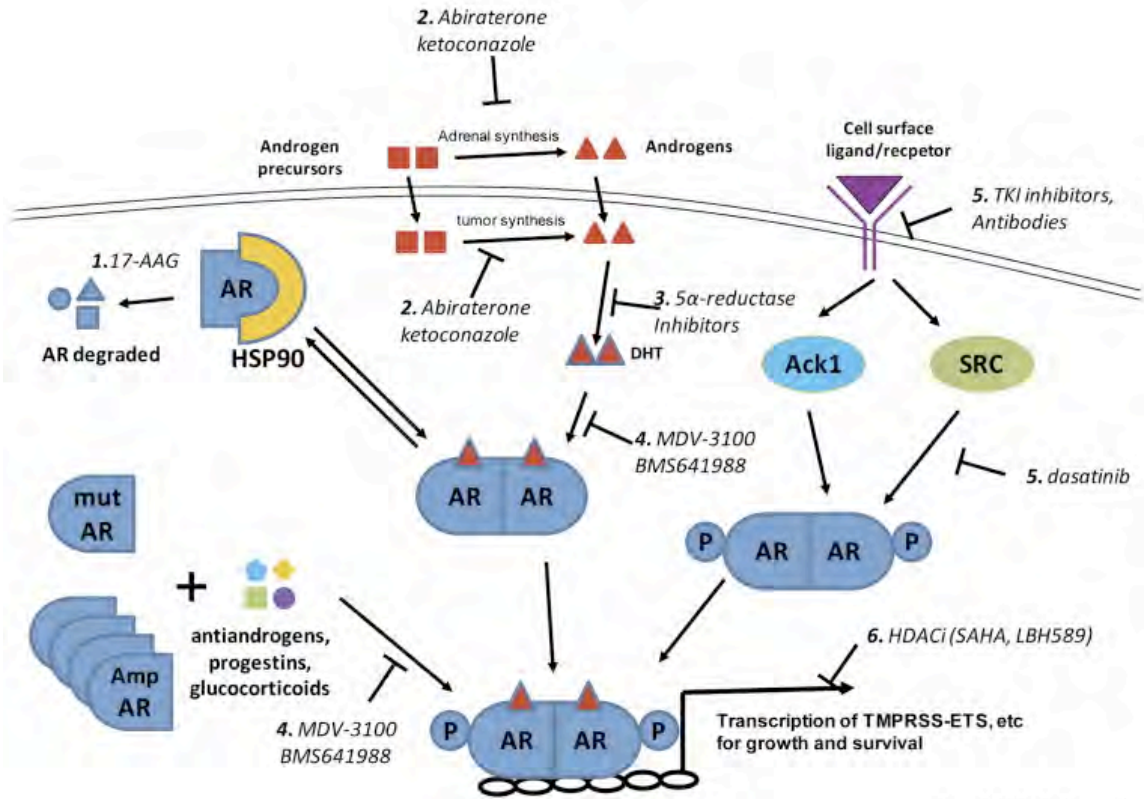
Figure 5. Schematic of therapies targeting the AR signaling pathway

1) HSP90 inhibitors, such as 17-AAG, cause AR degradation and decrease AR levels. **2)** Steroidogenesis inhibitors ketoconazole and abiraterone can block androgen synthesis by the adrenal glands and intratumoral androgen synthesis. **3)** Finasteride and dutasteride block 5α-reductase mediated conversion of testosterone to the more potent DHT. **4)** Antiandrogens such as MDV3100 block DHT binding and activation of AR. **5)** Activation of receptor tyrosine kinases, in particular HER2, can lead to downstream AR activation. Antibodies such as trastuzamab, and small molecular TKI inhibitors such as erlotinib target HER2, dasatinib targets SRC. **6)** HDAC inhibitors block transcription of AR target genes by disrupting chromatin structure and blocking coactivator and RNA polymerase recruitment. (*25*)

Reprinted from Curr Opin Pharmacol. 8(4), Chen Y, Sawyers CL, Scher HI. Targeting the androgen receptor pathway in prostate cancer. 440-8. Copyright 2008, with permission from Elsevier.

14

Other strategies to treat prostate cancer have included the use of histone deacetylase (HDAC) inhibitors, which aim to disrupt AR transcription complex formation, and HSP90 inhibitors, that attempt to destabilize the androgen receptor and lead to its degradation (*25*). Neither approach has been very successful in early clinical trials, but there is effort to optimize these therapeutic strategies. Tyrosine kinase inhibitors and monoclonal antibodies against EGFR and Her2 have also been tested for activity in CRPC, but have not shown promising results (*25*).

Until recently, the only therapy shown to modestly improve survival and provide palliative benefits for patients with metastatic castration-resistant disease was docetaxel-based chemotherapy (*24*). In the last several years there have been many advances in the treatment of CRPC, targeting different aspects of disease pathobiology. In April 2010, the first therapeutic cancer vaccine, sipuleucel-T (Provenge), was approved for men with minimally symptomatic CRPC. The following year, abiraterone acetate (Zytiga), the novel and more specific steroidogenesis inhibitor of 17 alpha-hydroxylase/C17,20 (CYP17), received FDA approval for patients with metastatic CRPC. Finally, the novel diarylthyohydantoin antiandrogen enzalutamide (Xtandi) received FDA approval for patients with CRPC in August 2012.
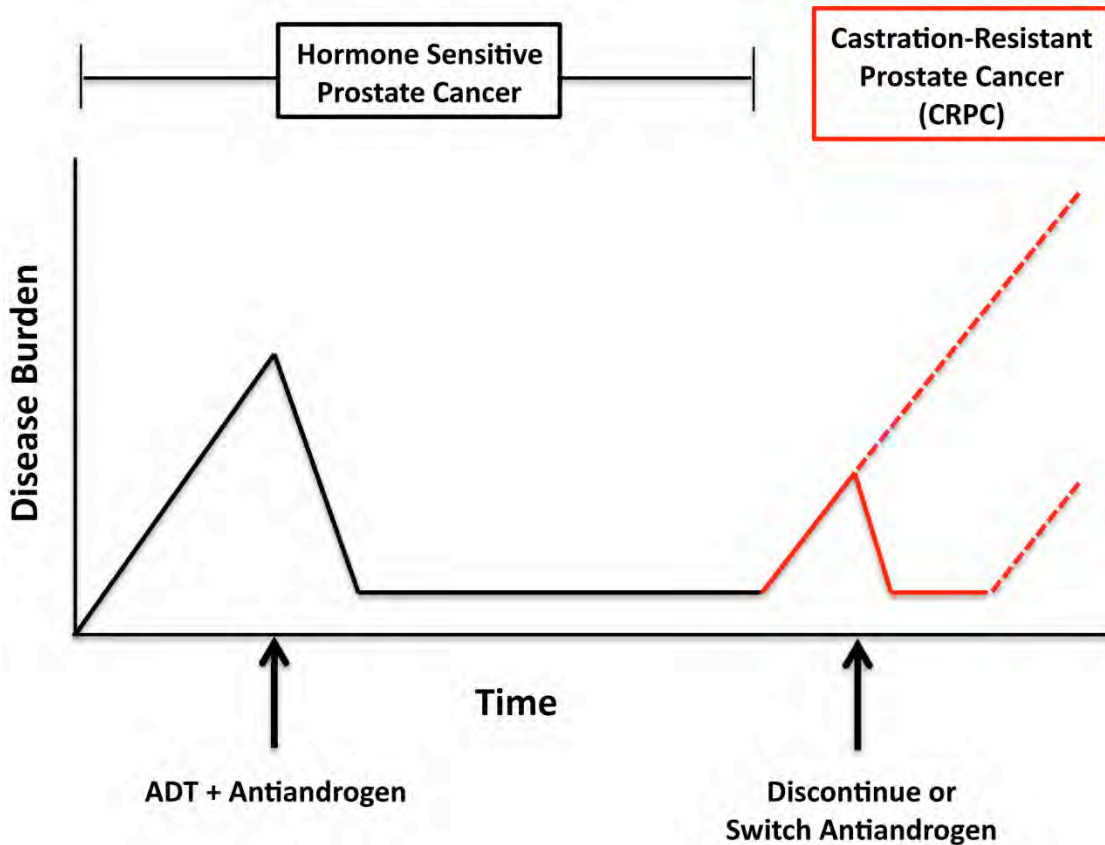
Figure 6. Typical response to hormonal therapy

Prostate tumors go through an initial stage where they are exquisitely sensitive to hormonal therapy and tumors respond rapidly to androgen deprivation therapy (ADT), which often includes the use of AR antagonists (antiandrogens).   After a period of inhibition, the tumors eventually begin to regrow with hormonal therapy.   Alternative hormonal manipulations often provide some benefit, and these tumors still largely depend on androgen signaling. This stage of disease is known as castration-resistant prostate cancer (CRPC).

Mechanisms of Resistance to Targeted Therapy

Targeted therapy has been employed for infectious disease for many decades, using drugs that specifically inhibit different aspects of bacterial or viral replication and survival. Resistance to these targeted therapies often develops, but the use of combination therapy can effectively overcome this resistance (*26*). With the increasing use of targeted therapies in cancer, mechanisms of acquired drug resistance are well documented and the limitations of these therapies appreciated. There are many parallel mechanisms of resistance shared between targeted antimicrobials and antitumor agents, and can include mutation or amplification of the gene that encodes the drug target, upregulation of a parallel bypass pathway, drug destruction or modification, and persistence of insensitive (stem-like) cells (*26*).

Mutation of an anticancer drug target as a mechanism of resistance was originally demonstrated with the discovery of mutations in the kinase domain of BCR-ABL in patients with chronic myeloid leukemia (CML), conferring resistance to the small molecule tyrosine kinase inhibitor imatinib (*27*). Since this study, mutations as a mechanism of acquired resistance to targeted therapies have been described in many tumor types, including gastrointestinal stromal tumors (*28*), melanoma (*29*), and non-small cell lung cancer (*30*). Recent studies have also described resistance to targeted therapies through activation of a parallel signaling pathway or a signal downstream of the original target (*31, 32*).

Mechanisms of Resistance in CRPC

Many studies have demonstrated that CRPC still requires and maintains androgen signaling for growth, and that despite hormonal therapies that aim to shut it down, these tumors often develop various mechanisms to reactivate androgen receptor signaling. This frequently involves sensitizing the tumor to low level of androgens through overexpression of AR (**Figure 7**), which in roughly 30% of CRPC tumors occurs through amplification of the receptor (*33, 34*). Antiandrogens, such as bicalutamide and hydroxyflutamide, lose their antagonism for AR and behave as partial agonists in the setting of AR overexpression, which could be due to an imbalance in coregulators, permitting a conformation that is suboptimal for receptor activation, but still allows coactivator recruitment (*35*).
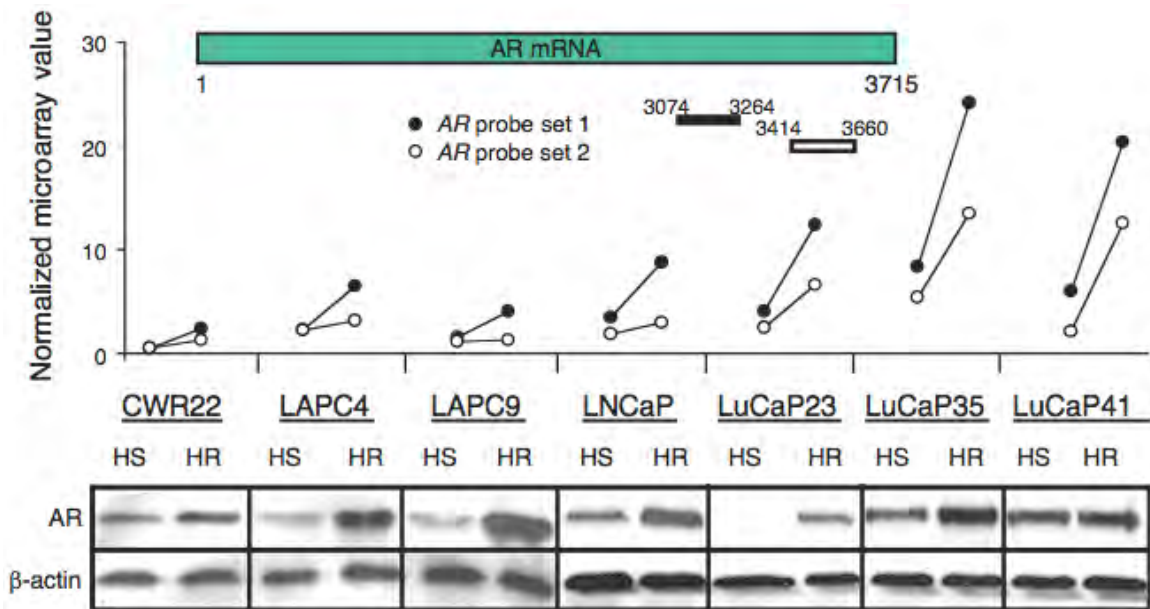
Figure 7. AR expression in hormone sensitive (HS) and hormone refractory (HR) xenografts

Microarray analysis of genes that were differentially expressed from the "hormone-sensitive" to "hormone-refractory" state found that AR was the only gene consistently upregulated in seven distinct human xenograft pairs. Western blot analysis showed that protein expression was also higher in the HR tumors. (*35*)

Reprinted by permission from Macmillan Publishers Ltd: NATURE MEDICINE, 10(1):33-9, copyright 2004.

http://www.nature.cornl:nrnljoumal/v10/n1/full/nm972.html

Although mutation of AR does not seem to be common in early stages of prostate cancer, mutations have been well documented upon relapse in the setting of ADT and antiandrogen therapy (*36*). There has been a wide degree of difference in reports of incidence of AR mutations (*13*), but recent next gen sequencing studies confirm that they occur in 20% of patients with metastatic CRPC (*37*). These mutations often increase ligand promiscuity, allowing other endogenous androgens (or hormones) to activate AR signaling, and some can convert antiandrogens into agonists of the mutant receptor (*38*) (**Figure 8**). The clinical observation of antiandrogen withdrawal syndrome, where PSA levels decrease or tumors regress upon withdrawal from bicalutamide or flutamide treatment, correlates with the presence of AR mutations.
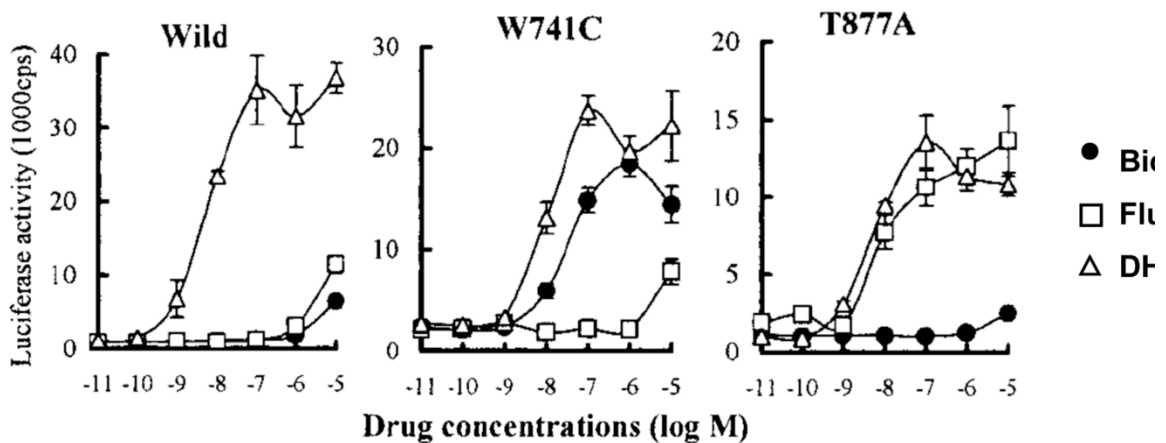
Figure 8. Distinct AR mutations confer agonism on different antiandrogens

Luciferase reporter assay showing agonist conversion of the antiandrogens bicalutamide (Bical) and flutamide (Flut) with the W741C and T877A mutations, respectively (*38*).

Reprinted by permission from the American Association for Cancer Research: Hara et al., Novel mutations of androgen receptor: a possible mechanism of bicalutamide withdrawal syndrome, Cancer Research, January 1, 2003, 63(1), 149-53.

Interestingly, these tumors often show further response when there is a switch to a different antiandrogen therapy. In vitro studies have shown that the LNCaP prostate cancer cell line, which already harbors the T877A mutation that alters the receptor's affinity for several ligands and confers agonist properties on flutamide (*39*), can acquire additional mutations when cultured long-term in the presence of bicalutamide (*38*). These secondary mutations (W741C/L) convert bicalutamide into an agonist of the mutant receptor.

Levels of intratumoral androgens in men with castrate resistant disease are not significantly lower than in normal prostate and an increase in the expression of genes that mediate the conversion of adrenal androgens to testosterone and DHT has also been observed in CRPC (*40, 41*). These data suggest that tumors adapt to reduced systemic testosterone levels by increasing expression of enzymes involved in the conversion of adrenal androgens into testosterone. These results have led to the design of a selective inhibitor of Cyp17, abiraterone acetate (Zytiga), to more completely turn off androgen biosynthesis (*42*). Alteration of androgen receptor transcriptional coregulators has also been implicated in castration resistance. There is evidence that a change in the coactivator/ corepressor balance can lead to constitutive active of AR, and certain AR coactivators are overexpressed in the progression of prostate cancer (*6*).

Recent work has also shown that expression of AR splice variants, that have distinct C-terminal extensions encoded by cryptic exons from the intronic regions between canonical coding exons of AR, occurs in castration resistance (*43*). These variants often the ligand-binding domain (LBD) and some data suggests that they may exhibit constitutive AR activation. Although work from our group has shown that these variants still require full-length AR to function (*44*), recent studies have suggested that

expression of these variants is sufficient to elicit transcription of AR target genes in the absence of androgen and confer resistance to the novel antiandrogen enzalutamide (*45*).

Novel Antiandrogens: Enzalutamide and ARN-509

Recent work has focused on the development of new antiandrogens, with the objective to overcome mechanisms of resistance seen with the previous generations of antiandrogens. Because AR overexpression is the most common mode of antiandrogen resistance, a library of compounds was screened for antagonism using human prostate cancer cells engineered to overexpress the androgen receptor (*46*). The novel bisaryl thiohydantoin antiandrogen enzalutamide (formerly MDV3100) was selected for further development from this structure-activity relationship (SAR) screen. Further studies revealed another compound, ARN-509, that scored in this assay and has also shown success in preliminary clinical trials (*47*).

Enzalutamide binds AR with much higher affinity than bicalutamide, and in the setting of AR overexpression, inhibits AR nuclear translocation, prevents coactivator recruitment and DNA binding to AREs (*46*). In contrast, bicalutamide gains partial agonist properties in cells that overexpress AR, permitting translocation of AR into the nucleus, coactivator recruitment, binding to AREs and results in transcription of AR target genes (*35*). In vitro studies using cell lines that overexpress AR demonstrate that enzalutamide treatment inhibits cell growth and AR-mediated transcriptional activity, while bicalutamide does not. Enzalutamide treatment also induced tumor regression in xenograft tumors growing in castrate male mice, while mice treated with bicalutamide displayed variable responses and at best, only modestly slowed tumor growth (*46*) (**Figure 9**).

22
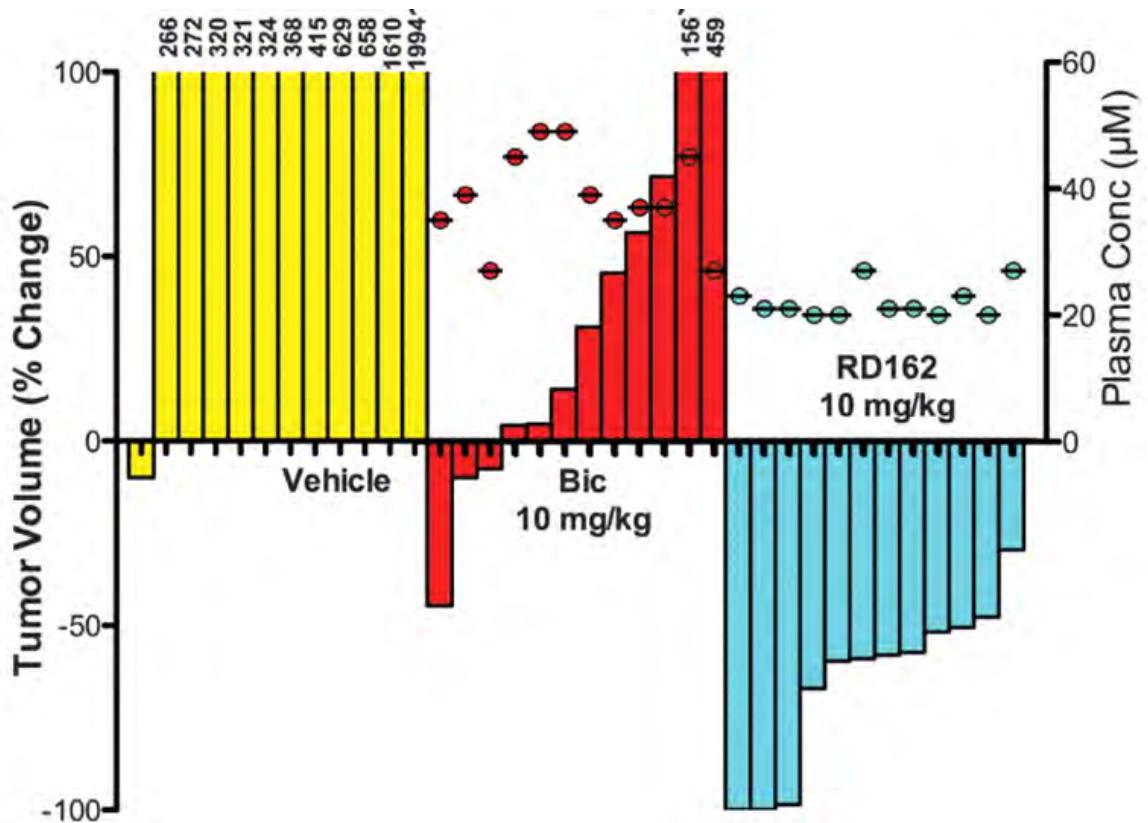
Figure 9. Waterfall plot of change in CRPC xenograft tumor volume

RD162 (MDV3100 analog) induces tumor regression, while bicalutamide has a limited and variable effect on tumor growth. Serum concentrations are comparable in the 2 drug treatment groups. (*46*)

From Science 2009 May 8; 324(5928):787-90. Reprinted with permission from AAAS.

These promising preclinical results lead to the advancement of enzalutamide for clinical development. In a phase 1-2 study, enzalutamide was tested for pharmacokinetics, safety and tolerability, and to define a maximum tolerated dose. This study also aimed to assess tumor response based on changes in serum PSA levels, imaging studies, circulating tumor cell (CTC) counts, and time to disease progression in patients with histologically confirmed castration-resistant disease (*48*).

The results of this study suggested that AR signaling continues to play a critical role in prostate tumorigenesis in the castrate-resistant stage, with evidence that MDV3100 provides significant benefit for men with CRPC who had failed on previous chemotherapy or hormonal treatments. Based on these promising clinical data, MDV3100 underwent testing in a phase 3 randomized trial, comparing it to placebo in men with progressive advanced prostate cancer who had received previous docetaxel therapy. The primary endpoint of this study was overall survival, and secondary endpoints included measures of response (PSA reduction, soft-tissue response, quality-of-life benefit) and measures of progression (time to PSA progression, radiographic progression-free survival, time to skeletal-related event) (*5*).

At a predetermined interim analysis point, there was a 37% reduction in the risk of death for patients receiving enzalutamide compared to placebo (*5*). The benefit for patients in the enzalutamide group was shown for all secondary endpoints as well. Based on these results, an independent data and safety monitoring committee suggested the trial be ended and patients in the placebo arm offered enzalutamide treatment. On the basis of these studies, enzalutamide received Food and Drug Administration (FDA) approval in August 2012.

ARN-509 is another diaryl-thiohydantoin compound that came out of SAR screens for compounds that remain active in cells that overexpress the androgen receptor. Like enzalutamide, ARN-509 remains a potent AR antagonist, efficiently blocking AR nuclear translocation and DNA binding. Studies in preclinical models showed that ARN-509 potently inhibits tumor growth and achieves similar efficacy as MDV3100 in xenograft models of CRPC (*49*). These promising preclinical data led to clinical evaluation of ARN-509, which showed that it is safe and well-tolerated. ARN-509 is currently in phase II studies to determine its activity in 3 different patient populations:

1) non-metastatic CRPC patients who are treatment-naïve (haven't received prior chemotherapy or enzalutamide); 2) metastatic CRPC patients who are treatment-naïve; and 3) metastatic CRPC patients who have received abiraterone acetate, but are chemotherapy naïve. The primary endpoint for these trials was a 50% or greater decline in PSA after 12 weeks, with secondary endpoints being safety, time to PSA progression and objective response rates. Preliminary analysis of these data show that a subset of patients show a 50% decline in PSA in each of the separate patient populations: 1) 91% (non-metastatic, treatment-naïve; 2) 88% (metastatic, treatment-naïve; and 3) 29% (metastatic, post-abiraterone treatment) (*47*). Final analysis of the phase II trial is ongoing.

Despite the FDA approval of enzalutamide and the initial outcomes of the ARN-509 clinical trials showing a benefit to many CRPC patients, a subset of patients do not respond up front. In addition most patients who respond initially, ultimately progress on this therapy. (**Figure 10)** There is a need to identify factors that modify response to this novel antiandrogen therapy in order to intelligently stratify patients and direct future studies.

Overall Survival
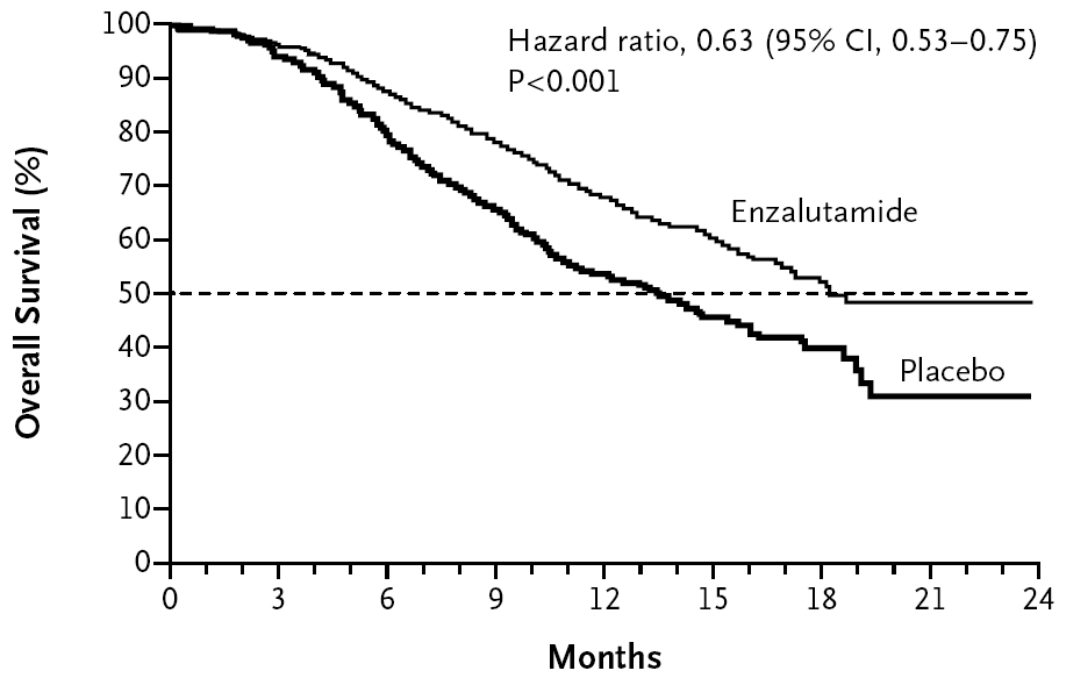
Figure 10. Enzalutamide therapy provides survival benefit for men with CRPC

Overall survival for men on phase 3 trial of enzalutamide vs. placebo, showing survival benefit for men in the enzalutamide arm. (*5*)

Reproduced with permission from N Engl J Med. 2012 Sep 27; 367(13):1187-97, Copyright Massachusetts Medical Society.

Saturation Mutagenesis Screens

Unbiased mutagenesis screens have been utilized for decades to discover gene function in bacteria and yeast systems. More recently, saturation mutagenesis approaches have been used to uncover mutations that alter drug sensitivity in mammalian cells. Such studies have been performed for oncogenic kinases, including BCR-ABL and EGFR, and often use growth in the presence of drug to assess resistance. In the case of Abl kinase inhibitors to study CML drug sensitivity, the Baf-3 cell line is a useful tool. When transduced with BCR-ABL, Baf-3 cells, which normally require interleukin-3 (IL-3) for growth, lose their dependence on this cytokine. To screen for mutations that might confer resistance to Abl kinase inhibitors, Baf-3 cells can be transduced with a randomly mutagenized BCR-ABL cDNA library and screened for mutations that allow transformation and colony formation in the presence of drug and absence of IL-3 (*50*). This method was used to prospectively identify BCR-ABL mutants that confer resistance to dasatinib, with the mutations later clinically validated in patients who relapsed on this therapy (*51, 52*).

In my thesis work, I have designed and optimized a novel mutagenesis screening method to prospectively identify AR mutations that confer resistance to second-generation antiandrogens. The design and optimization of this screen is described in Chapter 2 of my thesis, while the screen conducted to identify enzalutamide-resistance mutations is described in Chapter 3, and our efforts to validate our in vitro findings in patients who relapse on these therapies is discussed in Chapter 4 of my work.

Chapter 2 – A reporter-based system to screen for AR activity

Introduction

We developed a reporter-based system to screen AR mutations for sensitivity to novel antiandrogens. This EGFP reporter assay will be useful to identify AR mutants that maintain AR transcriptional activity in the presence of different AR antagonists, either by precluding antiandrogen binding or altering the conformation of the receptor once bound by the antiandrogen in such a way that it now behaves as an agonist. To optimize our screening system we tested several different EGFP reporters of AR activity, and ultimately chose a lentiviral EGFP construct that contains the probasin promoter region and PSA enhancer elements driving EGFP expression (Pb.PSE.EGFP) (*53*). The combination of the probasin promoter and PSA enhancer displayed the highest specificity and strong inducibility in the AR-positive LNCaP cancer cell line, with very low background and no EGFP induction in AR-negative HuH7 cells (*53*) (**Figure 11**).

We chose to use LNCaP cells to develop our screen assay system because of their exquisite sensitivity to MDV3100, and also to bicalutamide, which was to be used for our proof-of-concept validation screen. These cells endogenously express AR and the necessary cofactors for AR-regulated transcription. LNCaP cells display strong induction of canonical AR target genes with androgen stimulation, which is efficiently quenched with MDV3100 exposure (*46*). Although LNCaP cells respond very well to antiandrogen treatment, in terms of AR target gene repression, they only exhibit a modest growth response in vitro. For this reason, we chose to strictly use short-term EGFP-reporter expression to readout antiandrogen response. We single-cell cloned

LNCaP cells transduced with the Pb.PSE.EGFP reporter to minimize the variability in

EGFP reporter expression due to different viral integration sites or copy number of the

reporter construct.
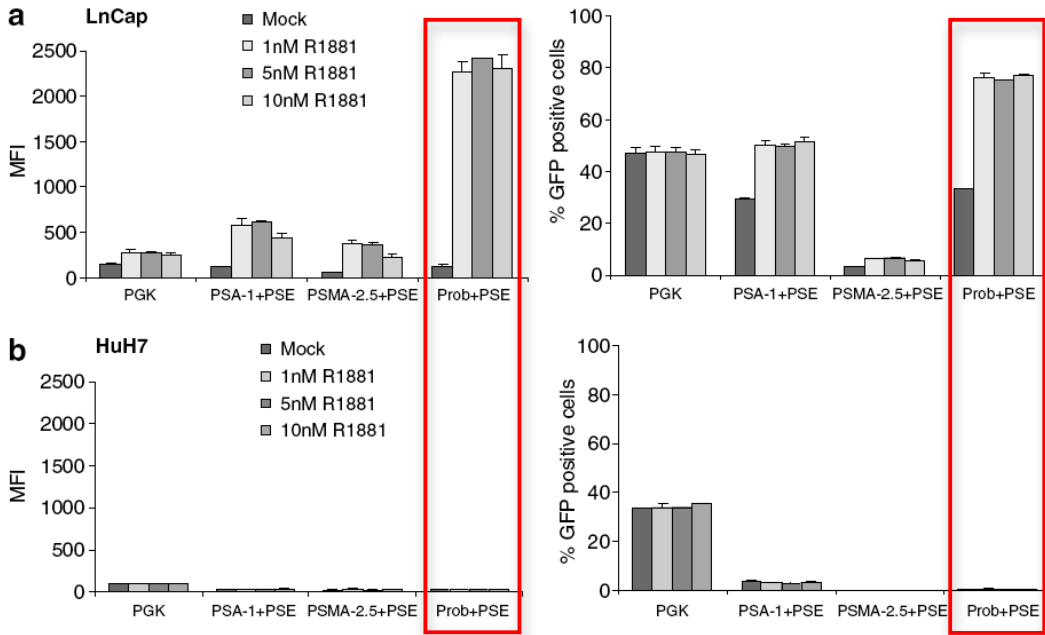
Figure 11. AR-regulated EGFP reporter

A lentiviral reporter construct with a probasin promoter and PSA enhancer driving EGFP expression (outlined in red), displays (a) high AR-regulated inducibility (b) with low background. Modified from (*53*).

Reprinted by permission from Macmillan Publishers Ltd: CANCER GENE THERAPY 13(10):919-29, copyright 2006.

http://www.nature.com/cgt/journal/v13/n10/full/7700966a.html

Materials and Methods

<u>Materials and Cell Lines</u>

The LNCaP cell line was obtained from ATCC. Fetal bovine serum (FBS) and charcoal-stripped, dextran-treated fetal bovine serum (CSS) were purchased from Omega Scientific. Bicalutamide (Investigational Drug Pharmacy), hydroxyflutamide (LKT Labs), DHT (Sigma), and R1881 (Perkin Elmer) were commercially obtained; all other ligands were synthesized at MSKCC. Serial dilutions of all drugs were made using DMSO. Antibodies used for immunoblot assays were β-actin (AC-15, Sigma), FKBP5 (IHC-00289, Bethyl), β-tubulin (D-10), androgen receptor (N-20), and PSA (C-19) (all 3 from Santa Cruz Biotechnology). Protein lysates were prepared in M-PER protein extraction reagent (Pierce). Nontarget and human AR siRNA pools were from the ON-TARGETplus collection (Dharmacon). All oligos were ordered from Operon Biotechnologies.

<u>Plasmids & Cell Transduction</u>

The human AR cDNA plasmid, pWZL-AR, was provided by William Hahn (Dana-Farber Cancer Institute, Boston). All mutant AR constructs were generated in pWZL-AR with the QuikChange II XL site directed mutagenesis kit (Agilent) and primers designed using Agilent's online QuikChange Primer Design tool. Stable cell lines were generated by pantropic retroviral infection (Clontech) and selected with blasticidin (Invivogen). LNCaP cells were infected with the lentiviral AR-regulated EGFP reporter construct, Pb.PSE.EGFP (*53*), provided by C. Bignon (EFS Alpes Méditerranée, Marseilles, France).

Single Cell Cloning

LNCaP-Pb.PSE.EGFP cells were plated at a low density (1×10^4 cells) in a 15-cm tissue culture plate in conditioned RPMI +10% FBS. Media was replaced every 4 days, and cells examined under the microscope for single cell expansion. Once colonies started to emerge, sterile cloning rings were placed around the colony and the cells were trypsinized, collected, and transferred to one well of a 24-well tissue culture plate. These cells were expanded, frozen down, and tested for modulation of EGFP expression in response to androgens and antiandrogens.

Flow Cytometry Analysis and FACS-sorting

LNCaP-Pb.PSE.EGFP cells for flow cytometric analysis were treated with antiandrogens (1µM or 10µM) for 4-6 days, changing media and drug every 2-3 days. Cells were collected using Accumax dissociation solution (Innovative Cell Technologies) and dead cells were counterstained using TO-PRO3-Iodide (Invitrogen). EGFP expression was measured using the BD-FACSCalibur flow cytometer using the 488nm laser and 530/30 bandpass filter to detect EGFP expression, and the 633nm laser and 661/16 bandpass filter to detect TO-PRO3-Iodide labeled dead cells. For each sample, 2-5 x 10^4 cell events were collected and analysis was done using FlowJo software. FACS-sorting of LNCaP-Pb.PSE.EGFP cells was performed on a BD FACSVantage cell sorter. Dead cells were counterstained with DAPI (Invitrogen). EGFP expression was detected using the 488nm laser and 530/30 bandpass filter, and DAPI-labeled dead cells were detected using the 355nm laser and 450/50 bandpass filter.

FACS-based Bicalutamide Proof-of-Concept Screen

We introduced 4 additional synonymous mutations into our pWZL-AR W741C construct to aid in distinguishing wild-type (WT) AR and AR W741C, using the QuikChange Multi Site-Directed Mutagenesis Kit (Agilent). We then designed and optimized quantitative PCR primers across these mutation sites, so that they specifically amplified AR W741C. We overexpressed AR WT or AR W741C in our LNCaP-Pb.PSE.EGFP reporter cells, mixed different ratios of cells expressing either WT or W471C, treated these cells with 1μM bicalutamide for 4 days, and FACS-sorted the cells that maintained/induced EGFP expression. Gates for EGFP positivity were set using WT or W741C expressing cells treated with bicalutamide. Sorted cells were expanded in culture (without drug) until they reached approximately 60 million cells, we then isolated gDNA and froze down a small fraction, and the brief bicalutamide treatment and sorting was repeated on the remainder.

Table 1. Site-Directed AR Mutagenesis Primers

G142V - sense	cgccagcaaggtgctgccgcagc
G142V - antisense	gctgcggcagcaccttgctggcg
K179R - sense	ctgctccgctgaccttagagacatcctgagc
K179R - antisense	gctcaggatgtctctaaggtcagcggagcag
D221H - sense	tcccacttcctccaagcacaattacttaggggg
D221H - antisense	cccccctaagtaattgtgcttggaggaagtggga
P340L - sense	gggacacttgaactgctgtctaccctgtctctc
P340L - antisense	gagagacaggggtagacagcagttcaagtgtccc
T575A - sense	gtcactatggagctctcgcatgtggaagctgcaag
T575A - antisense	cttgcagcttccacatgcgagagctccatagtgac
C619Y - sense	tcttgtcgtcttcggaaatattatgaagcagggatgac
C619Y - antisense	gtcatccctgcttcataatatttccgaagacgacaaga
Q670R - sense	attgaaggctatgaatgtcggcccatctttctgaatgtc
Q670R - antisense	gacattcagaaagatgggccgacattcatagccttcaat
I672T - sense	ctatgaatgtcagcccacctttctgaatgtcctgg
I672T - antisense	ccaggacattcagaaaggtgggctgacattcatag
L701H - sense	ctcctttgcagccttgcactctagcctcaatgaac
L701H - antisense	gttcattgaggctagagtgcaaggctgcaaaggag
V715M - sense	gagacagcttgtacacatggtcaagtgggccaa
V715M - antisense	ttggcccacttgaccatgtgtacaagctgtctc
R726H - sense	ccttgcctggcttccacaacttacacgtgga
R726H - antisense	tccacgtgtaagttgtggaagccaggcaagg
R726L - sense	ccttgcctggcttcctcaacttacacgtgga
R726L - antisense	tccacgtgtaagttgaggaagccaggcaagg
V730M - sense	cttccgcaacttacacatggacgaccagatggc
V730M - antisense	gccatctggtcgtccatgtgtaagttgcggaag
W741L - sense	gtcattcagtactccttgatgggggctcatggtg
W741L - antisense	caccatgagcccccatcaaggagtactgaatgac
M749I - sense	gctcatggtgtttgccataggctggcgatc
M749I - antisense	gatcgccagcctatggcaaacaccatgagc
A748T - sense	gatggggctcatggtgtttaccatgggctg
A748T - antisense	cagcccatggtaaacaccatgagccccatc
E872Q - sense	cgtgcagcctattgcgagacagctgcatca
E872Q - antisense	tgatgcagctgtctcgcaataggctgcacg
H874Y - sense	cctattgcgagagagctgtatcagttcacttttgacc
H874Y - antisense	ggtcaaaagtgaactgatacagctctctcgcaatagg
T877S - sense	gagagctgcatcagttctcttttgacctgctaatc
T877S - antisense	gattagcaggtcaaaagagaactgatgcagctctc
M886I - sense	acctgctaatcaagtcacacatagtgagcgtggac
M886I - antisense	gtccacgctcactatgtgtgacttgattagcaggt

Table 2. Primers for W741C Proof of Concept Screen

Synonymous Mutagenesis	Sense Primers
W741C-S1	acagcttgtacacgtcgtcaagtgggccaag
W741C-S2	acagcttgtacacgtcgtgaagtgggccaag
W741C-S3	taccgcatgcacaagtcgcggatgtacagccag
W741C-S4	taccgcatgcacaagtcgcgcatgtacagccag
Quantitative PCR primers	
pWZL-AR control- forward	gtcccctacatcgtgacctg
pWZL-AR control -reverse	gaggttcaagggggagagac
pWZL-AR.W741C-SM - forward	agagacagcttgtacacgtcgtg
pWZL-AR.W741C-SM - reverse	acacactggctgtacatgcgc

Results

<u>Isolation of a clonal cell line expressing the Pb.PSE.EGFP reporter</u>

We isolated and expanded two single-cell clones with different basal levels of EGFP expression when grown in complete media, and evaluated the response of the EGFP reporter for each clone in response to androgen and antiandrogen treatment. Upon antiandrogen treatment, both clones showed clear downregulation of EGFP expression, as measured by flow cytometry, with maximal reduction after 4 days of exposure. Both clones showed EGFP reduction in response to MDV3100 and bicalutamide treatment (**Figure 10**), and induction of EGFP expression with either DHT or R1881 treatment (data not shown).
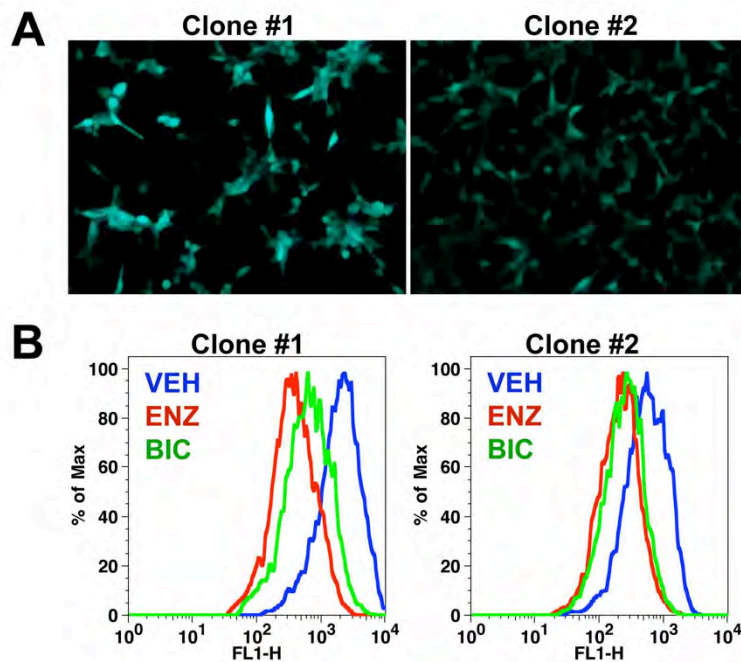
Figure 12. Modulation of EGFP expression in LNCaP-Pb.PSE.EGFP cells

(A) Images showing the basal level of EGFP expression in clones 1 and 2 of LNCaP-Pb.PSE.EGFP cells (images were taken using the same exposure time). (B) Representative flow cytometry histogram plots showing modulation of EGFP expression (FL1-H) by 1µM enzalutamide (ENZ) or 1µM Bicalutamide (BIC).

Although clone#1 appeared to display a greater degree of response to antiandrogen exposure (fold-reduction in EGFP expression), this clone did not proliferate as well as clone #2 and displayed poor attachment. Due to the extremely high basal EGFP expression in clone #1, we were also concerned that there may have been some adverse effects on the viability of these cells due to EGFP toxicity. For these reasons, we chose to use clone #2 for our resistance screen system. From here on, clone #2 will simply be referred to as LNCaP-Pb.PSE.EGFP cells.

EGFP expression is AR-dependent in LNCaP-Pb.PSE.EGFP cells

To demonstrate that our EGFP signal in LNCaP-Pb.PSE.EGFP cells is due to AR expression, we performed siRNA knockdown experiments, with small-interfering RNA (siRNA) against AR or a non-targeting (NT) sequence. We transfected parental LNCaP-Pb.PSE.EGFP reporter cells, as well as reporter cells stably expressing wild-type (WT) AR or AR W741C, with the AR and NT siRNAs. We collected protein lysates from our transfected cells to ensure that we achieved good knockdown of AR protein. We then treated these siRNA transfected cells with different antiandrogens, and performed flow cytometry to measure EGFP expression.

We achieved significant knockdown of AR protein, as measured by western blot. In the case of parental cells and those overexpressing WT-AR, knockdown of the androgen receptor was equivalent to MDV3100 treatment in terms of reduction in EGFP expression (**Figure 13**). We also showed that the induction of EGFP expression in AR W741C expressing cells with bicalutamide treatment was completely reversed by knockdown of AR expression. These data gave us confidence that EGFP expression in our LNCaP-Pb.PSE.EGFP reporter cell line was dependent upon AR.
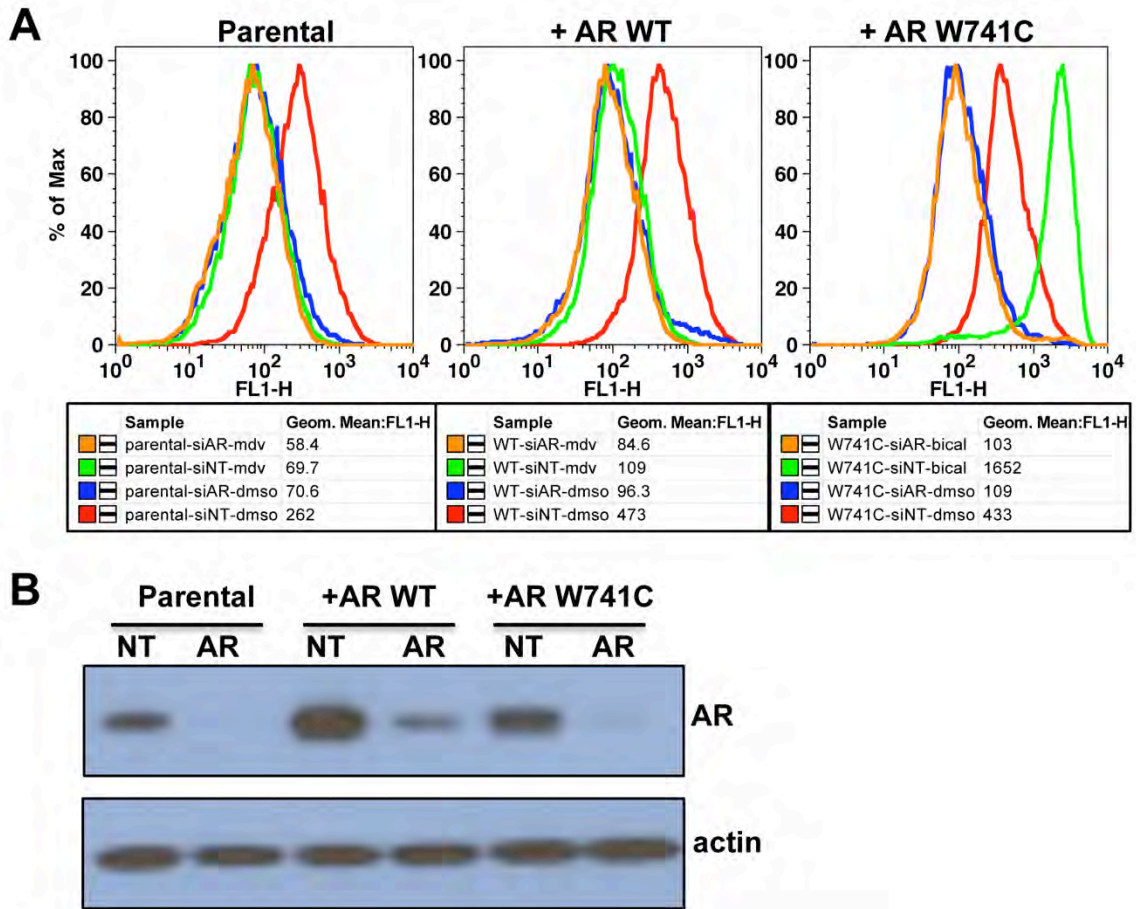
Figure 13. EGFP expression is AR-dependent in LNCaP-Pb.PSE.EGFP cells

LNCaP-Pb.PSE.EGFP cells, or those overepxressing AR WT or AR W741C, were transfected with either a non-targeting siRNA (siNT) or a pooled siRNA against AR (siAR), and then treated with 1µM MDV3100 (mdv) or 1µM bicalutamide (bical). Flow cytometry analysis of EGFP expression is shown in (**A**) and a western blot (**B**) shows that significant knockdown of AR protein was achieved.

EGFP is a reliable readout of AR activity

Because we are using an artificial system to measure AR activity (EGFP reporter), we wanted to be sure that regulation of EGFP expression was comparable to an endogenous AR target gene, PSA. In order to determine if EGFP was a true readout of AR activity, we treated our parental LNCaP-Pb.PSE.EGFP reporter cells, as well as those stably expressing either WT AR or AR-W741C, with either MDV3100 or bicalutamide and collected RNA at various time points. We then performed qRT-PCR to determine relative expression levels of EGFP and PSA transcripts (**Figure 14**). Our data show that in the parental cells, both EGFP and PSA expression are reduced in a similar time-course by both bicalutamide and MDV3100. In reporter cells overexpressing WT AR, bicalutamide has little effect of EGFP or PSA expression, while MDV3100 efficiently lowers both transcripts. And finally in reporter cells overexpressing AR W741C, bicalutamide rapidly induces both EGFP and PSA transcription, while MDV3100 represses transcription of these genes. These data demonstrate that expression of our EGFP reporter is representative of AR activity.
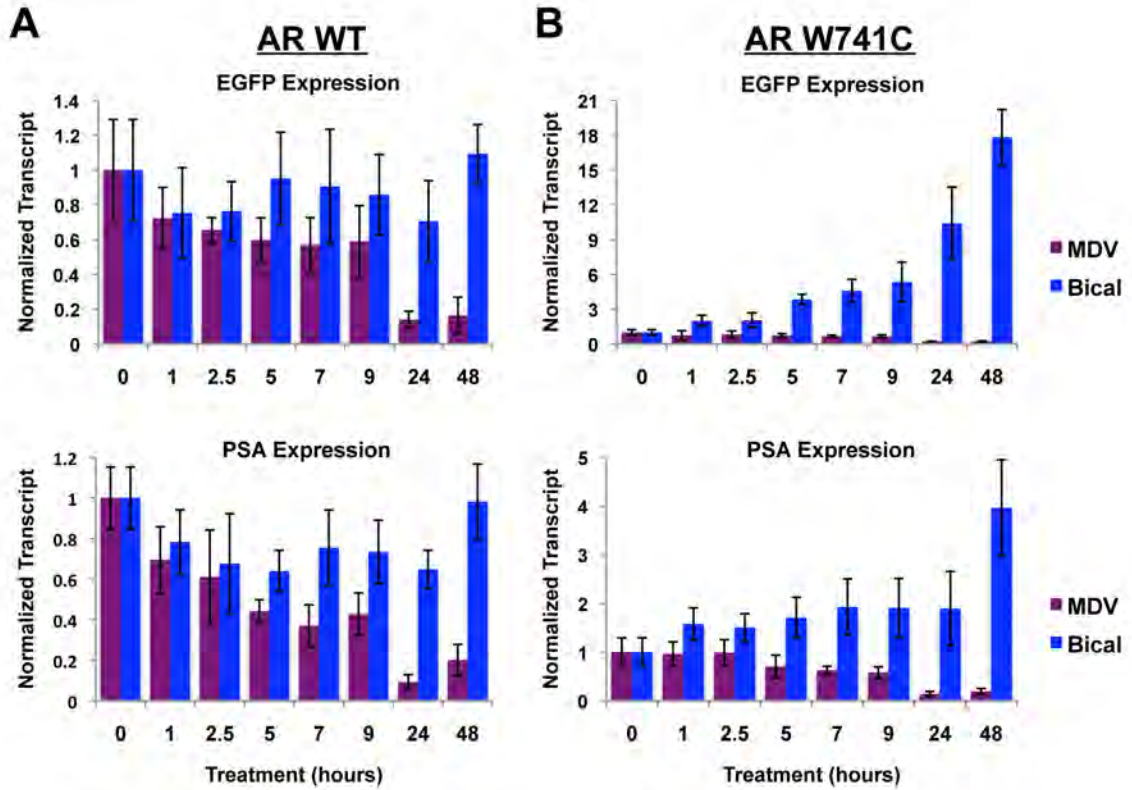
Figure 14. EGFP expression is a reliable readout of AR activity

EGFP expression is regulated in a manner similar to endogenous AR-target gene PSA (KLK3). LNCaP-Pb.PSE.EGFP cells overexpressing either AR WT or AR W741C were treated with 1µM of either Bicalutamide (Bical) or MDV3100 (MDV), RNA collected at the indicated timepoints, and qRT-PCR performed for EGFP and PSA transcript expression.

Clinically Annotated AR Mutations and Variants

A large number of AR mutations have been described in patients with advanced prostate cancer. Although we knew that some of the common AR mutants (T877A, W741C, and H874Y) remain sensitive to enzalutamide, we made a library of other clinically described AR mutations and tested them individually in our LNCaP-Pb.PSE.EGFP cell line reporter system. In addition to single nucleotide changes that result in amino acid substitutions, some result in a premature stop codon and produce truncated AR mutants. There are also several AR splice variants that have recently been described, that have distinct C-terminal extensions, encoded by cryptic exons in the intronic regions between canonical coding exons in AR. These variants lack the ligand-binding domain (LBD) and data suggests that they may exhibit constitutive AR activation.

We used a compiled list of AR mutations annotated in patients with prostate cancer (*36*), and the AR splice variants that commonly occur in castration-resistant disease, AR-V1 and AR-V7, to create our mutant and variant library. To create these point mutants, we again used site-directed mutagenesis (QuikChange, Agilent) in the pWZL-AR retroviral plasmid. We sequenced the entire AR cDNA in this plasmid, to ensure that we only introduced the specific point mutation of interest. The AR variants, AR-V1 and AR-V7, were cloned out of 22Rv1 cells, and subcloned into QCXIH and QCXIN respectively (*44*). We infected our LNCaP-Pb.PSE.EGFP reporter cells with each of these constructs, and selected them with the appropriate antibiotic.

To ensure expression of each mutant and variant AR, we collected lysates of each stable cell line and performed western blot analysis for AR expression. All point mutants expressed very high levels of mutant AR protein (data not shown). For each of these stable cell lines expressing mutant AR, we plated cells and treated them with

either vehicle (DMSO) or 1 µM MDV3100 for four days, and then performed flow cytometry analysis of EGFP expression. All of the point mutants that we evaluated remained sensitive to MDV3100 (**Table 3**). Of the two variants we tested in our reporter-based MDV3100 sensitivity assay, only AR-V7 remained sensitive to MDV3100. Cells stably expressing AR-V1 had much higher basal expression of EGFP, and this was not significantly downregulated by MDV3100 treatment (**Figure 15**). One caveat of these data is that AR-V1 was expressed at significantly higher levels than AR-V7. In addition, endogenous full-length AR is significantly reduced in the AR-V1 expressing cells, suggesting that there may be feedback regulating the total level of AR expression in these cells. This result may also indicate that splice variant AR-V1 is constitutively active, while AR-V7 requires full-length androgen receptor, as our previous work has shown (*44*).
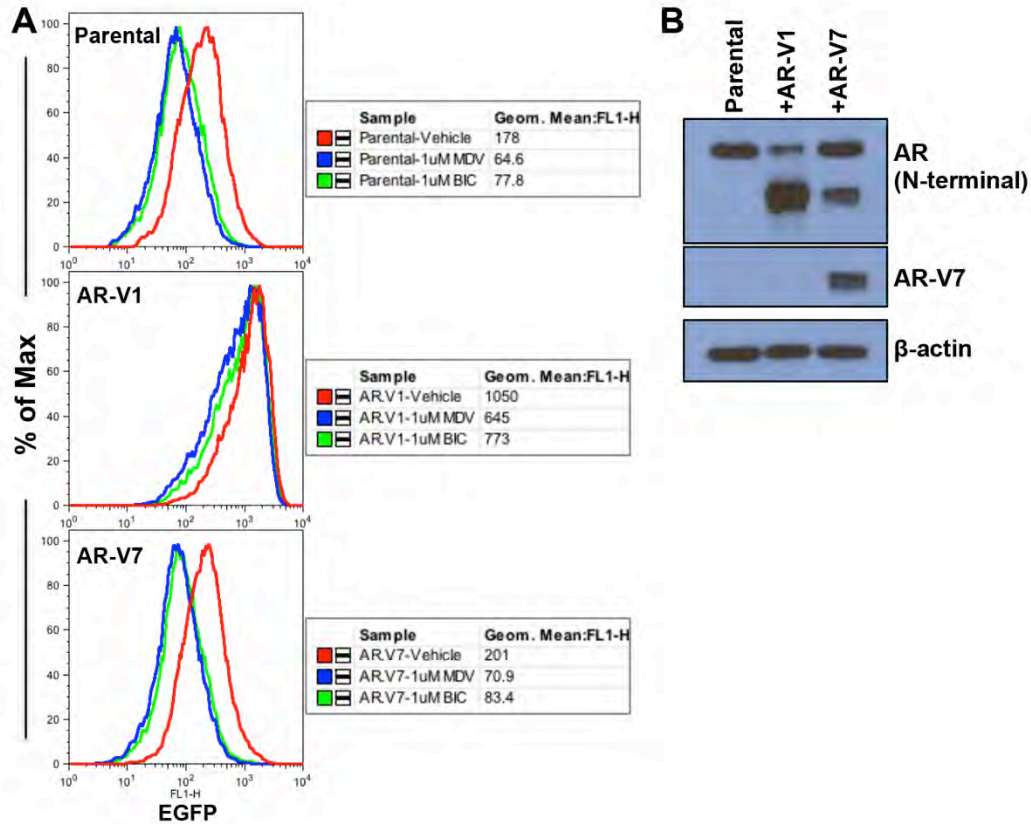
Figure 15. AR-V1 displays constitutive activity and MDV3100 resistance in our EGFP reporter assay

(**A**) LNCaP-Pb.PSE.EGFP cells transduced with either AR-V1 or AR-V7 were treated with either 1µM MDV3100 (MDV) or bicalutamide (BIC) and analyzed by flow cytometry for EGFP expression. The adjacent table shows the geometric-mean fluorescent intensity (MFI) of EGFP expression for each treatment. (**B**) Western blot analysis of lysates from each of these cell lines.

Table 3. MDV3100 Sensitivity of Annotated AR Mutants and Variants

AR Alteration	Location	Functional Properties	MDV3100 Sensitive
G142V	NTD	ITA. MICoA, MICoR	Yes
K179R	NTD	ITA, MN/CI, MICoA	Yes
D221H	NTD	ITA. MICoA, MICoR	Yes
P340L	NTD	DTA, MICoA	Yes
T575A	DBD	DTA	Yes
C619Y	DBD	ANT, DTA, MICoA	Yes
Q670R	Hinge	BLS	Yes
I672T	Hinge	BLS	Yes
L701H	LBD	BLS, TAF, MIH	Yes
V715M	LBD	BLS, weak TAF	Yes
R726H	LBD	BLS	Yes
R726L	LBD	BLS	Yes
V730M	LBD	ND	Yes
W741C	LBD	BLS, TAB	Yes
W741L	LBD	BLS, TAB	Yes
M749I	LBD	BLS, TAB	Yes
A748T	LBD	DTA, MIH	Yes
E872Q	LBD	BLS, MiCoA, MICoR	Yes
H874Y	LBD	BLS, TAF, MICoA	Yes
T877A	LBD	BLS, TAF, MICoA, MICoR	Yes
T877S	LBD	BLS, TAF	Yes
M886I	LBD	MICoA, MICoR	Yes
AR-V1	Hinge truncation	CA	No
AR-V7	Hinge truncation	CA	Yes

ITA, increased transactivation activity; DTA, decreased transactivation activity; MICoA, modified interaction with coactivators; MICoR, modified interaction with corepressors; MN/CI, modified N/C interaction; CA, constitutive activity; BLS, broadened ligand specifity; TAF, transcriptional activation with flutamide; TAB, transcriptional activation with bicalutamide; MIH, modified interaction with Hsp90.

Bicalutamide-AR.W741C proof-of-concept screen

In order to optimize and validate our screening approach, we took advantage of the antiandrogen bicalutamide and one of the clinically described and well-characterized AR mutations that convert it into an AR agonist, W741C. This antiandrogen/ mutation validation screen helped us to determine the sensitivity of detection and optimal growth conditions for our assay, in order to reduce the background noise and find the conditions that would best modulate reporter activity. This also enabled us to determine the best method for DNA extraction, PCR amplification of our AR cDNA, and subsequent sequencing efforts.

We used a PCR based site-directed mutagenesis method (QuikChange, Agilent) to generate the bicalutamide-resistant AR W741C mutant in the retroviral pWZL-AR plasmid. In addition to the single nucleotide change that results in the W741C substitution, we also introduced additional synonymous mutations roughly 100 base pairs on either side of this mutation to facilitate detection and relative quantification of the mutant AR (**Figure 16**). We designated this W741C construct with additional synonymous mutations AR W741C-SM. We then designed real-time quantitative PCR primers, spanning these regions of synonymous mutations, that specifically amplify the AR W741C mutant. We also designed control quantitative PCR primers for the pWZL-AR vector to use as a normalization control.

We infected our LNCaP-Pb.PSE.EGFP reporter cells with either wild-type (WT) AR or AR W741C-SM and made stable cell lines. We first mixed different ratios of each cell line, treated them with vehicle (DMSO) or 1µM bicalutamide and performed flow cytometry to determine the best method to set gates for EGFP positivity. (**Figure 17**)

44
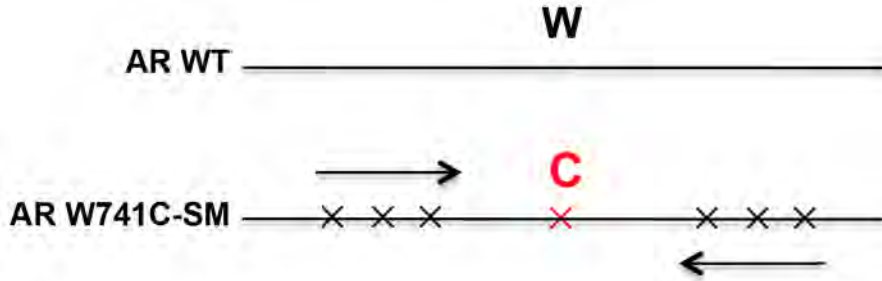
Figure 16. Schematic of method to distinguish AR WT and AR W741C

Several additional synonymous mutations were engineered into the AR W741C expression construct (AR W741C-SM) using site-directed mutagenesis. We then designed qPCR primers that spanned these regions, to specifically detect the mutant but not the wild-type allele.
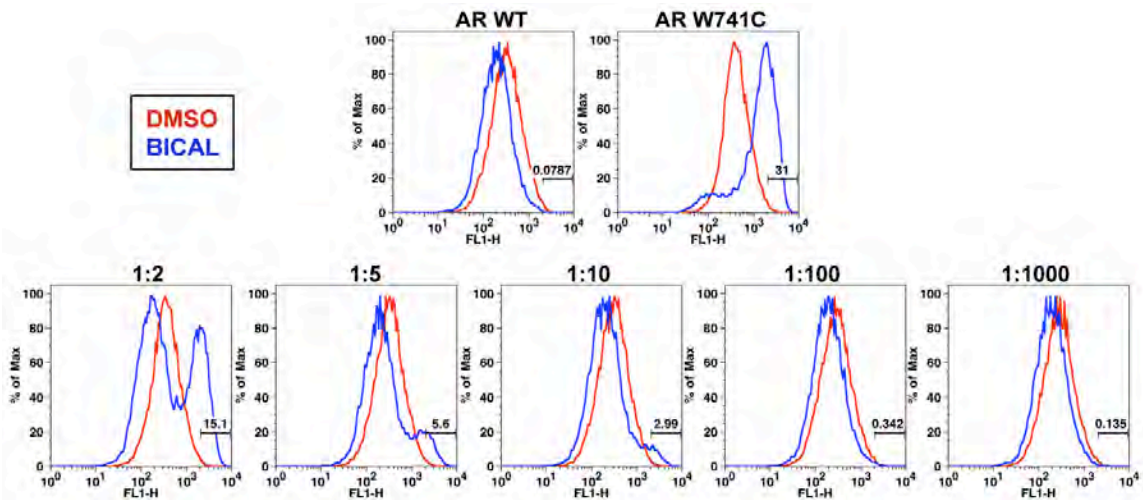
Figure 17. FACS plots of WT, W741C, or mixtures of W741C:WT cells

Cell mixtures were treated with either vehicle (DMSO) or 1µM bicalutamide, and analyzed by flow cytometry for EGFP expression (FL1-H). The gate was set so that in the AR WT expressing cells, less than 0.1% of the cells were EGFP positive.

We collected genomic DNA from each individual cell line and each mix, and performed qPCR to ensure that our primers were selective and quantitative. Titration experiments were then done with WT AR and AR W741C-SM cells combined in ratios of 1:100 and 1:1000 (W741C-SM: WT). About 60 million cells of both of these cell mixtures were treated with 1 μM bicalutamide for 4-6 days, replenishing media and drug every 2-3 days. These cell mixtures were subjected to FACS-sorting, sorting the cells that remained EGFP-positive in the presence of bicalutamide. Gates for EGFP positivity were set based on AR WT and AR W741C cells treated with bicalutamide, selecting the top 0.5% EGFP-positive in the AR WT treated cells, which corresponds to roughly 30% EGFP-positive in the AR W741C-SM treated cells. After the first round of sorting in the 1:100 and 1:1000 ratio mixes, cells were replated and expanded until they reached approximately 80 million cells. At this point, we isolated genomic DNA (gDNA) from a small fraction of the cells, froze down about 20 million cells (2 vials), and repeated the brief bicalutamide exposure (4-6 days) and subsequent FACS-sorting of EGFP-positive cells on the remaining cells. We performed four rounds of this short bicalutamide treatment and EGFP sorting. We then evaluated the fraction of cells that expressed our AR W741C-SM mutant after each sort by performing qPCR. We saw enrichment of the AR W741C-SM expressing cells after each sort, and after the final sort, these cells dominated the final population (**Figure 18**).

46
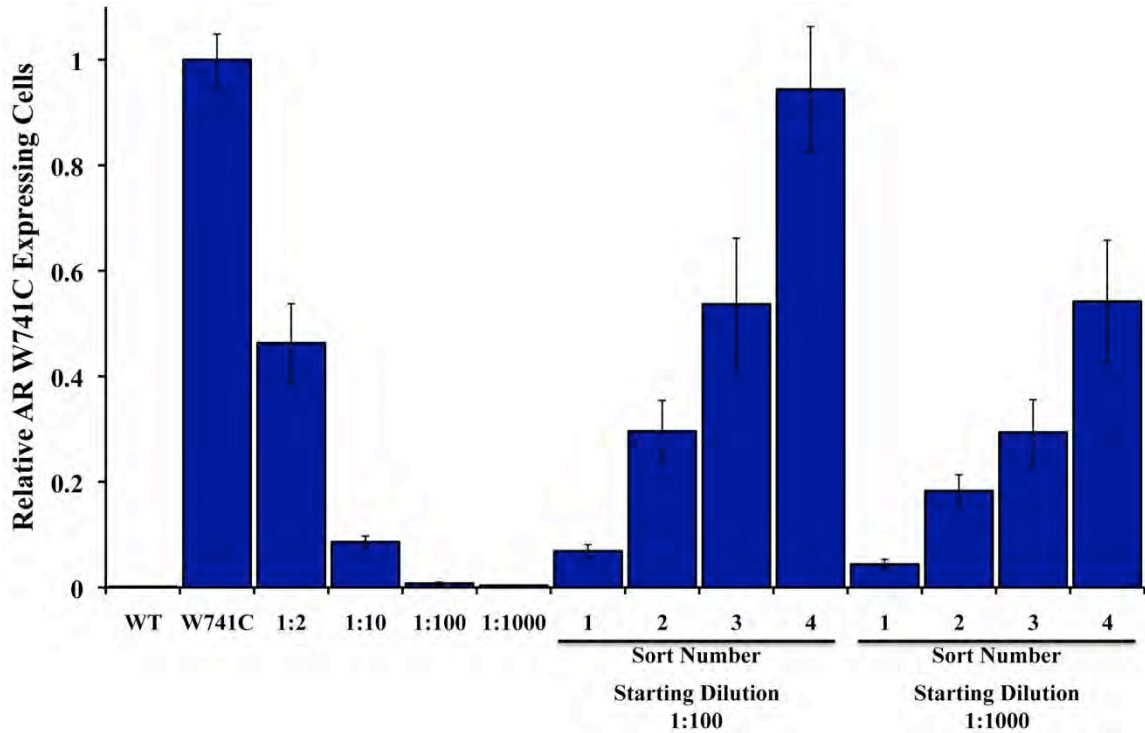
Figure 18. Enrichment of AR W741C mutant expressing cells

Genomic DNA was isolated from LNCaP-Pb.PSE.EGFP cells ectopically expressing either wild-type (WT) AR or mutant AR W741C, or different ratios of mutant-to-WT, and quantitative PCR was performed to test the sensitivity of the W741C-specific primers. With starting ratios of 1:100 and 1:1000 mutant-to-WT, we treated these cell mixtures with 1mM bicalutamide for 4 days, and then FACS-sorted those that maintained/ induced EGFP expression. Sorted cells were expanded and the brief bicalutamide treatment and FACS-sorting was repeated (4 rounds). Genomic DNA was isolated from the sorted cell populations, and quantitative PCR was performed to test for enrichment of the W741C mutant cells.

Discussion

We generated a useful clonal cell line in which expression of EGFP, as measured by flow cytometry analysis and validated with qRT-PCR, was a clear measure of AR activity and responses to antiandrogens or androgens. We tested a large library of known AR mutations in our screening system, and found that none of the point mutations conferred resistance to enzalutamide. We did find that one of the AR splice variants (AR-V1) displays constitutive activation and enzalutamide resistance in our screening assay. These data suggest that known point mutations in AR are not likely to be isolated from our screen, but that truncation mutants are a possibility. The results from our proof-of-concept screen convinced us that our reporter and FACS-based screening approach was selective and efficient, and that if a resistance mutation exists for enzalutamide, analogous to those described for previous antiandrogens, we would be able to isolate it from our screen.

Chapter 3 – Overcoming mutation-based resistance to antiandrogens with rational drug design

Abstract

The second generation antiandrogen enzalutamide was recently approved for patients with castration resistant prostate cancer. Despite its success, the duration of response is often limited. For previous antiandrogens, one mechanism of resistance is mutation of the androgen receptor (AR). To prospectively identify AR mutations that might confer resistance to enzalutamide, we performed a reporter-based mutagenesis screen and identified a novel mutation, F876L, which converted enzalutamide into an AR agonist. Ectopic expression of AR F876L rescued the growth inhibition of enzalutamide treatment. Molecular dynamics simulations performed on antiandrogen-AR complexes suggested a mechanism by which the F876L substitution alleviates antagonism through repositioning of the co-activator recruiting helix 12. This model then provided the rationale for a focused chemical screen which, based on existing antiandrogen scaffolds, identified three novel compounds that effectively antagonized AR F876L (and AR WT) to suppress the growth of prostate cancer cells resistant to enzalutamide.

Introduction

The recent FDA approval of enzalutamide (formerly MDV3100) confirms the continued critical role AR signaling plays in castration-resistant prostate cancer (*46, 54*). In spite of these promising results, patient responses to enzalutamide are varied and often short-lived. Reactivation of AR signaling has been implicated in resistance to previous antiandrogen therapy (*34, 35*), and one well-documented mechanism of reactivation is point mutation in the ligand-binding domain (LBD) of AR (*36*). Many of

these mutations broaden ligand specificity and some confer resistance by converting the AR antagonist into an agonist of the mutant receptor (*38, 39, 55*). Because prior work with targeted therapies that inhibit oncogenic kinases has shown that unbiased mutagenesis screens in preclinical models can identify *a priori* clinically relevant mutations that alter drug activity (*50, 51*), we designed a novel screening method to prospectively identify AR mutations that confer resistance to enzalutamide.

Mutagenesis screens to identify kinase inhibitor-resistant alleles of kinase targets such as BCR-ABL have relied upon cytokine-dependent test cells that become cytokine-independent after introduction of the target kinase.   Cells expressing drug-resistant kinase alleles selectively expand in the presence of drug, allowing rapid identification of mutations that confer drug-resistance. There is no comparable strategy available for antiandrogens because introduction of AR does not confer a comparable growth advantage in AR-negative cells. We instead chose to identify and select cell populations with persistent AR transcriptional activity in the presence of enzalutamide. We reasoned that targeting the biological process of interest (transcriptional activation of a target gene), rather than a distal symptom of resistance to drug (*i.e.* persistent viability, elevated proliferation) might identify resistant clones more quickly. To this end, an AR-regulated EGFP reporter, with a probasin promoter and PSA enhancer elements driving EGFP expression (Pb.PSE.EGFP) (*53*), was used to screen for and enrich cell populations bearing biologically active mutations (**Fig. 19A**).

Results

With our proof-of-concept bicalutamide screen in hand, we next conducted the enzalutamide resistance screen with the Pb.PSE.EGFP reporter and a randomly

mutagenized AR library. After five iterations of enzalutamide exposure and FACS sorting, we identified a population of cells with durable EGFP expression (**Figure 19B**). Moreover, enzalutamide promoted AR transcriptional activity in these cells, reflected by induction of EGFP expression compared to vehicle control (**Figure 19B**). Analysis of endogenous AR target gene expression confirmed that enzalutamide behaved as an agonist in the enriched cell population (**Figure Supplement 1**), and siRNA knockdown of AR showed that these pharmacologically induced changes remained AR-dependent (**Figure Supplement 2**).

To identify AR mutations in these cells, we amplified the exogenously expressed AR cDNA, and Sanger sequenced the PCR product. In two of three replicates, a single dominant point mutation emerged, resulting in the amino acid substitution F876L (**Figure 19C**). Importantly, this mutation clearly enriched throughout the selection process (**Figure Supplement 3**).
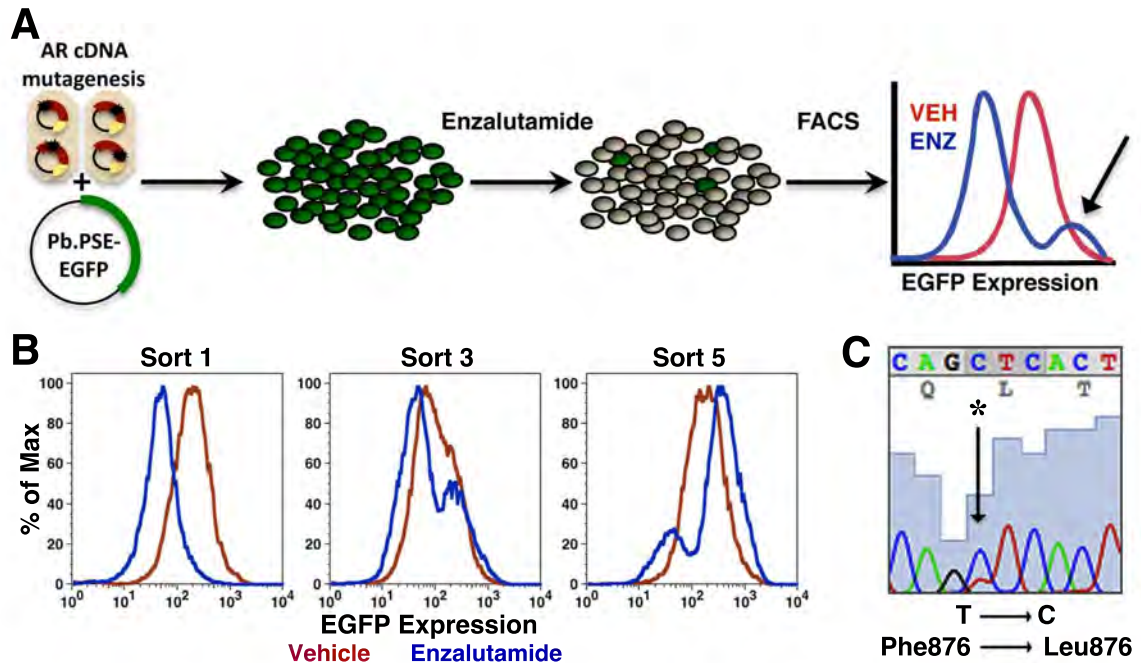
Figure 19. Mutagenesis screen for enzalutamide resistance identifies novel AR mutation

(A) A cartoon of the AR mutagenesis screen developed to identify enzalutamide resistance mutations. Briefly, cells were co-transduced with a randomly mutagenized AR cDNA library (AR*) and EGFP reporter of AR activity (Pb.PSE.EGFP), treated with 1 mM enzalutamide, and EGFP-positive cells were sorted using FACS. AR was PCR amplified and sequenced to identify relevant mutations. **(B)** Representative FACS histograms showing the progressive enrichment of an EGFP-positive subpopulation of LNCaP/AR*/Pb.PSE.EGFP cells post multiple rounds of enzalutamide treatment and cell sorting. **(C)** A Sanger sequencing trace of exon 8 within AR on the exogenous AR allele from LNCaP/AR*/Pb.PSE.EGFP cells after the fifth FACS sort. The position of the mutation is highlighted with an arrow. The alignment was performed against AR WT.

To validate the results of the screen, an AR F876L vector was engineered and transduced into parental LNCaP cells expressing the Pb.PSE.EGFP reporter. Treatment of these cells with enzalutamide resulted in a dose-dependent induction of EGFP expression (**Figure 20A, Figure Supplement 4**). We also introduced AR F876L cDNA into AR-negative CV1 cells along with an AR-dependent luciferase construct, and upon enzalutamide treatment, luciferase activity was induced ~50-fold (**Figure 20B**). These results were comparable to those seen with the previously reported AR mutations T877A and W741C, which confer agonism to hydroxyflutamide and bicalutamide respectively. Moreover, enzalutamide treatment potently induced nuclear localization of AR F876L (**Figure Supplement 5A**), and chromatin immunoprecipitation studies showed that enzalutamide recruited AR F876L to the enhancers of AR target genes (**Figure Supplement 5B**). Consistent with these results, endogenous AR target gene expression was either no longer repressed by enzalutamide (**Figure 20C**, left) or strongly induced by enzalutamide in cells expressing AR F876L (**Figure 20C,** right). A competition assay with $16\beta[^{18}F]$fluoro-5α-DHT (18F-FDHT), to measure relative AR binding affinity (*46*), showed that enzalutamide binds with higher affinity to AR F876L than wild-type AR (**Figure Supplement 6**), similar to what has been shown for hydroxyflutamide and the AR T877A mutant (*56*). Notably, F876L similarly impacted the pharmacology of ARN-509 (*49*), a structurally discrete antiandrogen sharing the bisaryl-thiohydantoin core motif (**Figure 20B, Figure Supplement 7 and 8**).

In vitro growth assays were conducted to examine the consequences of AR F876L expression on enzalutamide sensitivity in prostate cancer cell lines. Although enzalutamide treatment potently inhibits the growth of parental VCaP cells (*46*), overexpression of AR F876L entirely reversed this phenotype (**Figure 20D**). Enzalutamide also rescued the growth of VCaP/AR F876L cells in androgen-depleted

media, similar to that seen with the endogenous androgen DHT (**Figure 20E**). Finally, these results were recapitulated in CWR22Pc cells, another prostate cancer cell line that is sensitive to enzalutamide (**Figure Supplement 9**).

In vivo, LNCaP/AR cells overexpressing either AR WT or F876L were grafted subcutaneously into castrate SCID mice and time to tumor emergence/ progression was determined in the presence or absence of drug. While the growth of wild-type AR tumors was almost completely inhibited by enzalutamide treatment, tumors expressing AR F876L grew rapidly in the presence of enzalutamide, similar to vehicle treated tumors of either genotype (**Figure 20F**).

We next asked whether the F876L mutation spontaneously arises in antiandrogen-sensitive human prostate cancer models after prolonged treatment with enzalutamide or ARN-509. After culturing CWR22Pc cells *in vitro* with enzalutamide for several months, more than 50% of the cells expressed the F876L mutation (**Table 4**). Prolonged culture of these cells with ARN-509 also selected for a small population (~1.3%) expressing AR F876L. *In vivo*, long-term enzalutamide or ARN-509 therapy in mice bearing LNCaP/AR xenograft tumors also resulted in the outgrowth of tumor cell populations expressing AR F876L (**Table 4**). Sequencing revealed that AR F876L predominated in one tumor (~71%), was present at low frequency in four other tumors (~1-2%), and that a distinct amino acid substitution at this residue, F876I, was enriched in one enzalutamide-resistant tumor (**Table 5**).

54
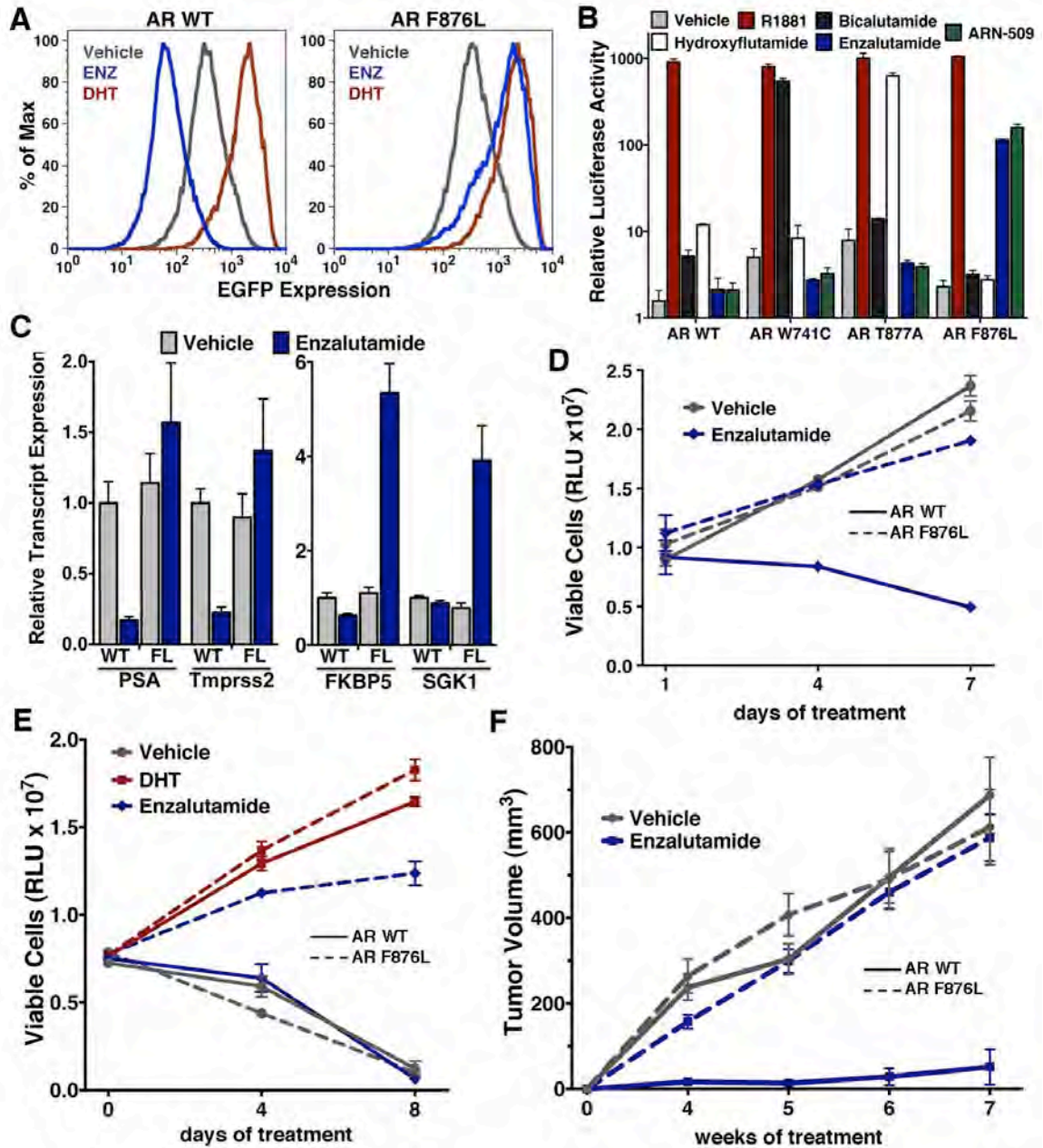
Figure 20. AR F876L mutation converts enzalutamide into an agonist and rescues enzalutamide-induced growth inhibition

(A) A representative FACS histogram shows the induction of AR-dependent EGFP expression by enzalutamide in LNCaP-Pb.PSE.EGFP cells ectopically expressing AR F876L. The magnitude of induction by enzalutamide (10 µM) is comparable to that conferred by the endogenous androgen DHT (1 nM). Enzalutamide treatment of LNCaP-Pb.PSE.EGFP cells ectopically expressing AR WT effectively suppressed EGFP expression. Geometric-mean fluorescence intensity for WT treated cells: vehicle (348), enzalutamide (66.4), DHT (1554); for F876L cells: vehicle (345), enzalutamide (1051), DHT (1699). **(B)** Co-transduction of CV1 cells with an AR-regulated firefly luciferase construct, a constitutive Renilla luciferase construct, and one of the indicated AR

constructs, recapitulates the pharmacology observed in the EGFP reporter system. These cells were treated with vehicle (DMSO), antiandrogens (1 µM), or the synthetic androgen R1881 (1 nM). A dual luciferase assay was conducted on cell lysates, the firefly signal was normalized to the constitutive Renilla activity, and the data are reported as relative light units (RLUs). Notably, the bisaryl-thiohydantoin antiandrogens (enzalutamide and ARN-509) effectively induce AR F876L transcriptional activity, while structurally discrete antiandrogens (hydroxyflutamide and bicalutamide) do not impact AR F876L activity in this assay. As expected, the transcriptional activity of AR W741C or AR T877A was induced by bicalutamide or hydroxyflutamide, respectively. **(C)** Quantitative reverse transcription-polymerase chain reaction analysis of LNCaP/AR F876L cells shows that enzalutamide (1 µM) can induce the expression of canonical AR regulated gene products (*i.e. PSA*, *TMPRSS2*, *SGK1*, and *FKBP5*). Relative gene expression post therapy for LNCaP/AR WT cells is included as positive controls. FL = AR F876L, data are normalized to GAPDH and represented as mean ± SD, n=3. **(D)** Cell proliferation data shows that overexpression of AR F876L in a human prostate cancer cell line sensitive to enzalutamide therapy can rescue cell growth. VCaP cells overexpressing either AR WT (solid lines) or AR F876L (dashed lines) were cultured in media containing full serum, treated with either vehicle (DMSO) or 10 µM enzalutamide, and the viable cell fraction was determined at the indicated time points (data is represented as mean ± SD, *n* = 3). **(E)** Cellular proliferation data shows that enzalutamide also rescues the growth of VCaP cells expressing AR F876L in androgen-depleted media. VCaP cells overexpressing either AR WT (solid lines) or AR F876L (dashed lines) were treated with vehicle (DMSO), 1 nM DHT, or 10 µM enzalutamide, and the viable cell fraction was determined at the indicated time points (mean ± SD, *n* = 3). **(F)** A time to progression study for mice bearing subcutaneous LNCaP/AR-WT (solid lines) or LNCaP/AR-F876L (dashed lines) xenografts further highlights the genotype-dependent pharmacology of enzalutamide. Inoculated animals were treated once daily *via* oral gavage with either vehicle or enzalutamide (30 mg/kg), and tumor size was monitored weekly (11-16 tumors per treatment group). While enzalutamide potently suppressed the growth of LNCaP/AR-WT tumors, LNCaP/AR-F876L tumors exposed to enzalutamide grew with kinetics roughly equivalent to either vehicle treatment arm.

Table 4. Enrichment of F876 mutant cells after Enz/ARN exposure

	F876 Mutation *	Treatment
CWR22PC (in vitro)	52% of all reads	Enzalutamide
	1.3% of all reads	ARN-509
	not detected	Vehicle
LNCaP/AR (in vivo)	3/8 tumors *	Enzalutamide
	3/14 tumors	ARN-509
	0/5 tumors	Vehicle
* 1 tumor F876I, all others F876L		

Table 5. F876 mutation frequency in drug-resistant LNCaP/AR xenograft tumors

Treatment	Frequency	Mutation	endogenous or exogenous locus
Enzalutamide	1.06%	F876L	exogenous
Enzalutamide	1.82%	F876L	exogenous
Enzalutamide	2.19%	F876I	exogenous
ARN-509	1.10%	F876L	exogenous
ARN-509	1.39%	F876L	exogenous
ARN-509	71.23%	F876L	endogenous

To further explore the function of Phe876 as the "gateway" residue governing enzalutamide and ARN-509 pharmacology, we used site-directed mutagenesis to make additional amino acid substitutions at residue 876. A conservative F876Y substitution did not alter the pharmacology of either drug, but aliphatic substitutions structurally similar to F876L, such as F876I (also found in one xenograft with acquired resistance), conferred agonism to both enzalutamide and ARN-509 (**Figure Supplement 10**).

Notably, we observed that bicalutamide did not induce AR F876L transcriptional activity in our luciferase reporter assay, either at low (**Figure 20B**) or high (**Figure Supplement 10**) concentrations, suggesting that it retains weak antagonist activity against this mutant. We conducted EGFP reporter assays to determine if AR F876L transcriptional activity is inhibited by bicalutamide, and found that while at low doses it is an effective inhibitor of AR F876L, it loses potency at higher concentrations (**Figure Supplement 11**). We also observed only minimal growth inhibition in CWR22Pc cells expressing AR F876L with bicalutamide treatment (**Figure Supplement 9**). These data, along with the knowledge that AR overexpression is a common resistance mechanism in patients with CRPC (*34*) and confers partial agonism on bicalutamide (*35*), suggest that bicalutamide is not a viable treatment option for patients who fail on enzalutamide due to AR F876L mutation.

That F876L so dramatically impacted the pharmacology of enzalutamide and ARN-509 suggested that a clear structural change in the drug-receptor complex might be occurring. This consideration prompted us to investigate the structural basis of this antagonism-to-agonism conversion. Because a crystal structure depicting AR bound to an antagonist does not yet exist, we performed structural modeling using ligand docking

and molecular dynamics (MD) simulations (*57, 58*). In designing the study, we noted that both enzalutamide and ARN-509 share identical A rings with bicalutamide (**Figure 21A**) and its derivative S1 that were respectively co-crystallized with the LBD of AR W741L and AR WT in agonist conformations (PDB ID 1Z95 and 2AXA) (*17, 18*). 2AXA was chosen as a structural template as it bears fewer amino-acid substitutions compared to 1Z95. After initial quantum-mechanical geometry optimization of the small molecules, each was independently docked into AR WT or AR F876L with the mutually-shared A ring overlaid with that of S1, whereupon 10-ns explicit-solvent MD simulations were performed.

The docked enzalutamide and ARN-509 molecules demonstrated strikingly different interaction patterns with AR compared to bicalutamide (**Figure 21B** and **21C**). Notably, the thiohydantoin B-ring prevents the compound from accessing the "H12 pocket" occupied by bicalutamide. Instead, the conformationally-restricted thiohydantoin forces the C-ring to bind a region near the C terminus of helix 11 and the loop connecting helices 11 and 12, that we termed the "H11 pocket". As seen in the MD simulations using the WT receptor with enzalutamide and ARN-509 (**Figure 21D** and **21E** (in red)**, Figure Supplement 12**), accommodation of the C-ring in this region is coupled to significant conformational rearrangements of residues on H11 and the H11-H12 connecting loop that prevents H12 from adopting the agonist conformation required for efficient co-activator recruitment. To investigate how the F876L mutation might alleviate antagonism, we performed similar MD simulations using the F876L receptor (**Figure 21D** and **21E** (in cyan), **Figure Supplement 12**). For WT receptors in complex with enzalutamide and ARN-509, the average RMSDs to the crystal agonist conformation for the helix 11 terminus (residues 875-882) were measured at 2.24 Å and 1.94 Å respectively, and those for the helix 12 terminus (residues 893-900) were 1.81 Å

and 2.08 Å respectively. For the F876L mutants, in comparison, the average RMSDs for helix 11 were somewhat lower at 1.01 Å and 1.70 Å for enzalutamide and ARN-509 respectively, and those for helix 12 went down to 1.37 Å for both ligands. The results demonstrate that despite inducing similar dislocations in the H11 pocket the mutation allows the receptor to reposition H12 in a more agonist-like conformation that is compatible with co-activator recruitment (**Figure 21D** and **21E, Figure Supplement 12**). A close look in the H11 pocket (**Figure Supplement 13**) indicated the following: (1) F876 in AR WT likely interacts with the C ring end of enzalutamide or ARN-509 through favorable pi stacking or van der Waals contacts, and (2) the loss of such favorable contacts upon F876L mutation concurrently affects the conformational choices of helices 11 and 12, which interact through both bonded and non-bonded forces. Importantly, these structural modeling results are consistent with the differential resistance profiles for enzalutamide and bicalutamide involving residues 741 and 876 respectively (**Figure 20B**).

Another notable insight from these simulations was that the substituent on the 4 position of the B ring (*i.e.* the geminal (gem)-dimethyl group on enzalutamide, the spiro-cyclobutyl ring on ARN-509, **Figure 22A**) was predicted to lie in close proximity to residues on H12 of the mutant receptor (**Figure 21D** and **21E**). Moreover, the steric girth of the substituent appeared to impact the positioning of H12, as the bulkier spiro-cyclobutyl moiety on ARN-509 elicited greater H12 displacements in AR WT than did enzalutamide's gem-dimethyl group (**Figure 21E**).
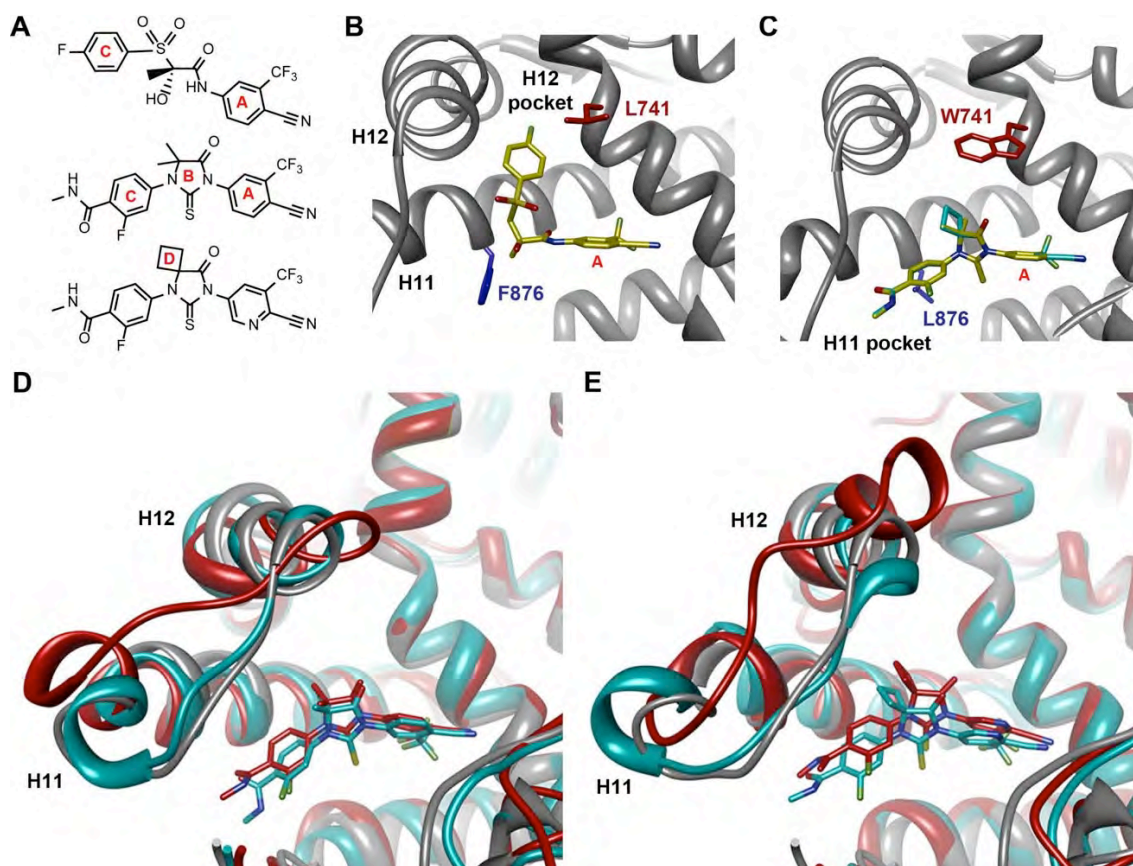
Figure 21. Molecular dynamics simulations predict a novel binding mode for bisaryl-thiohydantoin antiandrogens and the basis for agonism toward AR F876L

(A) Structures of the antiandrogens bicalutamide (top), enzalutamide (middle), and ARN-509 (bottom) oriented to highlight the common and discrete regions of the molecules. The A-D annotation of the rings is indicated. **(B)** A magnified view of the co-crystal structure of AR W741L (grey) and bicalutamide (gold) shows the antiandrogen's spatial relationship to the H11 and H12 pockets and residue F876 (blue). In this agonist conformation, the C ring of bicalutamide does not interact with F876. **(C)** A magnified view of the initial-docked models of enzalutamide (gold) and ARN-509 (cyan) calculated using coordinates from 2AXA in which residue 741 is a tryptophan.   The model suggests that the loss of torsional freedom imposed by the thiohydantoin B ring imposes conformational restrictions on the antagonists that force the C-ring towards F876 and the "H11 pocket". **(D)** The lowest energy 10 ns MD models for enzalutamide with AR WT (red) and AR F876L (cyan) overlaid on 1Z95 (grey – agonist reference structure). The F876L mutation allows for cooperative changes in neighboring residues which, when bound to enzalutamide, enable H12 to adopt a more agonist-like conformation. **(E)** An analogous view of the lowest energy 10 ns MD models for ARN-509 with AR WT (red) and AR F876L (cyan) overlaid on 1Z95 (grey) shows a similar effect for F876L on the positioning of H11 and H12. These simulations also point to the comparatively larger dislocation in H12 by ARN-509 in AR WT, presumably owing to favorable steric interactions between the spiro-cyclobutyl ring and H12.

To restore the positioning of H12 into the antagonist conformation for AR F876L, we designed and synthesized a series of analogues bearing saturated hydrocarbon spirocycles of incrementally greater size and complexity on the B ring of the enzalutamide scaffold (DR100-103, **Figure 22A**). We defined these ring extensions on the B ring as the D ring (**Figure 21A**). The merit of this approach was also supported by prior medicinal chemistry, which had shown that discrete bisaryl-thiohydantoin compounds bearing similar D rings, were effective antagonists of AR WT (*59*). In this regard, we were optimistic that, minimally, the larger inhibitors we designed should be tolerated within the ligand-binding pocket.

Consistent with this precedent, the DR100-103 series inhibited the transcriptional activity of AR WT in the EGFP reporter assay (**Figure 22A**, **Figure Supplement 14**). Whereas DR100-102 behaved as strong agonists for AR F876L (**Figure Supplement 14A**), (±)-DR103 potently inhibited the mutant receptor and antagonized DHT induction (**Figure Supplement 14B** and **15**). We also found that (±)-DR103 was a more potent inhibitor of AR F876L than AR WT (**Figure Supplement 16)** a phenomenon we're currently working to understand.

This striking structure-activity relationship prompted us to empirically investigate the significance of the position of the gem-dimethyl group on the D ring of (±)-DR103. Remarkably, a compound with the gem-dimethyl group on the 4 (rather than 3/5) position of the D ring (DR104) was a modest agonist of AR F876L (albeit an antagonist of AR WT). Moreover, a compound with gem-dimethyl groups at the 3 and 5 positions of the D ring (DR105) inhibited AR F876L (and AR WT) (**Figure Supplement 14C**), further underscoring the biological importance of the steric interactions brought about by these moieties in the context of the mutant receptor. Encouragingly, transplanting the D ring

from (±)-DR103 onto the ARN-509 scaffold [(±)-DR106] also resulted in AR F876L inhibition (**Figure Supplement 14B**). We interpret this result to be supportive of the model advanced by the prior MD simulations, as the F876L substitution appeared to impact the ability of enzalutamide and ARN-509 to induce H12 conformational choices in a roughly equivalent manner. Finally, to underscore the importance of the steric interactions conferred by the D ring, we synthesized DR107, a compound built on the enzalutamide scaffold bearing only hydrogen atoms at position 4 on the B ring. This molecule was an agonist both for AR WT and AR F876L (**Figure Supplement 14C**), pointing directly to the pharmacological significance of interactions between H12 and the substituent at the 4 position of the B ring.

In line with this pharmacology, (±)-DR103 inhibited the growth of prostate cancer cell lines expressing both the WT and mutant receptor (**Figure 22B, Figure Supplement 17**). (±)-DR103 also inhibited endogenous AR signaling and induced PARP cleavage (**Figure Supplement 18**). DR101, a close structural analogue that behaved as an agonist for AR F876L, did not inhibit cell growth at equivalent doses (**Figure 22B**). Finally, the dose of (±)-DR103 required to observe antiproliferative effects (10 μM) did not impact the growth of DU145 (an AR null human prostate cancer cell line), supporting the specificity of the antiandrogen (**Figure Supplement 19**).

Structural modeling studies for (±)-DR103 reinforced our pharmacological model for AR antagonism by bisaryl-thiohydantoins. Unlike the results for enzalutamide and ARN-509, MD simulations using (*S*)-DR103 suggested that an agonist-like conformation of H12 cannot be achieved for either WT or mutant AR (**Figure 22C, Figure Supplement 20**). The modeling study instead showed that the D ring on (*S*)-DR103 was capable of directly displacing the N-terminal residues of H12. A magnified view of

63

the H12 pocket (**Figure Supplement 21**) shows that (*S*)-DR103 occupies a region in the H12 pocket that neither enzalutamide nor ARN-509 can access, thus imposing antagonist-like dislocation of helix 12. Whereas in the H11 pocket (**Figure Supplement 21**), (*S*)-DR103 did not show a significant difference in binding with residue L876, compared to either enzalutamide or ARN-509, which suggests that the restored antagonism was not achieved by simply regaining interactions at the mutation site in AR. Similar MD simulations for the complex of AR F876L and (*R*)-DR103 showed a slightly less pronounced H12 dislocation (**Figure Supplement 20)**, suggesting that the two enantiomers might cause different levels of antagonism.
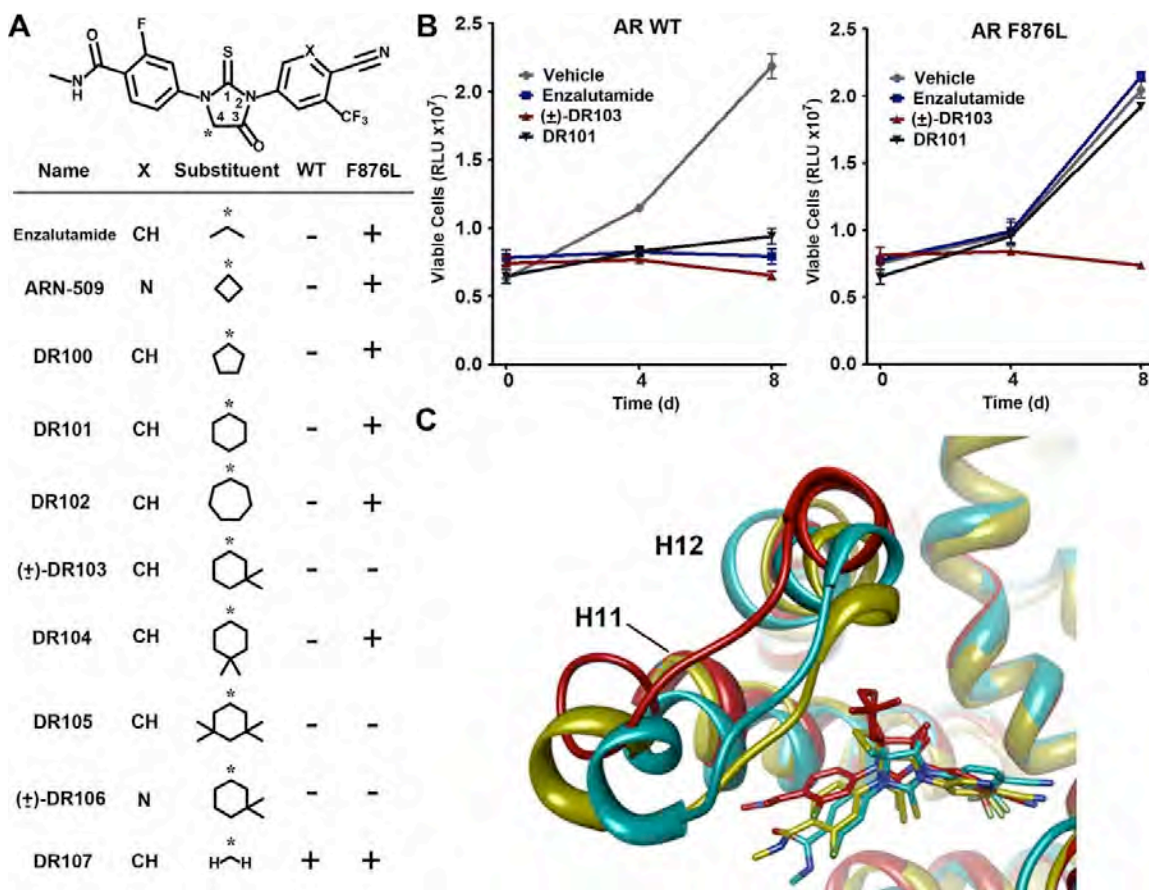
Figure 22. A focused chemical screen identifies novel antagonists of AR F876L

(A) A tabular summary of the bioactivity of the novel antiandrogens in the LNCaP/AR/Pb.PSE.EGFP cell-based assay shows the importance of a carefully designed D ring for competent inhibition of AR F876L. Antagonism is indicated with a "–" symbol, and agonism is indicated with a "**+**" sign. The asterisk is situated over the shared carbon atom in the 4-position that joins the bisaryl-thiohydantoin scaffold to the respective "substituent". The source data is outlined in **Figure 4 – figure supplement 1.** **(B)** A proliferation assay for VCaP prostate cancer cells overexpressing either wild-type AR (left) or AR F876L (right) shows that (±)-DR103 effectively inhibits the growth of both models, while enzalutamide and the close structural analogue DR101 only inhibit the growth of VCaP/AR WT. Data are reported as mean ± SD, *n* = 3. **(C)** A view of the lowest energy conformations of enzalutamide (cyan), ARN-509 (gold), and (*S*)-DR103 (red) in complex with AR F876L highlights the greater dislocation of H12 and the loop between H11, H12 uniquely conferred by (*S*)-DR103. The color scheme invoked for AR F876L matches the respective antiandrogen.

Discussion

As is evident from prior work with ABL kinase inhibitors for chronic myeloid leukemia and antivirals for HIV and hepatitis (*26, 60*), understanding mechanisms of drug resistance is a crucial first step in developing strategies to prevent or overcome it. With its recent approval, the case for defining mechanisms that overcome enzalutamide therapy is timely and compelling. Because AR mutations are a cause of clinical resistance to antiandrogens (flutamide and bicalutamide) (*39, 55*), and prior work has shown that clinically relevant mutations can be discovered from screening platforms in preclinical models, we prospectively searched for such mutations in the context of enzalutamide using a novel saturation mutagenesis approach. This screen revealed that mutation of Phe 876 to Leu converts enzalutamide and ARN-509 into AR agonists and confers resistance to drug-induced growth inhibition *in vitro* and *in vivo*. Importantly, this mutation was also recovered "spontaneously" from enzalutamide-sensitive cell line and xenografts models treated with prolonged enzalutamide therapy.

That prostate cancer can spontaneously acquire gain-of-function mutations in AR (rather than acquiring mutations that simply preclude inhibitor binding) underscores the special challenge in pharmacologically overcoming this mechanism of resistance. By borrowing insight from studies of the progesterone receptor, showing that a single amino acid can determine sensitivity to RU486, and structural analyses of the estrogen receptor (*19, 61*), our attention was immediately directed to establishing and testing a structural model of the AR/ enzalutamide complex to explain enzalutamide's curious pharmacology in the context of AR F876L. Using MD simulations, a novel binding mode for the drug was identified, which provided a compelling explanation for how antagonism is retained against the bicalutamide-resistant Trp 741 mutation. More importantly, the

MD simulations argued that an altered spatial orientation of enzalutamide within the AR LBD might explain the onset of agonism, as the F876L mutation appeared to reposition the drug to eliminate steric clashes that promoted H12 dislocation in AR WT. Reassuringly, several larger compounds that the MD simulations predicted could restore H12 dislocation (the "D ring" series) effectively antagonized AR F876L.

Because the discovery of this mutation and its companion pharmacology provided the basis for our structural model, it is difficult to envision how the importance of the D ring might have otherwise emerged from prior (and ongoing) chemical screening efforts. Among the ~100 bisaryl thiohydantoins published to date, several compounds bearing structurally similar moieties to our bioactive series were essentially indistinguishable from enzalutamide, ARN-509, or other lead agents in conventional cell-based assays. Our own focused chemical screen further speaks to the unusually complicated pharmacobiology of AR F876L, as subtle changes in the position of geminal dimethyl moieties on DR103-5 radically impacted the respective bioactivity of the drugs.

Our success predicting the pharmacology of candidate inhibitors with MD simulations argues for a novel workflow by which *in silico* screening could guide future antiandrogen drug discovery (pending a co-crystal structure of an AR/antagonist complex). The data indicating that ~50% of patients fail to respond to enzalutamide has somewhat overshadowed the importance of the discovery of the bisarylthiohydantoin chemotype for AR, and the ongoing enthusiasm for developing better drugs based on this motif is most visibly reflected by the clinical trial with ARN-509. In this regard, our structural model provides a powerful tool to further refine the chemotype into drug candidates with improved properties.

Collectively, these findings demonstrate the importance of coordinated mutagenesis, structural modeling, and medicinal chemistry studies in designing drugs against an important cancer target for which appropriate drug affinity and binding conformation are mutually indispensible for competent inhibition. We are optimistic that discovery of the AR F876L mutation will facilitate solution of the enzalutamide/AR complex by X-ray crystallography. As for the potential clinical impact of *a priori* discovery of drug-resistance mutations to novel cancer drugs, our prior experience with the ABL kinase inhibitor dasatinib in chronic myeloid leukemia serves as an example. Within two years of reporting dasatinib-resistant mutations in BCR-ABL in a preclinical model, analogous mutations were recovered from dasatinib-resistant chronic myeloid leukemia patients (*51, 52*). We hope this report will guide a similar search for AR mutations in prostate cancer patients who develop clinical resistance to enzalutamide. Routine rebiopsy of tumor tissue in men with castration resistance prostate cancer is challenging due to the high frequency of osteoblastic bone lesions consisting primarily of stromal tissue. Blood based assays for AR mutation detection may be a compelling alternative, based on recent success in detection of tumor-specific mutations in circulating plasma DNA from patients with other cancers (*62, 63*).

Materials & Methods

<u>Materials and Cell Lines</u>

Fetal bovine serum (FBS) and charcoal-stripped, dextran-treated fetal bovine serum (CSS) were purchased from Omega Scientific. Bicalutamide (Investigational Drug Pharmacy), hydroxyflutamide (LKT Labs), DHT (Sigma), and R1881 (Perkin Elmer) were commercially obtained; all other ligands were synthesized at MSKCC. Serial dilutions of all drugs were made using DMSO. Antibodies used for immunoblot assays were β-actin (AC-15, Sigma) PARP (#9541; Cell Signaling Technology), FKBP5 (IHC-00289, Bethyl), β-tubulin (D-10) and androgen receptor (N-20) (both from Santa Cruz Biotechnology). Protein lysates were prepared in M-PER protein extraction reagent (Pierce). The chromatin immunoprecipitation assay was conducted using a kit (Upstate). Nontarget and human AR siRNA pools were from the ON-TARGETplus collection (Dharmacon). LNCaP/AR cells were previously described (*46*), and CWR22Pc cells (*64*) were provided by Marja T. Nevalainen (Thomas Jefferson University, Philadelphia). All other cell lines were obtained from ATCC. All LNCaP and CWR22Pc derived cells were maintained in RPMI +10% FBS. All CV1 and VCaP derived cell lines were maintained in DMEM +10% FBS. All oligos were ordered from Operon Biotechnologies.

For the analogue syntheses, all chemicals were acquired from Sigma-Aldrich at highest purity available and were used without further purification. Chromatography was done using Merck grade silica gel 60 and reactions were monitored by LC-MS (Waters Autopure, and Acquity systems in reverse phase and with mass, evaporative light scattering and diode array detections). Proton NMR experiments were executed on Bruker Advance DRX running at 500 MHz, and fluorine NMR was run on the same

machine but at 235 MHz. Chemical shifts are reported in parts per million (ppm) relative to tetramethylsilane.

Plasmids & Cell Transduction

The human AR cDNA plasmid, pWZL-AR, was provided by William Hahn (Dana-Farber Cancer Institute, Boston). All mutant AR constructs were generated in pWZL-AR with the QuikChange II XL site directed mutagenesis kit (Agilent) and primers designed using Agilent's online QuikChange Primer Design tool. Stable cell lines were generated by pantropic retroviral infection (Clontech) and selected with blasticidin (Invivogen). LNCaP cells were infected with the lentiviral AR-regulated EGFP reporter construct, Pb.PSE.EGFP (*53*), provided by Claude Bignon (EFS Alpes Méditerranée, Marseilles, France). We then single-cell cloned the LNCaP-Pb.PSE.EGFP cells to reduce the heterogeneity in EGFP expression, and isolated a clone that had a high level of EGFP expression, which was modulated effectively by antiandrogens and AR agonists. This clone was used for all flow cytometry assays and for the FACS-based resistance screens.

Flow Cytometry Analysis and FACS-sorting

LNCaP-Pb.PSE.EGFP cells for flow cytometric analysis were treated with antiandrogens (1μM or 10μM) for 4-6 days, changing media and drug every 2-3 days. Cells were collected using Accumax dissociation solution (Innovative Cell Technologies) and dead cells were counterstained using TO-PRO3-Iodide (Invitrogen). EGFP expression was measured using the BD-FACSCalibur flow cytometer using the 488nm laser and 530/30 bandpass filter to detect EGFP expression, and the 633nm laser and 661/16 bandpass filter to detect TO-PRO3-Iodide labeled dead cells. For each sample, 2-5 x 10^4 cell events were collected and analysis was done using FlowJo software. FACS-sorting of

LNCaP-Pb.PSE.EGFP cells was performed on a BD FACSVantage cell sorter. Dead cells were counterstained with DAPI (Invitrogen). EGFP expression was detected using the 488nm laser and 530/30 bandpass filter, and DAPI-labeled dead cells were detected using the 355nm laser and 450/50 bandpass filter.

FACS-based Enzalutamide Resistance Screen

Our randomly mutagenized AR cDNA library was generated as follows: we transformed the DNA-repair-deficient *Escherichia coli* strain XL-1 Red (Agilent) with the pWZL-AR plasmid and plated them on ampicillin-agar bacterial plates. After a 36-hour incubation, colonies were collected by scraping, and plasmid DNA was purified using a plasmid MAXI kit (Qiagen). This mutagenized AR plasmid stock was used to make pantropic retrovirus (Clontech) and infect LNCaP-Pb.PSE.EGFP cells at a MOI<1. Cells were selected for stable expression of our mutant pWZL-AR library using the blasticidin resistance cassette. Mutant library cells were cultured in 1µM enzalutamide for 4-6 days, collected with Accumax and resuspended in Accumax containing 0.5% BSA and 10mM HEPES. Cells that remained EGFP positive in the presence of enzalutamide were then FACS-sorted. Gates for EGFP positivity were set using LNCaP-Pb.PSE.EGFP cells transduced with the wild-type AR cDNA, treated with vehicle or 1µM enzalutamide. Sorted cells were expanded in culture (without drug) until they reached approximately 60 million cells, we then isolated gDNA and froze down a small fraction, and the brief enzalutamide treatment and sorting was repeated on the remainder. We performed the screen in triplicate, with 5 rounds of FACS and expansion for each replicate.

AR Mutation Detection

Exons 2 through 8 of the exogenously expressed AR cDNA were amplified from genomic DNA isolated from cells after each sort, by high-fidelity PCR (Qiagen, Hotstar)

on a Mastercycler (Eppendorf). The PCR product was subjected to bidirectional Sanger

sequencing, using previously published primers (*44*). Alignments were performed using

SeqMan Pro (DNASTAR) and Sanger traces were analyzed using 4Peaks software.

qRT-PCR

Total RNA was isolated using the QiaShredder kit (Qiagen) for cell lysis and the RNeasy

kit (Qiagen) for RNA purification. We used the High Capacity cDNA Reverse

Transcription Kit (Applied Biosystems) to synthesize cDNA according to the

manufacturer's protocol. Quantitative PCR was done in the Realplex MasterCycler

(Eppendorf) using the Power SYBR Green PCR Mastermix (Applied Biosystems).

Quantitative PCR for each sample was run in triplicate and each reaction contained 1µL

of cDNA in a total volume of 20 µL. PCR quantification was done using the $2^{-\Delta\Delta Ct}$ method

with normalization to GAPDH as described (Applied Biosystems). All primers were used

at a final concentration of 500nM and are listed 5' to 3' in Table X.

Chromatin Immunoprecipitation (ChIP)

LNCaP cells (10^7 cells/condition) were grown in phenol red free RPMI media

supplemented with 10% CSS for 4 days, then treated with DMSO, 10µM antiandrogens,

or 1nM DHT for 4 hours. The cells were cross-linked using 1% paraformaldehyde

(Electron Microscopy Sciences) for 15 minutes, glycine was then added, and samples

centrifuged (4^0 C, 2500rpm, 5 minutes) to stop further crosslinking. ChIP was performed

according to manufacturer's protocols using a ChIP assay kit (Upstate) with an antibody

for AR (PG-21, Upstate). Immunoprecipitated DNA was amplified by quantitative real-

time PCR (ABI Power SYBR Green PCR mix). All primers were used at 500nM and are

listed 5' to 3' in Table X.

Fluorescence Microscopy

LNCaP cells (10^6 cells/well of 6-well plate) were transfected with 2ug AR-EYFP plasmid (from Jeremy Jones and Marc Diamond, UCSF) or AR.F876L-EYFP plasmid (QuikChange II XL site-directed mutagenesis kit) using FUGENE HD (Roche). Six hours after transfection, media was removed and replaced with phenol red free RPMI media supplemented with 10% CSS. The next day cells were split and plated onto poly-lysine coated Nunc Labtek chamber slides in RPMI + 10% CSS containing DMSO, 1µM antiandrogens or 1nM DHT. Twenty-four hours later the cells were counterstained with NucBlue Live Cell Stain Hoechst 33342 (Molecular Probes) fixed with 4% paraformaldehyde, and mounted with a coverslip. Images were taken on a Leica TCS SP5-II Upright confocal microscope (MSKCC Microscopy Core and were analyzed for EYFP (AR) nuclear/ cytoplasmic localization using ImageJ.

AR Luciferase Reporter Assay

CV1 cells ($2x10^6$ cells/10 cm plate) were cotransfected with 50ng of SV40 Renilla Luciferase, 5ug of ARE(4X)-Luciferase, and 10ug of one pWZL-AR expression construct using Lipofectamine 2000 (Invitrogen). Transfection media was removed 4-6 hours later and replaced with phenol red free DMEM containing 10% CSS. The following day each plate was split into 48-well plates, in 10% CSS media, containing the indicated drugs in triplicate. Luciferase activity was assayed 24-48 hours later using Dual-Luciferase Reporter Assay System (Promega).

Ligand Binding Assay

The binding affinity of enzalutamide to AR WT and AR F876L, relative to dihydro-testosterone (DHT), was determined using a competition assay in which increasing

concentrations of cold competitor are added to cells pre-incubated with ^{18}F-FDHT. LNCaP/AR WT or LNCaP/AR F876L cells were cultured in phenol red free RPMI + 10% CSS for 2 days prior to the binding assay. Cells were trypsinized, washed in PBS, and mixed with 20,000 cpm ^{18}F-FDHT and increasing amounts of cold competitor (10 pM to 10 μM), in triplicate. The solutions were shaken on an orbital shaker at ambient temperature for 1 hour, then isolated and washed with ice-cold tris-buffered saline using a Brandel cell harvester (Gaithersburg, MD). Samples were counted using a scintillation counter, and the specific uptake of ^{18}F-FDHT determined. These data were plotted against the concentration of the cold competitor to give sigmoidal displacement curves and IC$_{50}$ values were determined using a one site model and a least squares curve fitting routine (Origin, OriginLab, Northampton, MA) with the R^{2} of the curve fit being >0.99.

Xenograft Experiments

In vivo xenograft experiments were done by subcutaneous injection of 2x10^{6} LNCaP/AR cells ectopically expressing AR WT or AR F876L (100uL in 50% Matrigel (BD Biosciences) and 50% growth media) into the flanks of castrated male SCID mice. Daily gavage treatment (using a formulation of 1% carboxymethyl cellulose, 0.1% Tween-80, 5% DMSO) was initiated on the day of injection. Once tumors were palpable, tumor size was measured weekly in three dimensions (l x w x d) with calipers.   All animal experiments were performed in compliance with the guidelines of the Research Animal Resource Center of the Memorial Sloan-Kettering Cancer Center.

Xenograft experiments in which AR F876 mutations emerged after long-term treatment with second-generation antiandrogens were performed as follows: 2x10^{6} LNCaP/AR cells (*46*) were injected subcutaneously into the flanks of castrated SCID mice.

Treatment with 30mg/kg enzalutamide or ARN-509 was initiated once tumors reached ~300mm^3, resulting in rapid tumor regression. After several months of continual dosing, these tumors regain the ability to grow. Once these "resistant" tumors reached their original volume, the mice were sacrificed, and tumors collected for analysis.

CWR22Pc drug resistant cell lines

CWR22Pc cells were cultured in RPMI + 10%FBS containing 0.1nM DHT and either 10µM enzalutamide or ARN-509. Treatment media was replaced every 4-5 days, and cells were passaged upon reaching confluence. Cell strains were designated as antiandrogen resistant when the time between consecutive passages was reduced to 4-6 days, which is a period of time equivalent to that of untreated CWR22Pc.

Deep Sequencing of AR

Genomic DNA (gDNA) was isolated (PureGene Core Kit A, Qiagen) from resistant CWR22Pc cell lines or LNCaP/AR xenograft tumors. With 20ng of gDNA as template, exon 8 of AR was PCR amplified with Kapa HiFi Ready Mix (Kapa Biosystems). RNA was extracted from LNCaP/AR xenograft tumors, reverse transcribed (High Capacity cDNA Reverse Transcription Kit, Applied Biosystems) and exons 2 through 8 of AR was PCR amplified using 200ng cDNA as template (Qiagen, HotStar).

PCR reactions were cleaned up with AMPure XP (Beckman Coulter Genomics) and pooled reaction yields were quantified using the Qubit fluorometer (Invitrogen). Library preparation was done using Nextera DNA Sample Preparation kit (Illumina) and run on the Illumina MiSeq sequencer using the 2x250 paired-end cycle protocol.

Genomic DNA was aligned to the hg19 build of the human genome using BWA (*65*) with duplicate removal using samtools (*66*) as implemented by Illumina MiSeq Reporter. cDNA FASTQ files were processed with a windowed adaptive trimming tool sickle (https://github.com/najoshi/sickle) using a quality threshold of 32. The reads were then mapped to the human genome build hg19 with TopHat 2 (*67*) using known AR transcripts NM_000044 and NM_001011645. Duplicates were then removed with Picard (http://picard.sourceforge.net). Variant detection was performed using VarScan 2 (*68*) with thresholds of a minimum of 10 supporting variant reads and variant allele frequencies of at least 1%.

Analogue Syntheses

General Strategy

The syntheses were executed according to a general schema, which involves starting from a given ketone and reacting it under Strecker reaction conditions, using sodium cyanide and 4-amino-2-fluoro-N-methylbenzamide.   The resulting cyanamine was then reacted with an aniline or 5-aminopyridine in the present of thiophosgene to give the desired thiohydantoins after acid hydrolysis of intermediate imine.
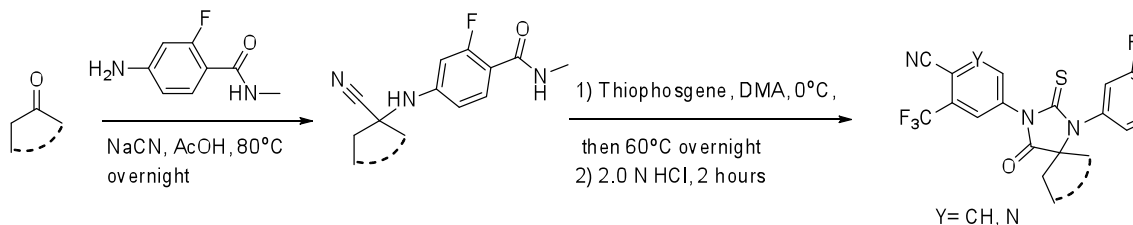

General Synthesis Schema

Below are two general procedures that apply to all molecules described.

Strecker reaction

To a mixture of 4-amino-2-fluoro-N-methylbenzamide (0.3 mmol) and the desired ketone (1.0-2.0 equivalents [eq]) in glacial acetic acid (2 mL) was added NaCN (100 mg, 2.0 mmol, 7.0 eq), and the mixture was heated to 80°C overnight. The solvent was then removed under reduced pressure and the residue was dissolved in water (20 mL), then pH was brought to neutrality with aqueous saturated NaHCO$_3$ solution. Extraction with ethyl acetate (3 x 50 ml), brief drying over Na$_2$SO$_4$ and concentration of the filtrate under reduced pressure and the residue was chromatographed on a short path silica gel column using the gradient hexane/ethyl acetate 2/1 to 1/1.5 (v/v) to yield desired product in more than 85% yield.

Thiohydantoin synthesis

Thiophosgene (5.1 μL, 66 μmol) is added dropwise to a solution of 5-amino-2-cyano-3-trifluoromethylpyridine or 4-amino-2-(trifluoromethyl)benzonitrile (60 μmol) and the given Strecker products above N-methyl-4-(1-cyanocycloalkylamino)-2-fluorobenzamides (60 μmol) in dry DMA (0.6 mL) under Argon at 0°C. After 5 min, the solution is stirred overnight at 60°C. At room temperature, this mixture was then diluted with MeOH (1 mL) and aq. 2.0 N HCl (0.5 mL), then the reaction was brought to reflux for 2 hours. After cooling to ambient temperature, the reaction mixture was poured into ice water (10 mL) and extracted with EtOAc (3 x 20 mL). The organic layer was briefly dried over MgSO$_4$, concentrated and the residue chromatographed on silica gel using the gradient system hexane/ethyl acetate 2/1 to 1.5/1 (v/v) to yield the desired thiohydantoin in up to 90 %.
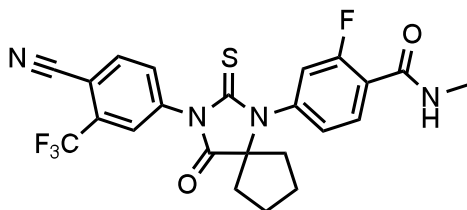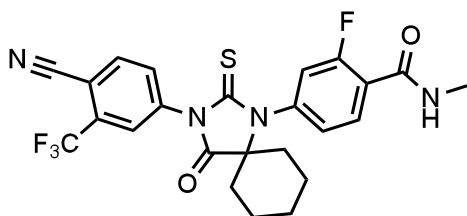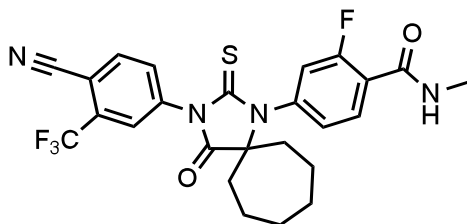
DR100, 4-(3-(4-cyano-3-(trifluoromethyl)phenyl)-4-oxo-2-thioxo-1,3-diazaspiro[4.4]nonan-1-yl)-2-fluoro-N-methylbenzamide

This compound was isolated as an off-white foam.

^{1}HNMR (CDCl$_3$): δ: 8.28 (t, 1 H, J = 8.5 Hz), 7.79 (d, 1 H, J = 8.3 Hz), 7.96 (bs, 1 H), 7.84 (dd, 1 H, J = 8.3 Hz, J = 1.5 Hz), 7.27 (dd, 1 H, J = 8.3 Hz, J = 1.8 Hz), 7.17 (dd, 1 H, J = 11.7 Hz, J = 1.5 Hz), 6.71 (m, 1 H), 3.07 (d, 3 H, J = 4.7 Hz), 2.36 (m, 2 H), 2.16 (m, 2 H), 1.91 (m, 2 H), 1.56 (m, 2 H).

^{19}FNMR (CDCl$_3$) δ: -61.98, -110.64.

LRMS for C$_{23}$H$_{18}$F$_4$N$_4$O$_2$S [M+H]$^+$ found: 491.22; calculated: 491.12

DR101, 4-(3-(4-cyano-3-(trifluoromethyl)phenyl)-4-oxo-2-thioxo-1,3-diazaspiro[4.5]decan-1-yl)-2-fluoro-N-methylbenzamide

The compound was obtained as an off-white foam.

^{1}HNMR (CDCl$_3$): δ: 8.27 (t, 1 H, J = 8.4 Hz), 7.98 (d, 1 H, J = 8.3 Hz), 7.93 (bs, 1 H), 7.82 (dd, 1 H, J = 8.2 Hz, J = 1.6 Hz), 7.19 (dd, 1 H, J = 8.3 Hz, J = 1.8 Hz), 7.08 (dd, 1 H, J = 11.6 Hz, J = 1.6 Hz), 6.70 (m, 1 H), 3.08 (d, 3 H, J = 4.7 Hz), 2.07 (m, 4 H), 1.70 (m, 6 H).

^{19}FNMR (CDCl$_3$) δ: -61.97, -110.92.

LRMS for C$_{24}$H$_{20}$F$_4$N$_4$O$_2$S [M+H]$^+$ found: 505.30; calculated: 505.13

DR102, 4-(3-(4-cyano-3-(trifluoromethyl)phenyl)-4-oxo-2-thioxo-1,3-diazaspiro[4.6]undecan-1-yl)-2-fluoro-N-methylbenzamide

This compound was isolated as off-white solid.

^{1}HNMR (CDCl$_3$): δ: 8.28 (t, 1 H, J = 8.4 Hz), 7.98 (d, 1 H, J = 8.3 Hz), 7.93 (bs, 1 H), 7.82 (dd, 1 H, J = 8.2 Hz, J = 1.6 Hz), 7.24 (dd, 1 H, J = 8.3 Hz, J = 1.6 Hz), 7.14 (dd, 1 H, J = 11.6 Hz, J = 1.5 Hz), 6.72 (m, 1 H), 3.08 (d, 3 H, J = 4.7 Hz), 2.28 (m, 2 H), 2.17 (m, 2 H), 1.81 (m, 2 H), 1.60 (m, 2 H), 1.44 (m, 2 H), 1.32 (m, 2 H).

^{19}FNMR (CDCl$_3$) δ: -61.98, -110.82.

LRMS for C$_{25}$H$_{22}$F$_4$N$_4$O$_2$S [M+H]$^{+}$ found: 519.38; calculated: 519.15;
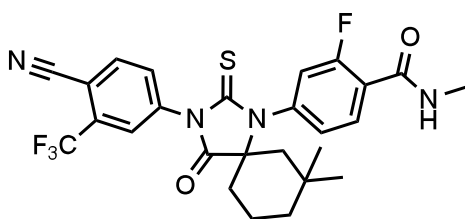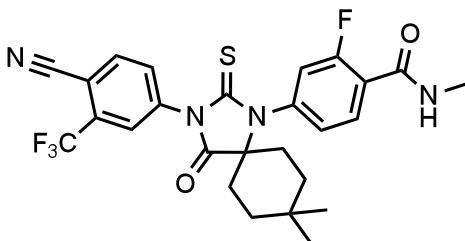

(±)-DR103, 4-(3-(4-cyano-3-(trifluoromethyl)phenyl)-7,7-dimethyl-4-oxo-2-thioxo-1,3-diazaspiro[4.5]decan-1-yl)-2-fluoro-N-methylbenzamide

Racemic DR103 was synthesized in 70% overall yield as an off-white powder.

^{1}HNMR (CDCl$_3$): δ: 8.27 (t, 1 H, J = 8.4 Hz), 7.98 (d, 1 H, J = 8.3 Hz), 7.92 (bs, 1 H), 7.80 (dd, 1 H, J = 8.2 Hz, J = 1.7 Hz), 7.17 (dd, 1 H, J = 8.3 Hz, J = 1.7 Hz), 7.07 (dd, 1 H, J = 11.6 Hz, J = 1.6 Hz), 6.70 (m, 1 H), 3.08 (d, 3 H, J = 4.7 Hz), 2.27 (m, 1 H), 2.17 (m, 1 H), 1.93 (m, 1 H), 1.67 (m, 1 H), 1.62 (m, 1 H), 1.57 (m, 1 H), 1.52 (m, 2 H), 1.20 (s, 3 H), 0.95 (s, 3 H).

^{19}FNMR (CDCl$_3$) δ: -61.98, -110.89.

LRMS for C$_{26}$H$_{24}$F$_4$N$_4$O$_2$S [M+H]$^{+}$ found: 533.33; calculated: 533.17
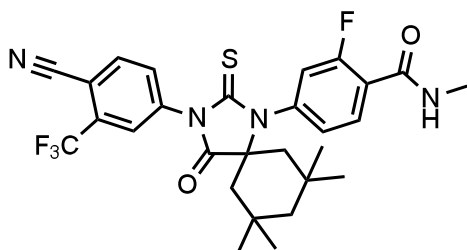

DR104, 4-(3-(4-cyano-3-(trifluoromethyl)phenyl)-8,8-dimethyl-4-oxo-2-thioxo-1,3-diazaspiro[4.5]decan-1-yl)-2-fluoro-N-methylbenzamide

It was isolated as an off-white powder.

^{1}HNMR (CDCl$_3$): δ: 8.30 (t, 1 H, J = 8.4 Hz), 7.98 (d, 1 H, J = 8.3 Hz), 7.93 (bs, 1 H), 7.82 (dd, 1 H, J = 8.2 Hz, J = 1.6 Hz), 7.22 (dd, 1 H, J = 8.3 Hz, J = 1.6 Hz), 7.11 (dd, 1 H, J = 11.6 Hz, J = 1.5 Hz), 6.72 (m, 1 H), 3.08 (d, 3 H, J = 4.7 Hz), 2.04 (m, 2 H), 1.93 (m, 4 H), 1.37 (m, 2 H), 0.99 (s, 3 H), 0.73 (s, 3 H).

^{19}FNMR (CDCl$_3$) δ: -61.98, -110.75.

LRMS for C$_{26}$H$_{24}$F$_4$N$_4$O$_2$S [M+H]$^+$ found: 533.33; calculated: 533.17.

DR105, 4-(3-(4-cyano-3-(trifluoromethyl)phenyl)-7,7,9,9-tetramethyl-4-oxo-2-thioxo-1,3-diazaspiro[4.5]decan-1-yl)-2-fluoro-N-methylbenzamide

This compound was isolated as a beige foam.

^{1}HNMR (CDCl$_3$): δ: 8.21 (t, 1 H, J = 8.4 Hz), 7.90 (d, 1 H, J = 8.3 Hz), 7.85 (bs, 1 H), 7.73 (dd, 1 H, J = 8.2 Hz, J = 1.2 Hz), 7.12 (dd, 1 H, J = 8.3 Hz, J = 1.2 Hz), 7.02 (dd, 1 H, J = 11.6 Hz, J = 1.2 Hz), 6.64 (m, 1 H), 3.01 (d, 3 H, J = 4.7 Hz), 1.94 (d, 2H, J = 14.4 Hz), 1.62 (d, 2H, J = 14.4 Hz), 1.50 (s, 2 H), 1.17 (s, 6 H), 0.83 (s, 6 H).

^{19}FNMR (CDCl$_3$) δ: -61.98, -110.89.

LRMS for C$_{26}$H$_{24}$F$_4$N$_4$O$_2$S [M+H]$^+$ found: 561.29; calculated: 561.20
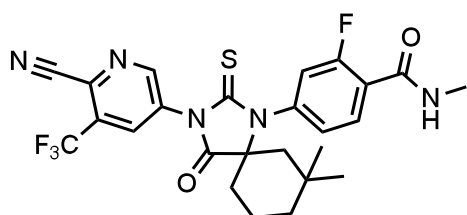

(±)-DR106, 4-(3-(6-cyano-5-(trifluoromethyl)pyridin-3-yl)-7,7-dimethyl-4-oxo-2-thioxo-1,3-diazaspiro[4.5]decan-1-yl)-2-fluoro-N-methylbenzamide

This compound was isolated as an off-white foam.

^{1}HNMR (CDCl$_3$): δ: 9.06 (d, 1 H, J = 1.9 Hz), 8.33 (d, 1 H, J = 1.9 Hz), 8.29 (t, 1 H, J = 8.4 Hz), 7.18 (dd, 1 H, J = 8.4 Hz, J = 1.6 Hz), 7.07 (dd, 1 H, J = 11.5 Hz, J = 1.5 Hz), 6.71 (m, 1 H), 3.08 (d, 3 H, J = 4.7 Hz), 2.30 (m, 1 H), 2.18 (m, 1 H), 1.94 (m, 1 H), 1.72 (m, 1 H), 1.63 (m, 1 H), 1.57 (m, 1 H), 1.52 (m, 2 H), 1.20 (s, 3 H), 0.94 (s, 3 H).

<superscript>19</superscript>FNMR (CDCl₃) δ: -61.87, -110.71.

LRMS for $C_{25}H_{23}F_4N_5O_2S$ [M+H]⁺ found: 534.31; calculated: 534.16
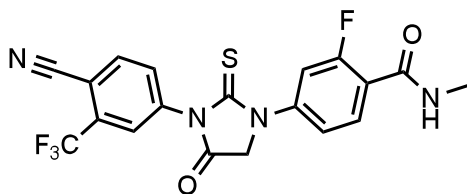
DR107, 4-(3-(4-cyano-3-(trifluoromethyl)phenyl)-4-oxo-2-thioxoimidazolidin-1-yl)-2-fluoro-N-methylbenzamide

This compound was isolated as a white to off-white powder.

¹HNMR (CDCl₃): δ: 8.26 (t, 1 H, J = 8.4 Hz), 8.02 (d, 1 H, J = 8.3 Hz), 7.91 (bs, 1 H), 7.79 (m, 2 H), 7.45 (dd, 1 H, J = 10.7 Hz, J = 1.3 Hz), 6.71 (m, 1 H), 4.71 (s, 2 H), 3.06 (d, 3 H, J = 4.7 Hz).

¹⁹FNMR (CDCl₃) δ: -62.05, -110.31.

LRMS for $C_{19}H_{12}F_4N_4O_2S$ [M+H]⁺ found: 437.19; calculated: 437.07;

Initial Models of AR–Antiandrogen Complex Structures

No structures have been solved experimentally for enzalutamide or ARN-509 in complex with AR (agonist or antagonist conformation). Therefore, 3D structures of antiandrogens were first built using the computer program Gaussview (version 4.1.2, part of the computer program Gaussian 03) (69) and then geometrically optimized in a quantum mechanical force field at the level of restricted Hartree-Fock (RHF) 6-31g* using the program Gaussian 03. The partial atomic charges were derived from the optimized structures by Restrained ElectroStatic Potential (70, 71) (RESP) fitting to the RHF/6-31g* potentials. The other parameters modeling the antiandrogens were taken from the CHARMm22 (72) force field after assigning CHARMm22 atom types to antiandrogens with an in-house program.

The initial AR-antiandrogen complex structures were then modeled with the molecular

modeling program CHARMM (*73, 74*). Starting with the atomic coordinates of AR WT and the A ring of S1 in the template crystal structure (PDB accession code, 2AXA), the side chain of residue F876 was replaced with CHARMm22-parameterized side chain of a leucine when needed and the CH group on the A ring was replaced with a nitrogen in cases of ARN-509. The rest of each antiandrogen was "grown" from the A ring using the ideal, unbound structures solved by geometry optimization. Missing side chain atoms were built using standard CHARMm22 parameters and hydrogen atoms were added with the HBUILD (*75*) module of CHARMM. All these newly-introduced atoms without 3D crystal coordinates treated flexible and the rest under harmonic constraints with the force constant of 100 Kcal/mol/Å^2, each AR-antiandrogen complex structure was energetically minimized with 1 round of 100-step steepest decent followed by 2 rounds of 100-step Adopted-Basis Newton–Raphson (ABNR) energy minimization. Harmonic constraints were reset at the beginning of each round of minimization. No nonbonded cutoff was used. Solvent effects were implicitly modeled in this stage with a distance-dependent dielectric constant.

Molecular Dynamics Simulations

The all-atom MD simulations were performed with explicit solvent atoms using the program CHARMM (version 36a1). Each initial AR–antiandrogen model was first centered and overlaid with a rhombic dodecahedron-shaped water box (edge length being 88 Å) of approximately 47,000 equilibrated water molecules. Any water molecule whose oxygen atom was within 2.8 Å away from any non-hydrogen atom of AR or antiandrgeon was removed. Proper amount of sodium and chloride ions were automatically added to achieve overall charge neutrality and physiological level of ion concentration (0.145 M). Their positions were optimized with 10 independent trajectories of randomly replacing water molecules and performing 50 steps of steepest

decent and 125 steps of ABNR energy minimization.

The molecular system including AR, antiandrogen, waters, and ions was heated to 300 K and equilibrated with two rounds of 0.1-ns MD simulations under successively weaker harmonic constraints on AR or antiandrogen atoms. After the MD equilibration, three sets of random velocities were assigned to initiate three independent 10-ns MD productions. The MD equilibration and production were performed using the crystal form of rhombic dodecahedron (RHDO) and the canonical ensemble (NVT). A nonbonded cutoff of 14 Å, periodic boundary conditions in conjunction with Ewald summation method, the leapfrog Verlet integrator, and the Hoover thermostat for pressure and temperature were used. The timestep was set at 2 fs. Parallel jobs for MD simulations were run on a computer cluster of Intel Xeon X5650 series (2.66 GHz and 4 GB memory per CPU).

<u>Molecular Visualization</u>

Structural models were visualized in a molecular graphics program, UCSF Chimera (*76*). The default option used when aligning structures.

Table 6. Site-Directed AR Mutagenesis Primers

Name	Sequence
W741C - sense	cattcagtactcctgcatggggctcatggtg
W741C - antisense	caccatgagccccatgcaggagtactgaatg
T877A - sense	gagagctgcatcagttcgcttttgacctgctaatc
T877A - antisense	gattagcaggtcaaaagcgaactgatgcagctctc
F876L - sense	cgagagagctgcatcagctcacttttgacctgct
F876L - antisense	agcaggtcaaaagtgagctgatgcagctctctcg
F876C - sense	gagagagctgcatcagtgcacttttgacctgctaa
F876C - antisense	ttagcaggtcaaaagtgcactgatgcagctctctc
F876I - sense	cgagagagctgcatcagatcacttttgacctgcta
F876I - antisense	tagcaggtcaaaagtgatctgatgcagctctctcg
F876S - sense	cgagagagctgcatcagtccacttttgacctgctaa
F876S - antisense	ttagcaggtcaaaagtggactgatgcagctctctcg
F876V -sense	cgagagagctgcatcaggtcacttttgacctgcta
F876V - antisense	tagcaggtcaaaagtgacctgatgcagctctctcg
F876Y - sense	tgcgagagagctgcatcagtacacttttgacctgctaa
F876Y - antisense	ttagcaggtcaaaagtgtactgatgcagctctctcgca

Table 7. Primers to amplify & sequence AR cDNA

PCR amplification of AR cDNA from gDNA	
AR-exon2-forward	ACATGCGTTTGGAGACTGC
AR-3UTR-reverse-1	TGGTCGACTAGATCCCCTATGA
AR-3UTR-reverse-2	CAAGGCACTGCAGAGGAGTA
AR sequencing primers	
AR-F1	TGTCCATCTTGTCGTCTTCG
AR-F2	GTCCTGGAAGCCATTGAGCCA
AR-F3	CCAGATGGCTGTCATTCAGTA
AR-R1	GAAGACCTTGCAGCTTCCAC
AR-R2	ACACACTACACCTGGCTCAAT
AR-R3	CAGGCAGAAGACATCTGAAAG

Table 8. ChIP quantitative PCR primers

Name	Sequence
PSA-Enhancer - forward	atgttcacattagtacaccttgcc
PSA-Enhancer - reverse	tctcagatccaggcttgcttactgtc
FKBP5-Enhancer - forward	ccccctattttaatcggagtac
FKBP5-Enhancer - reverse	ttttgaagagcacagaacacct

Table 9. Quantitative RT-PCR primers

| Name	Sequence
GAPDH - forward	GAAGGTGAAGGTCGGAGTC
GAPDH - reverse	GAAGATGGTGATGGGATTTC
PSA - forward	GGTGACCAAGTTCATGCTGTG
PSA - reverse	GTGTCCTTGATCCACTTCCG
Tmprss2 - forward	CACTGTGCATCACCTTGACC
Tmprss2 - reverse	ACACGCCATCACACCAGTTA
FKBP5 - forward	TCCCTCGAATGCAACTCTCT
FKBP5 - reverse	GCCACATCTCTGCAGTCAAA
SGK1 - forward	GCAGAAGGACAGGACAAAGC
SGK1 - reverse	CAGGCTCTTCGGTAAACTCG

Figure Supplements
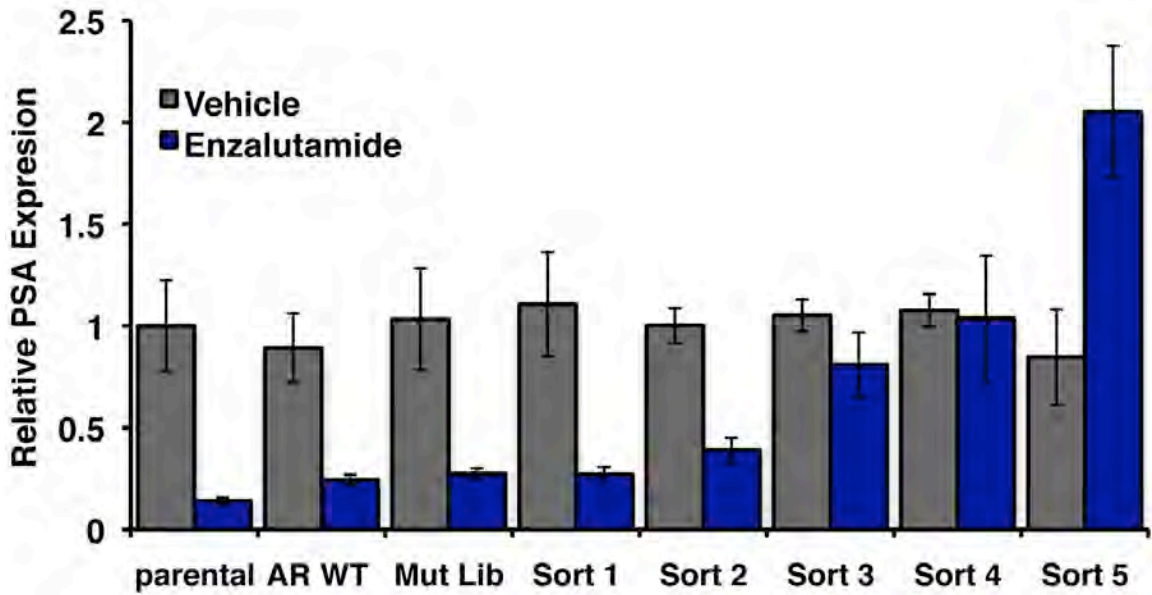
Figure Supplement 1. Enzalutamide induces PSA expression in FACS-sorted cells

Parental LNCaP-Pb.PSE.EGFP cells, and those overexpressing AR WT, the random AR mutant library (Mut Lib), and cells after each sort were treated with 1mM enzalutamide for 24 hours in media containing full serum. RNA was then collected, reverse transcribed, and quantitative PCR performed for AR target gene KLK3 (PSA).
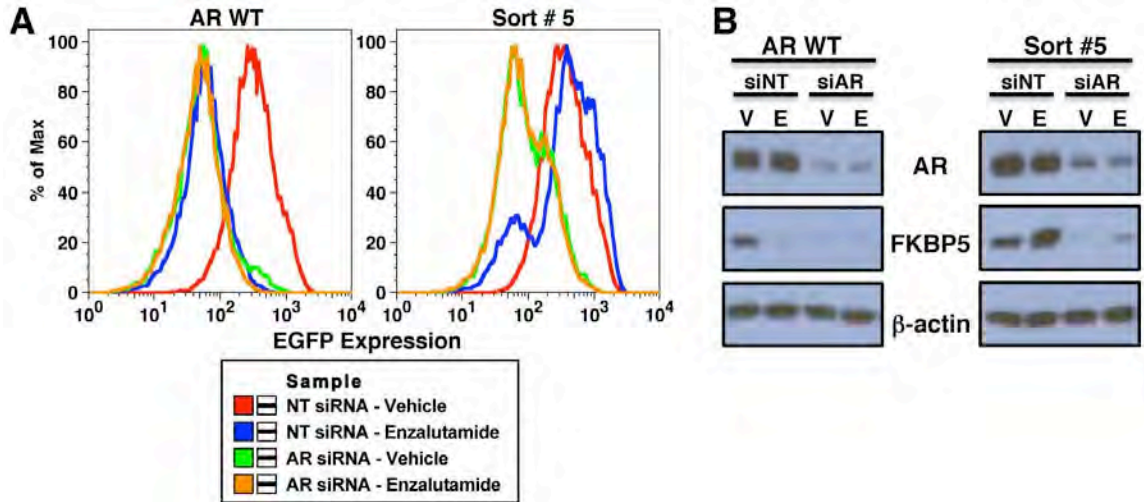
Figure Supplement 2. Expression of EGFP and FKBP5 remain AR-dependent in FACS-sorted cells

LNCaP-Pb.PSE.EGFP cells overexpressing AR WT and cells from the fifth sort of our screen were transfected with 10nM of either a non-targeting siRNA (siNT) or a siRNA against AR (siAR). They were also treated with either vehicle (V) or 1µM enzalutamide (E). After four days of enzalutamide treatment and siRNA knockdown, cells were collected for both **(A)** flow cytometric analysis of EGFP expression and **(B)** western blot analysis of the AR target gene FKBP5, and to ensure we achieved good AR knockdown.
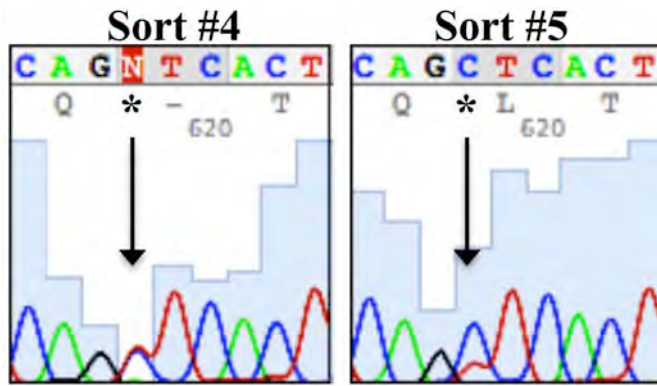
Figure Supplement 3. AR F876L mutant allele enriched from 4th to 5th sort

We PCR amplified AR from our LNCaP/AR*/Pb.PSE.EGFP cells after four rounds of enzalutamide treatment and FACS-sorting, and Sanger sequenced the PCR product. AR F876L (T $\rightarrow$ C) accounts for approximately 50% of the AR in these cells. This mutation is further enriched after the 5th sort, and accounts for approximately 80% of AR in that population of cells.
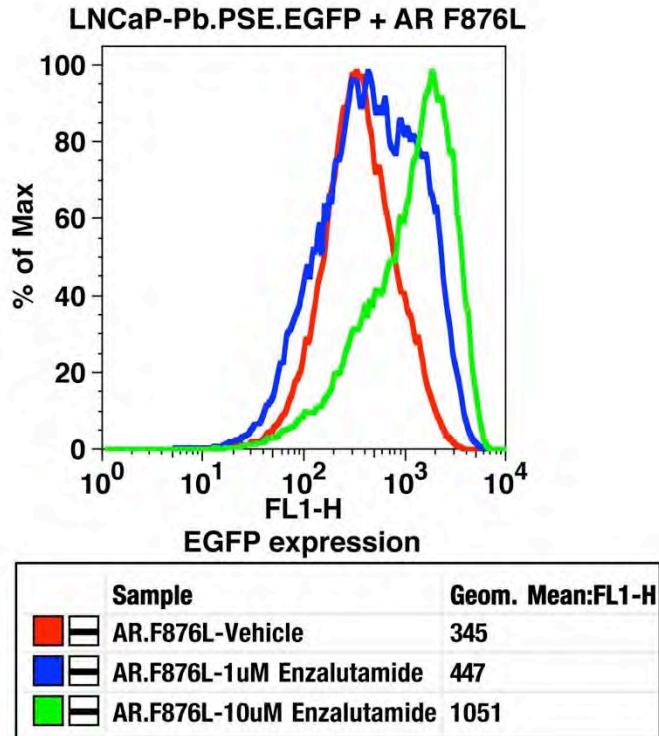
Figure Supplement 4. Dose-dependent induction of EGFP expression by enzalutamide in LNCaP-Pb.PSE.EGFP cells expressing AR F876L

LNCaP-Pb.PSE.EGFP cells ectopically expressing AR F876L were treated with vehicle, 1μM or 10μM enzalutamide for 4 days. Cells were then collected for FACS-analysis of EGFP expression (FL1-H). Geometric-mean fluorescence intensity is indicated in the table.
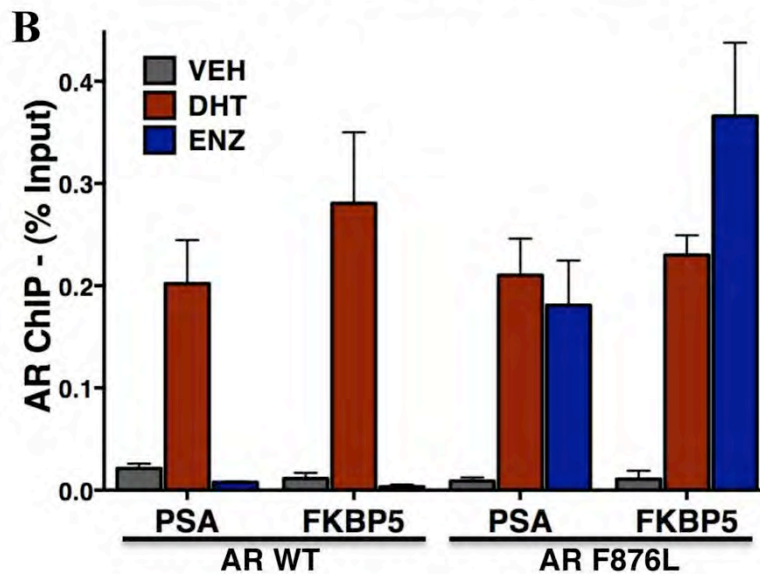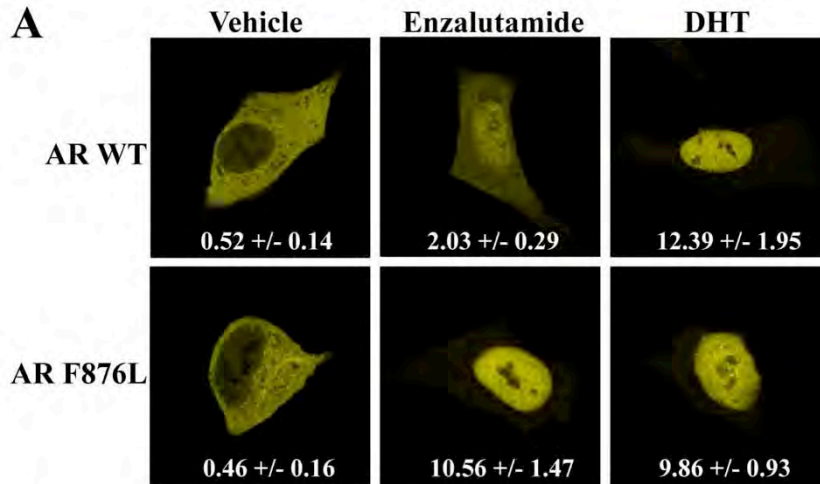
Figure Supplement 5. Enzalutamide induces AR F876L nuclear translocation and DNA binding

(A) LNCaP cells were transfected with EYFP tagged wild-type AR or AR F876L in androgen depleted media containing vehicle, 1µM enzalutamide, or 1nM DHT. Representative confocal images are shown. Average nuclear-to-cytoplasmic ratios for EYFP are displayed (± SD, n = 3). **(B)** LNCaP cells stably overexpressing either AR WT or AR F876L were cultured in androgen-depleted media for 4 days, then treated with vehicle (VEH), 10µM enzalutamide (ENZ), or 1nM DHT for 4 hours. AR chromatin immuoprecipitation was performed, and real-time PCR quantification of PSA enhancer and FKBP5 enhancer is shown (percent input mean ± SD, n=3).
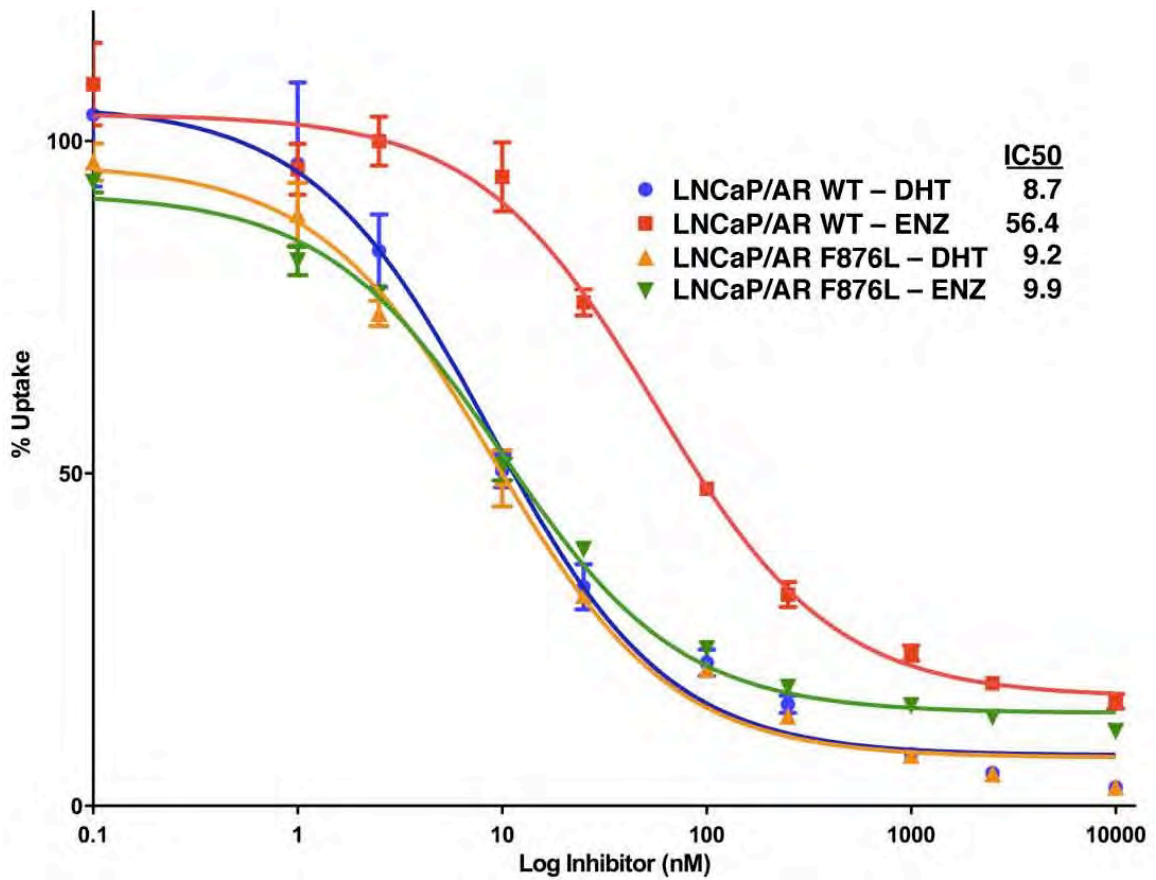
Figure Supplement 6. Enzalutamide binds to AR F876L with higher affinity than to AR WT

Representative competition binding curves, showing displacement of ^{18}F-FDHT in LNCaP/AR WT and LNCaP/AR F876L cells by increasing concentrations of cold DHT or enzalutamide (ENZ). The median inhibitory concentration (IC_{50}) values from this experiment are displayed (error bars represent the SD of triplicate measurements).
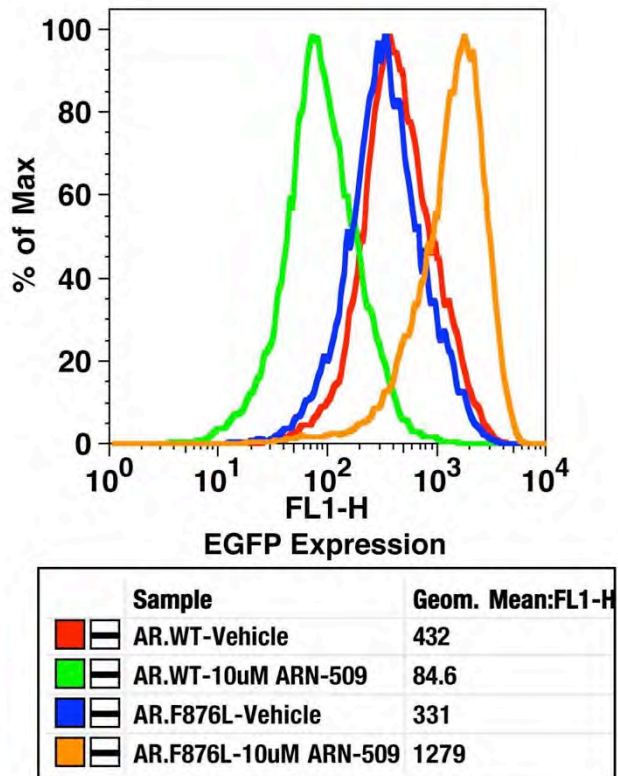
Figure Supplement 7. AR F876L mutation converts ARN-509 into an AR agonist

LNCaP-Pb.PSE.EGFP cells ectopically expressing either AR WT or AR F876L were treated with vehicle or 10μM ARN-509. After four days of treatment, cells were collected for analysis of EGFP expression (FL1-H), geometric-mean fluorescence is shown in the table below.
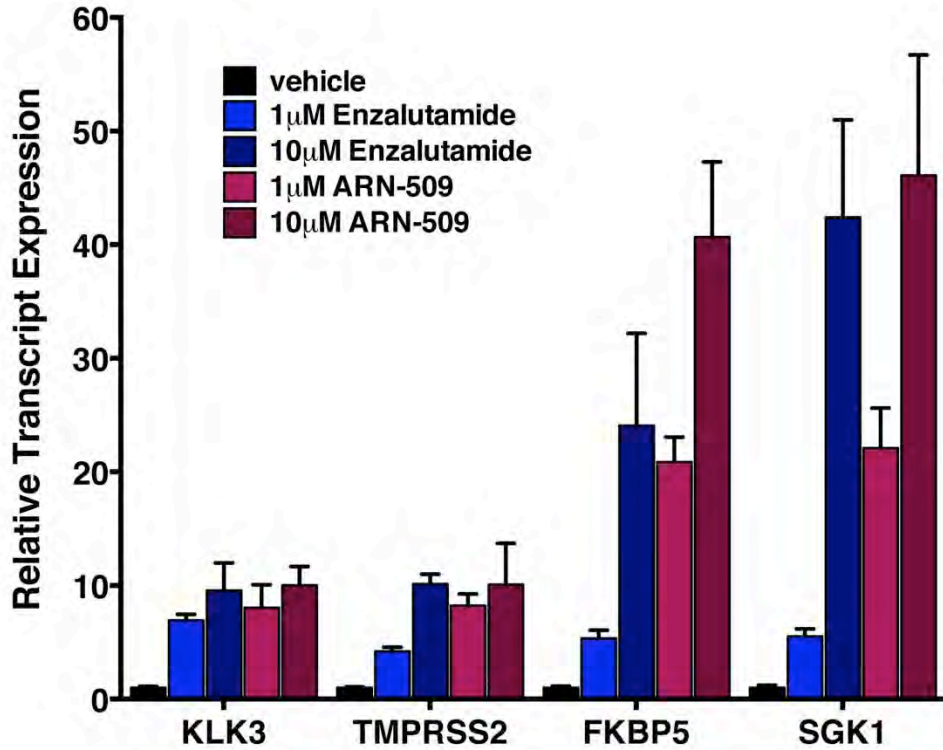
Figure Supplement 8. Dose-dependent induction of target genes in AR F876L expressing cells treated with enzalutamide or ARN-509

LNCaP cells ectopically expressing AR F876L were cultured in androgen-depleted media (10% CSS) for 48 hours, then treated with the indicated dose of antiandrogen for 24 hours, and qRT-PCR was performed to assess the expression of the indicated AR target gene.
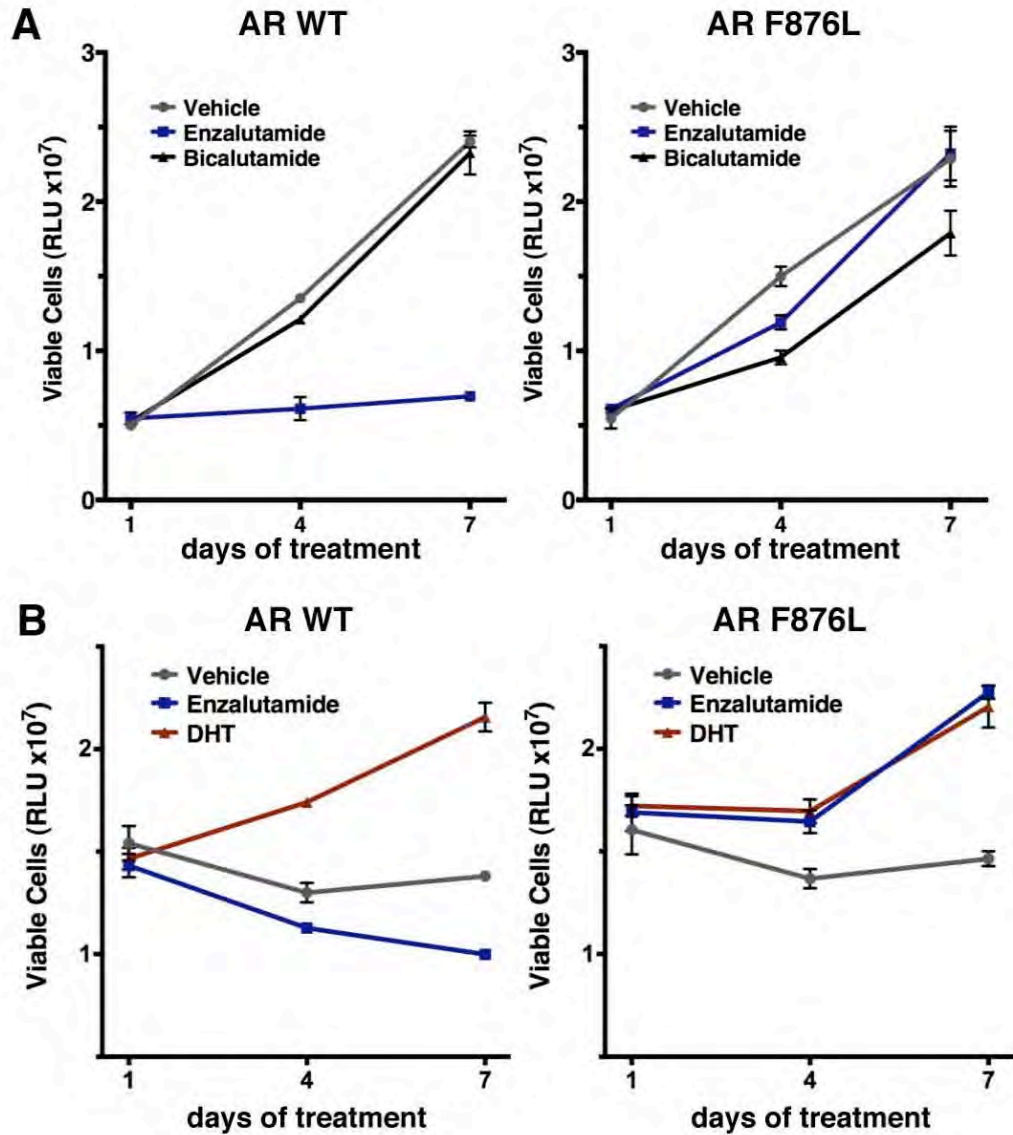
Figure Supplement 9. Enzalutamide treatment of CWR22Pc cells expressing AR F876L

(A) CWR22Pc cells stably expressing either AR WT or AR F876L were plated in 10% FBS media containing vehicle, 1µM enzalutamide, or 10µM bicalutamide. CellTiterGLO assay was performed on days 1, 4, and 7 to measure cell viability (mean relative light units (RLU) ± SD, n=3). **(B)** CWR22Pc cells stably expressing either AR WT or AR F876L were plated in 10% CSS media containing vehicle, 1µM enzalutamide, or 0.1nM DHT. CellTiterGLO assay was performed on days 1, 4, and 7 to measure cell viability (mean relative light units (RLU) ± SD, n=3).
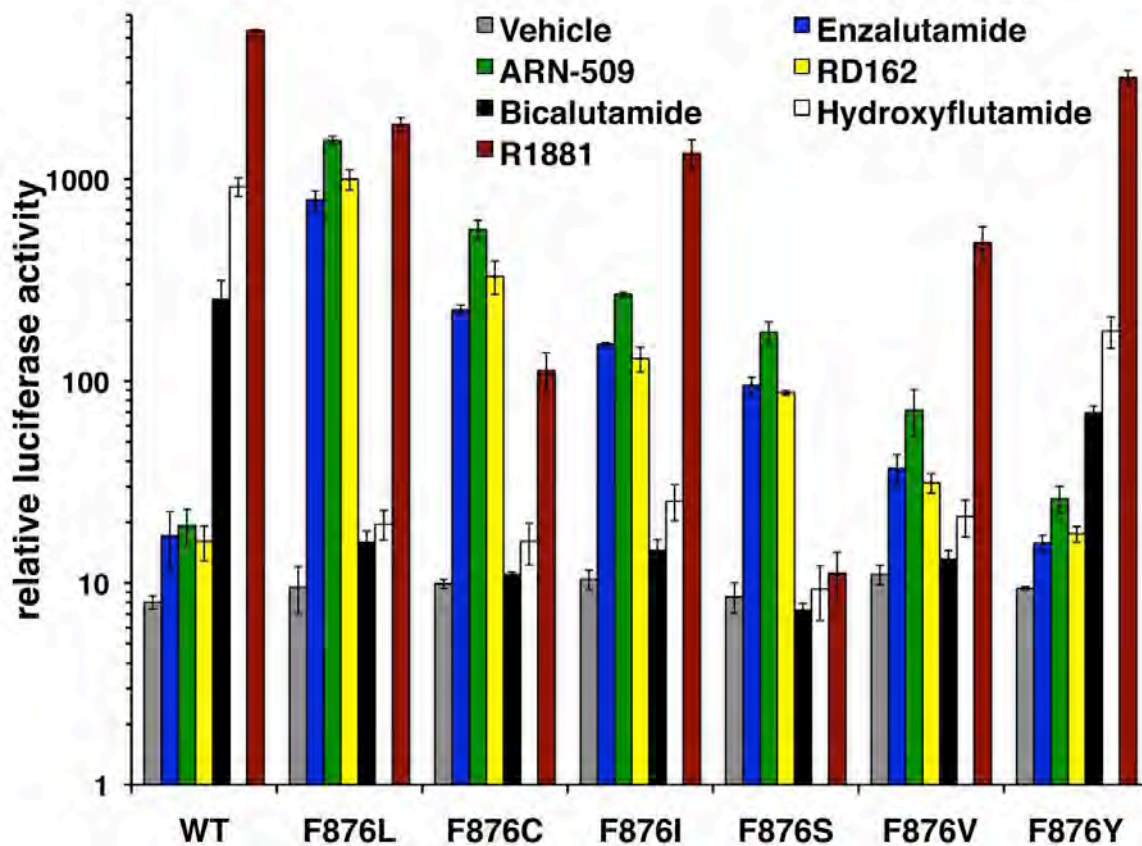
Figure Supplement 10. Other substitutions at Phe876 modify the pharmacology of second-generation antiandrogens

ARE(4X)-luciferase assay for additional F876 substitutions. CV1 cells were cotransfected with an ARE(4X)-firefly luciferase construct, SV40 Renilla luciferase construct and one of the designated AR constructs. The cells were treated with 10 μM of the indicated antiandrogens and a dual luciferase assay was performed on the lysates, and normalized to Renilla luciferase (mean ± SD, n=3).

Figure Supplement 11. Bicalutamide is a modest inhibitor of AR F876L transcriptional activity

Parental LNCaP-Pb.PSE.EGFP cells, and those transduced with AR WT or AR F876L were treated with Vehicle, 1 or 10 µM bicalutamide (BIC) for four days, and then collected for flow cytometri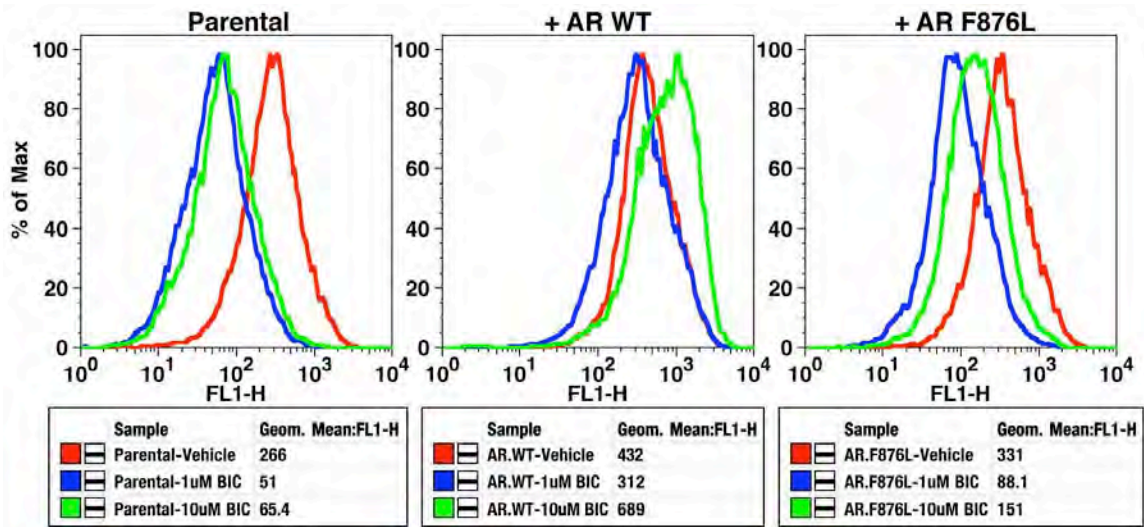c analysis of EGFP expression (FL1-H). Geometric-mean fluorescence intensity of EGFP is displayed in the table below each histogram plot.
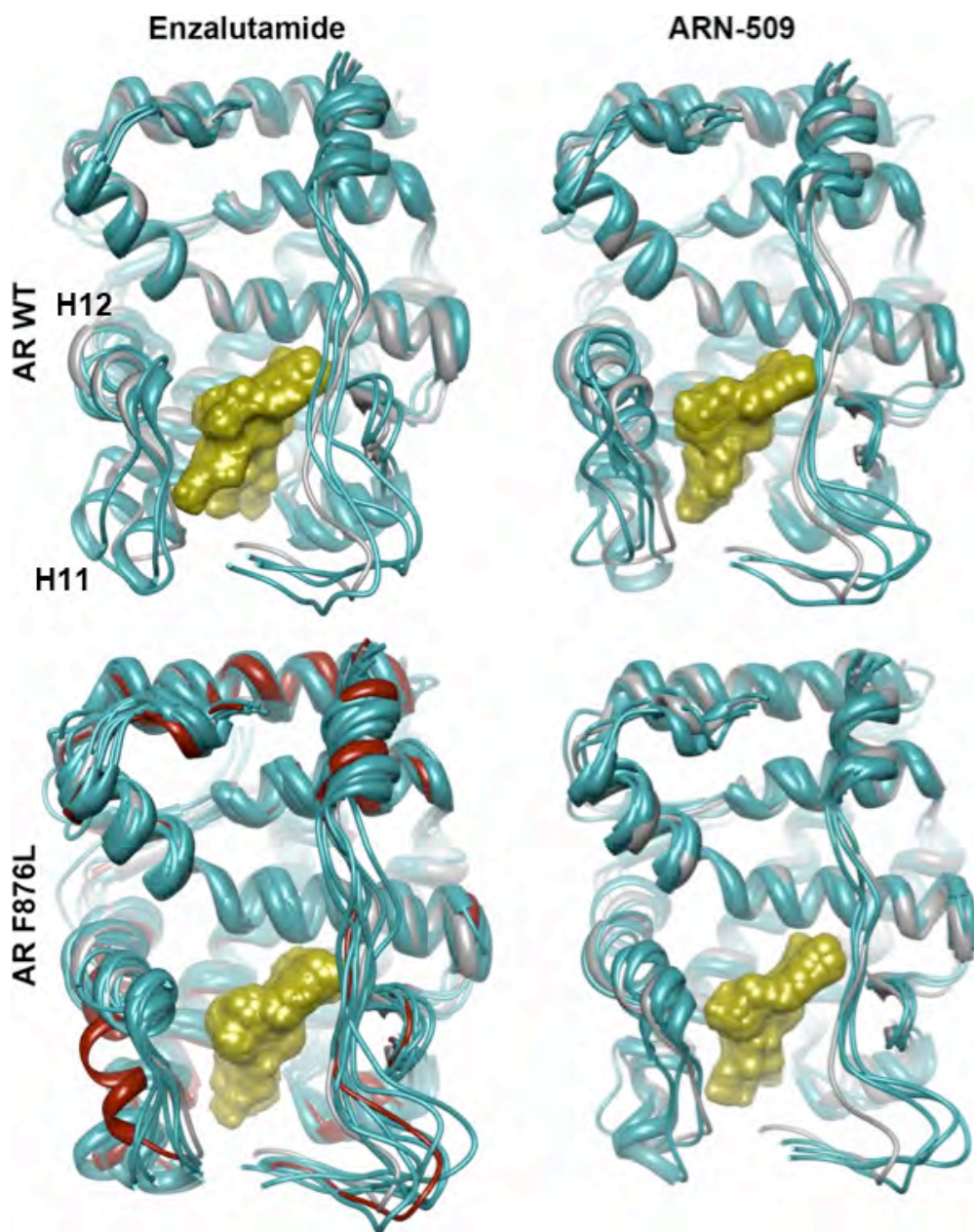
Figure Supplement 12. Predicted Enz/ARN simulations overlaid on agonist crystal structure

The coordinates for three 10ns simulations with the indicated receptor (cyan) and drug compound (gold) were overlaid on the 1Z95 structure (grey) to highlight structural differences between the agonist conformation of the AR W741L/bicalutamide complex. Note the evidence of H12 dislocation in AR WT/antiandrogen complexes that is less evident for AR F876L. Bicalutamide was deleted for visual clarity. For the simulations conducted for the enzalutamide/AR F876L complex, one suspected outlier (red) was detected among the initial 3 MD simulations. Five additional simulations were conducted and they recapitulated the majority tendency observed for the initial MD simulations.
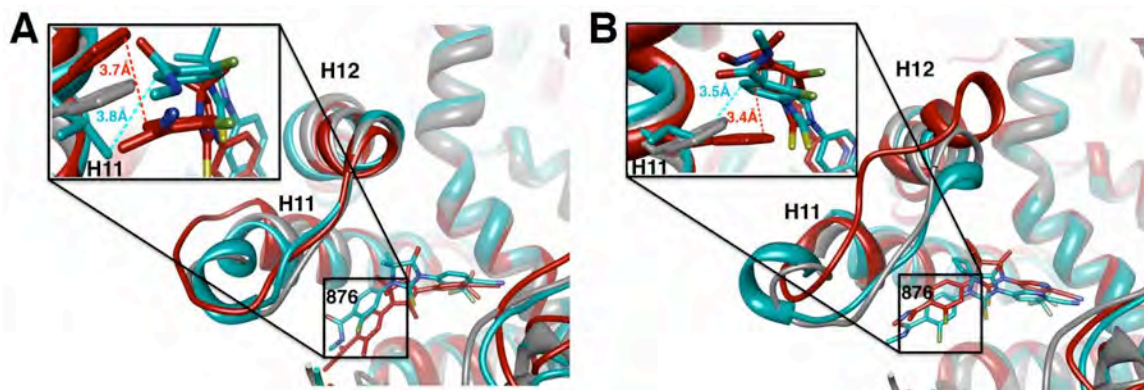
Figure Supplement 13. A zoomed in view of the H11 pocket from the enzalutamide and ARN-509 MD simulations

The lowest energy 10 ns MD models for enzalutamide **(A)** and ARN-509 **(B)** with AR WT (red) and AR F876L (cyan) overlaid on 1Z95 (grey – agonist reference structure), with an inset showing a zoomed in view of the region around residue 876, that includes distances between close hydrophobic atoms on each receptor:ligand pair.
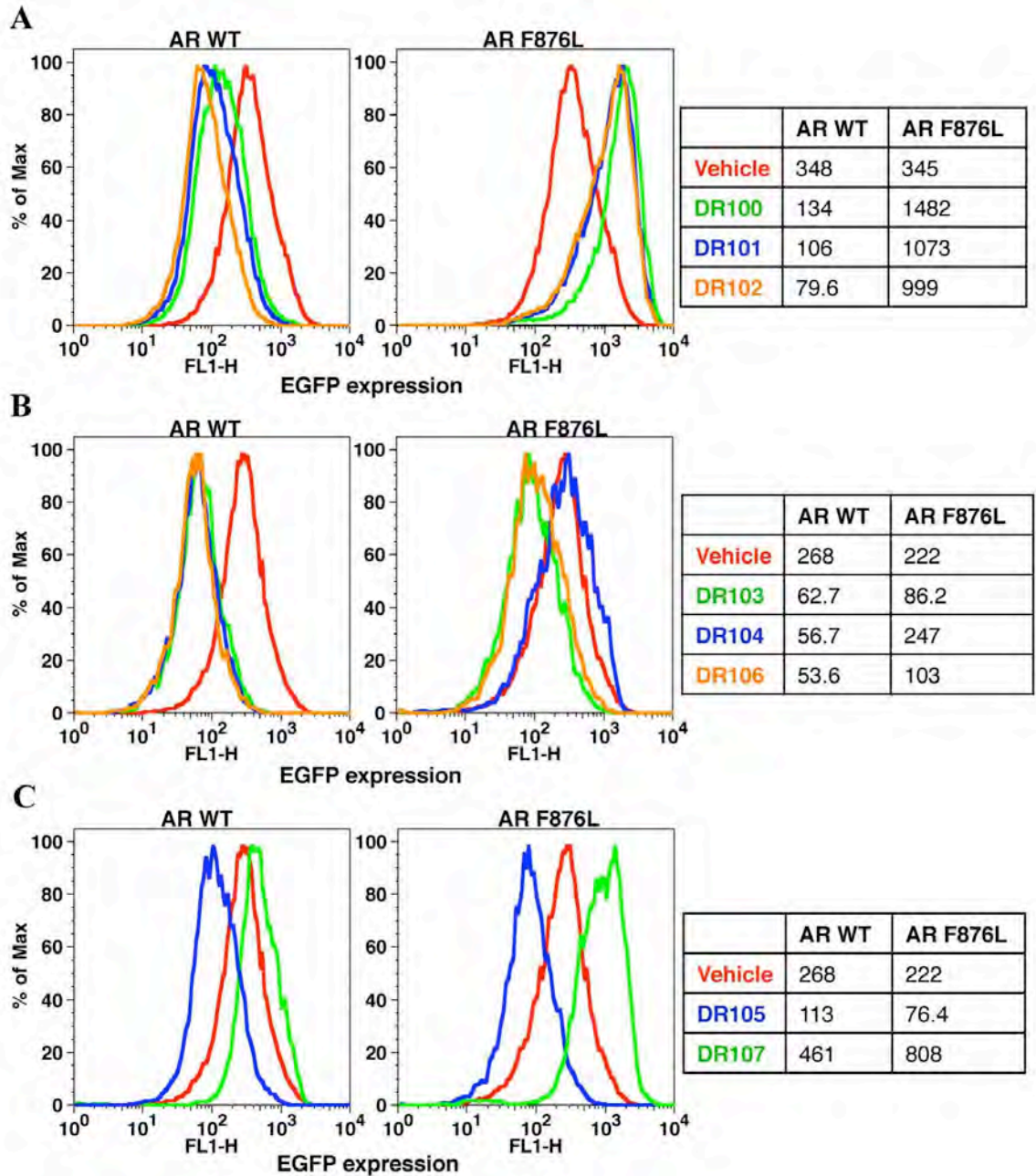
Figure Supplement 14. EGFP reporter assay for AR activity with DR-series compounds

LNCaP-Pb.PSE.EGFP cells ectopically expressing either AR WT or AR F876L were treated with vehicle (DMSO) or 10 µM of the indicated DR-series compound. After 4 days of treatment, cells were collected and FACS analysis for EGFP expression was performed. Geometric-mean fluorescence intensity is indicated in the adjacent table.
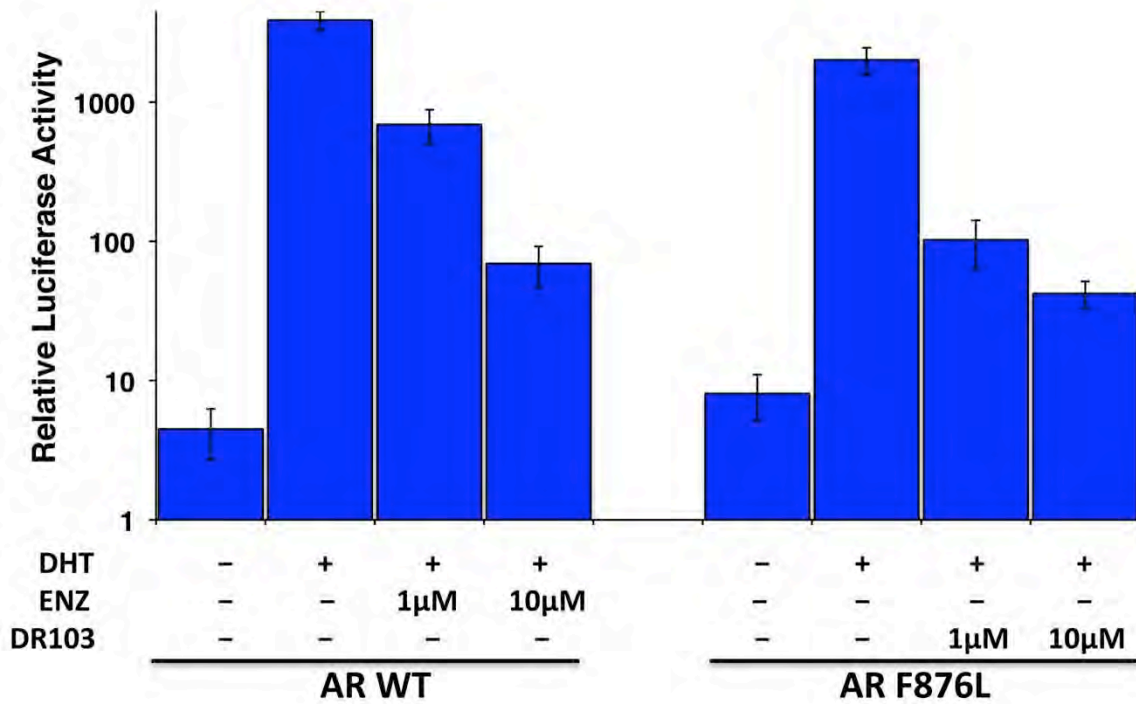
Figure Supplement 15. (±)-DR103 effectively competes with DHT for AR binding and induction of AR-regulated luciferase

CV1 cells were transfected with AR WT or AR F876L, 4XARE-luciferase, and SV40 renilla luciferase expression constructs. They were cultured in androgen-depleted media supplemented with the indicated androgen/ antiandrogen for 36 hours and a dual-luciferase assay was performed on cell lysates. Luciferase activity is represented by relative light units (RLU) ± SD, n=3.
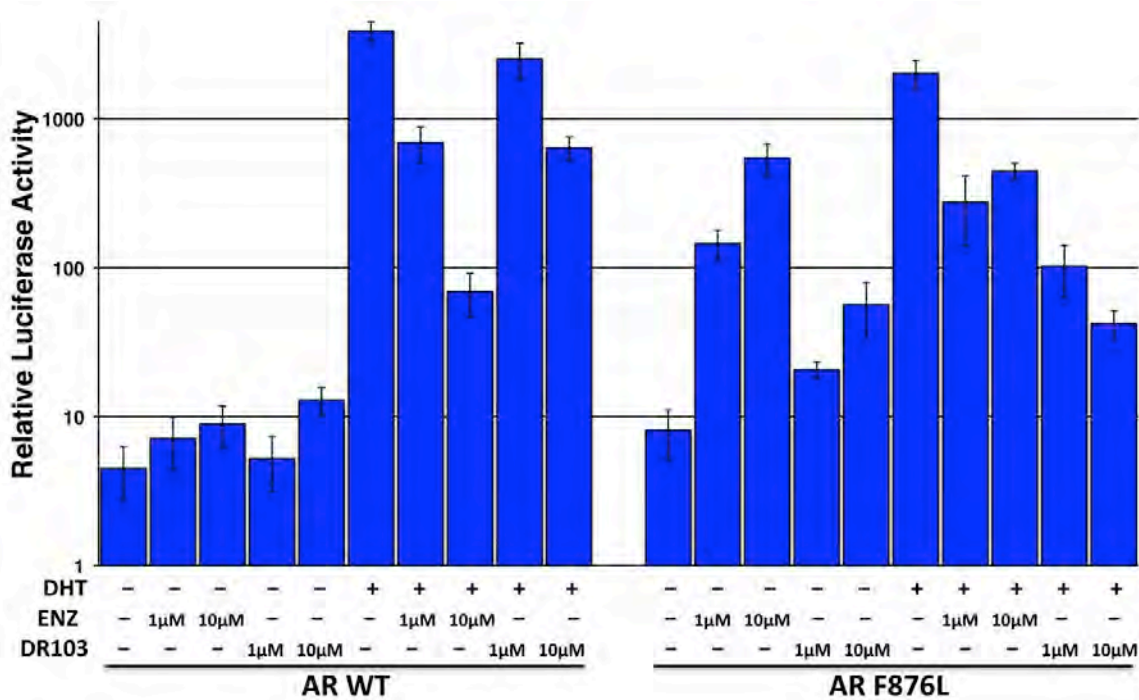
Figure Supplement 16. (±)-DR103 is a more potent antagonist for AR F876L than AR WT

CV1 cells were transfected with AR WT or AR F876L, 4XARE-luciferase, and SV40 renilla luciferase expression constructs. They were cultured in androgen-depleted media supplemented with the indicated androgen/ antiandrogens for 36 hours and a dual-luciferase assay was performed on cell lysates. DHT concentration was 1nM. Luciferase activity is represented by relative light units (RLU) ± SD, n=3.
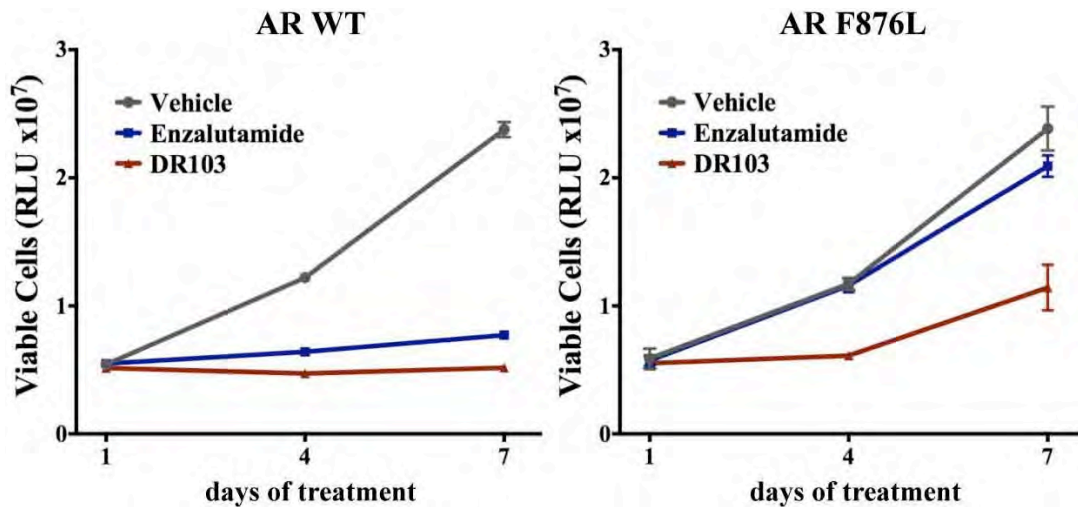
Figure Supplement 17. Growth inhibition of CWR22Pc cells overexpressing AR WT or AR F876L with (±)-DR103 treatment

CWR22Pc cells ectopically expressing wild-type AR or AR F876L, cultured in full-serum containing media, were treated with vehicle (DMSO) or 10 µM of enzalutamide or DR103. CellTiterGLO assay was performed on days 1, 4, and 7 to determine cell viability (relative light units (RLU) ± SD, n=3).
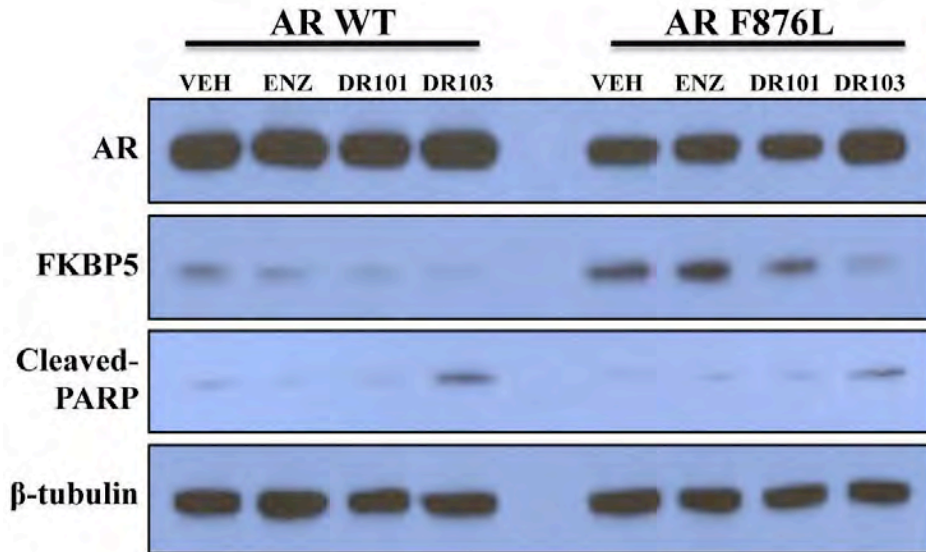
Figure Supplement 18. (±)-DR103, inhibits AR signaling and induces PARP cleavage in cells expressing both AR WT and AR F876L

VCaP cells ectopically expressing either AR WT or AR F876L were treated for 4 days with vehicle or 10 µM of the indicated antiandrogen (VEH=vehicle, DMSO; ENZ=enzalutamide) in media containing 10% FBS. Whole-cell lysates were analyzed by western blot.
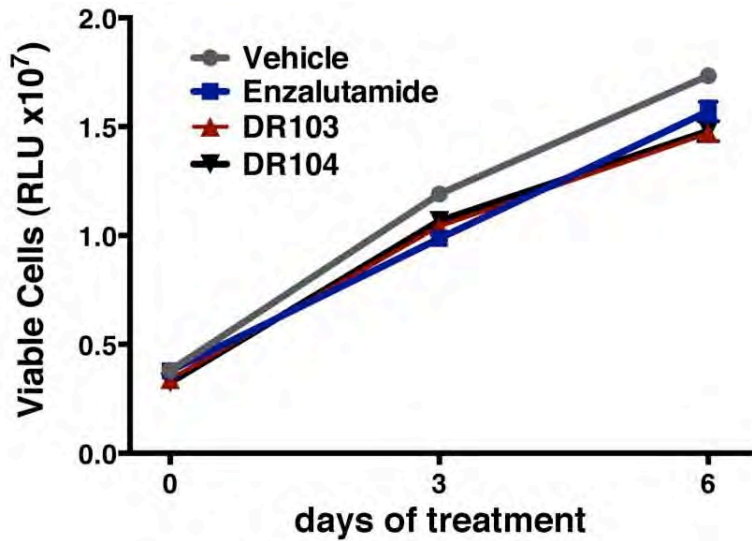
Figure Supplement 19. DU145 cells treated with (±)-DR103 and DR104 display no significant growth inhibition

DU145 cells were cultured in full serum containing media with 10 µM of the indicated antiandrogens. CellTiterGLO assay was performed on days 0, 3, and 6 to determine cell viability (relative light units (RLU) ± SD, n=3).
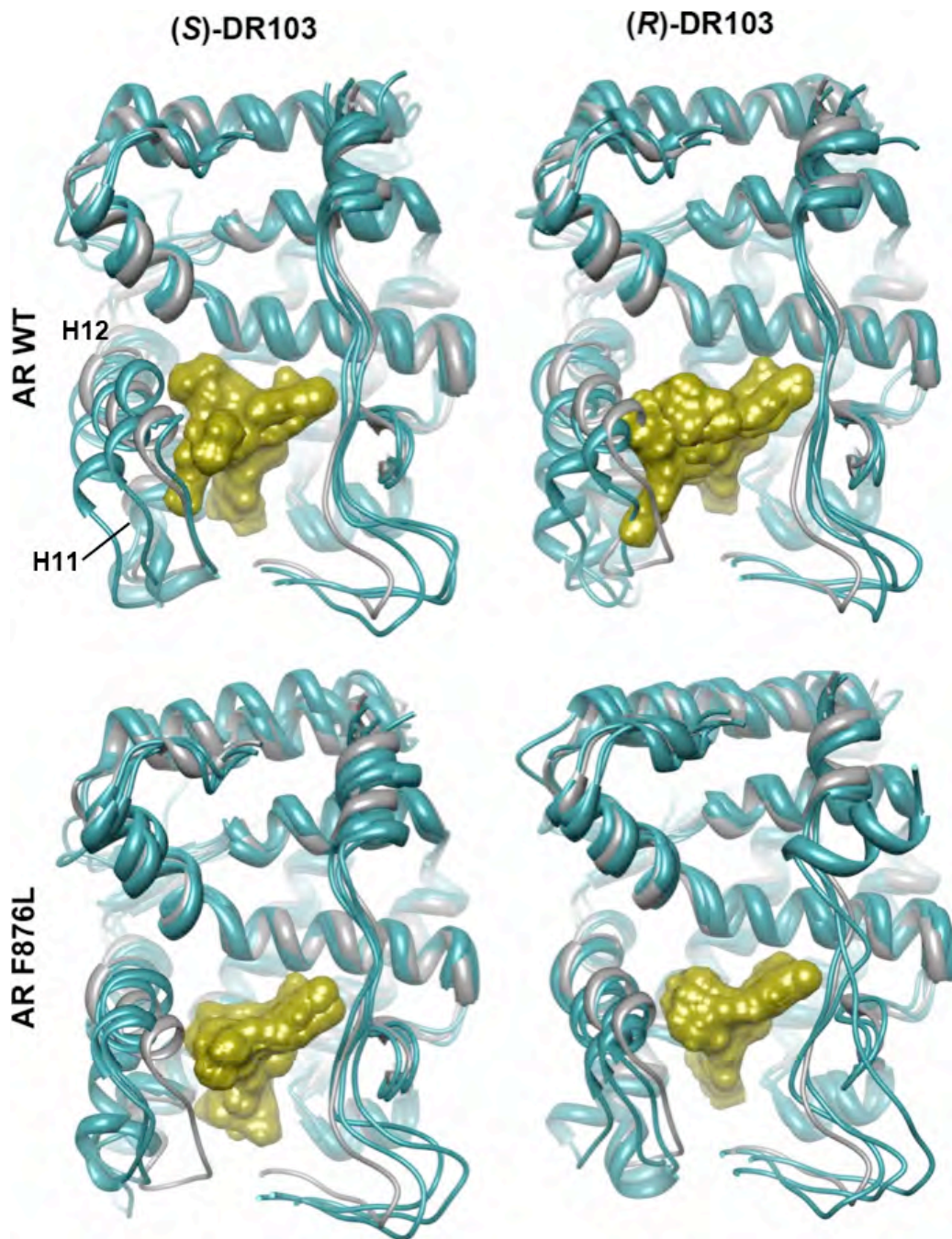
Figure Supplement 20. Overlay of predicted DR103 simulations and agonist crystal structure

An overlay of three 10 ns MD simulations for (*S*)-DR103 docked either in AR WT or AR F876L shows the dislocation of H12 in space compared to 1Z95 (grey), consistent with the pharmacological model predicted by prior MD simulations for enzalutamide and ARN-509 in AR WT. The predicted conformations of the AR variants are highlighted in cyan, and the respective conformations of (*S*)- and (*R*)-DR103 are represented in gold.
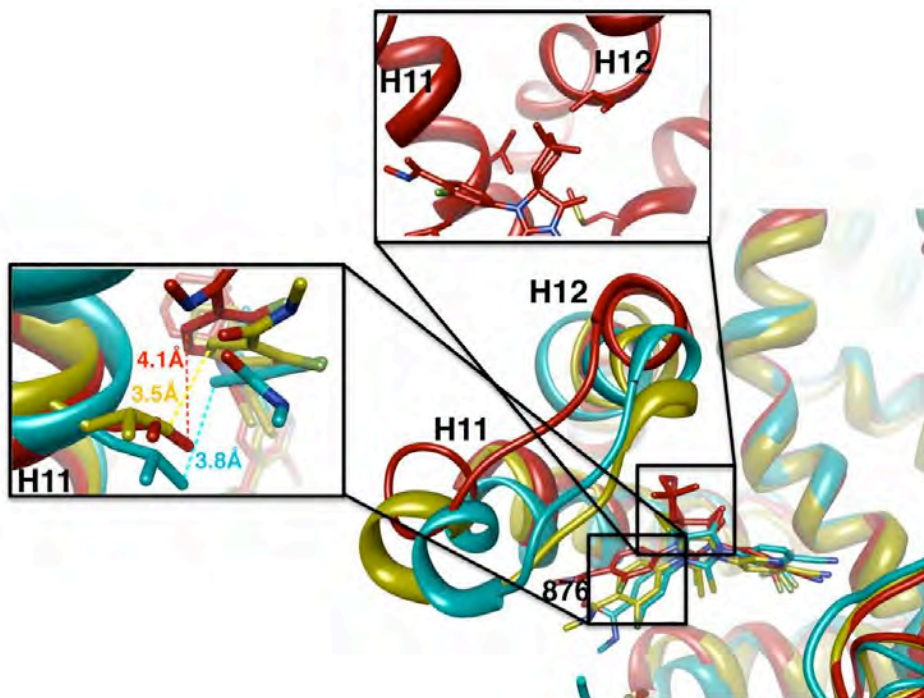
Figure Supplement 21. A zoomed in view of the H11 and H12 pockets of the MD simulations for AR F876L

A magnified view of the lowest energy conformations of enzalutamide (cyan), ARN-509 (gold), and (*S*)-DR103 (red) in complex with AR F876L, showing the structural framework and interactions in close proximity to the antagonist C and D-rings (with distances measured).

Chapter 4 – Future Directions

In addition to the F876L/I mutations that emerged from drug-resistant LNCaP/AR xenografts, several other AR mutations were identified. Using the reporter-based systems we optimized to measure AR activity, we tested each of these mutations to determine if they conferred resistance to enzalutamide or ARN-509. We have also begun to optimize assays to determine if F876L is a clinically relevant mutation in patients with acquired resistance to enzalutamide or ARN-509.

Additional AR Mutations

Several AR mutations emerged in the drug-resistant LNCaP/AR xenograft tumors described in Chapter 3, in addition to those described at Phe876. These mutations are listed in **Table 10** below. Most of these mutations only occurred in a single tumor, but one mutation was found in 4 tumors. This AR mutation, A597T, has been previously described in patients with partial androgen insensitivity syndrome (PAIS), and results in AR protein with impaired dimerization and transactivation ability. The remaining 9 mutations only occurred in single tumors, and many of them had also been previously described as AIS associated (77). Some of these mutations have not been previously described, but other amino acid substitutions at the same residue have been described. Because many of these AR mutations have been characterized and are known to result in transcriptionally impaired AR protein, cells that express these mutants may have acquired AR-independent mechanisms to overcome androgen blockade. Interestingly, several synonymous mutations were enriched in these drug-resistant tumors, suggesting that the presence of an AR mutation does not necessarily indicate there is a selection for a gain-of-function.

Table 10. Additional AR Mutations in LNCaP/AR Xenografts

AR Mutation	% of reads (Drug)	Clinical Annotation
E566K	1.56 (MDV)	
E589K	1.26 (ARN)	
A597T	6.25 (MDV), 1.04 (ARN), 6.99 (ARN), 10.34 (MDV)	PAIS (partial transactivation)
S648G	1.10 (MDV)	S648N (PCa)
E669K	1.71 (MDV)	
P683T	1.26 (ARN)	PAIS
D696E	12.08 (ARN)	D696H/N/Y/V (CAIS, MAIS or PAIS)
N728I	2.21 (MDV)	N728K (MAIS)
I738F	1.70 (MDV)	CAIS
V890M	1.07 (MDV)	CAIS or PAIS
R727H	1.67 (ARN)	PCa
W742C	1.42 (ARN)	PCa (Bical resistance)
W742L	1.88 (MDV)	PCa (Bical resistance)
G751S	1.03 (Vehicle)	G751D (CAIS)
P556P	1.19 (ARN)	
V737V	1.59 (ARN)	
V819V	7.17 (MDV), 10.09 (ARN), 7.92 (ARN)	

Pink: newly tested AR mutations; Blue: previously tested AR mutations (see chapter 2); Yellow: control tumor; Grey: synonymous mutations

***The numbering system used in Table 10 reflects the recent change in AR numbering (*77*)
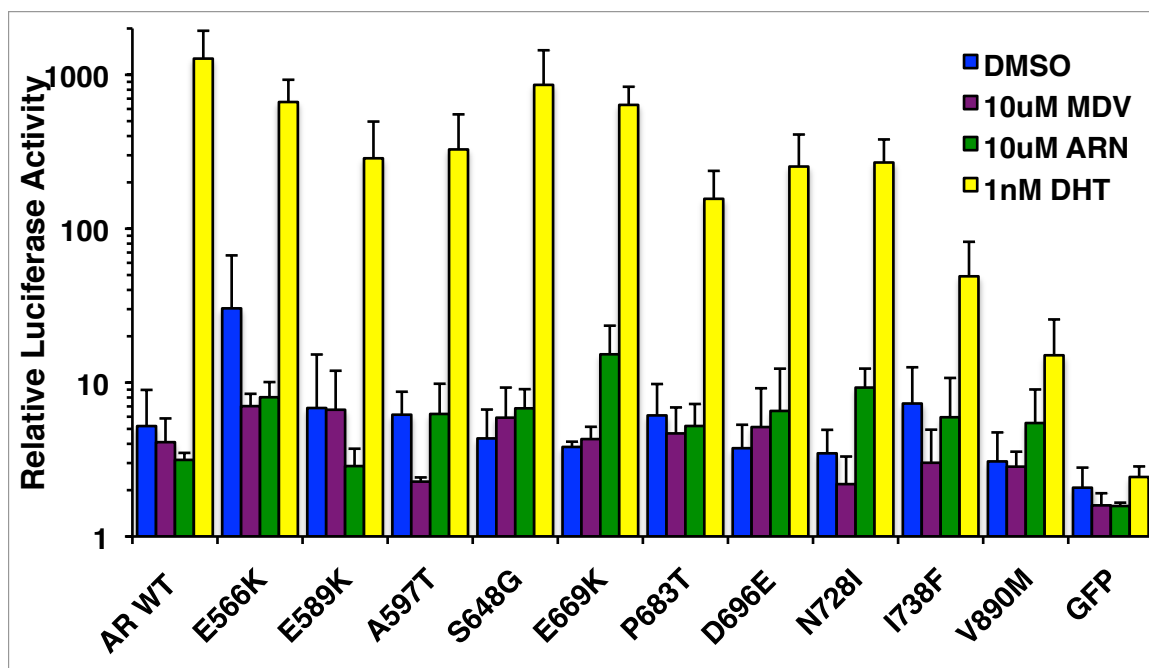
Figure 23. AR-regulated luciferase assay for additional AR mutations

CV1 cells were transfected with the indicated AR cDNA construct, 4XARE-luciferase (firefly) and SV40-renilla luciferase constructs, and cultured in androgen-depleted media containing the indicated androgen or antiandrogen for 24 hours and a dual-luciferase assay performed on cell lysates. Firefly luciferase was normalized to renilla luciferase activity.

We generated the 10 new AR point mutant cDNAs in the pWZL-AR retroviral vector using site-directed mutagenesis, and evaluated each mutant for enzalutamide and ARN-509 sensitivity in both our luciferase and EGFP reporter assays. In the luciferase reporter assay (**Figure 23**), neither enzalutamide (MDV) nor ARN-509 displayed agonism for any of the new AR mutants. All of the AR mutants also exhibited lower DHT induction compared to wild-type AR, suggesting that they have impaired AR transcriptional activity. All of these AR mutants remained sensitive to both enzalutamide and ARN-509 in the EGFP reporter assay (data not shown), and displayed comparable downregulation of EGFP expression as AR WT. These data indicate that an AR-

independent mechanism of resistance may be at play in the cells that harbor these AR mutations.

Detection of AR F876L mutation in CRPC patient samples

We are working to validate AR F876L mutation as a mechanism of acquired resistance to enzalutamide or ARN-509 therapy in patients who have been treated with and subsequently developed resistance to these drugs. For many reasons this is has been a challenging endeavor. Enzalutamide was approved by the FDA just over six months ago, so very few patients have been treated (and relapsed) outside the original clinical trials and, these trials were conducted by clinical investigators who, for the most part, did not obtain tumor tissue. Castration-resistant prostate cancer (CRPC) presents unique clinical challenges in obtaining tumor tissue, principally because most patients with this stage of disease present with bone metastases. It is difficult and uncommon to obtain bone biopsies, and there is often a great deal of stromal contamination.   These obstacles have led us to focus on developing new assays to detect AR mutations in blood, leveraging recent advances in circulating tumor cells (CTCs) and circulating tumor DNA (ctDNA). Both of these sources for tumor DNA are extremely attractive because they are minimally-invasive and allow serial collection/analysis to monitor patients' response to therapy.   This is challenging work that we are actively pursuing with collaborators.

Methods for detecting rare mutations in CTCs or ctDNA

Circulating Tumor Cells (CTCs)

The loss of single cells from a tumor marks an early event in tumor progression and metastasis. Though metastatic development in prostate cancer is not completely

understood, circulating tumor cell (CTC) count is becoming routine in clinical practice for diagnosis of minimal residual disease, estimating prognosis and monitoring treatment response for many tumor types (*78*). Circulating tumor cells (CTCs) account for a tiny fraction of all the cells in the peripheral blood circulation, and methods to detect and isolate them are varied. Enrichment methods often include density gradient centrifugation and antibody-capture methods, either using a negative selection for the leukocyte antigen CD-45 or positive selection for tumor-associated antigens, or combinations of both. Positive selection typically involves antibodies for EpCAM (epithelial cell adhesion molecule) and antibodies against cytokeratins specific for epithelial cells. The only FDA approved and analytically validated CTC isolation method is CellSearch, in which CTCs are captured using an EpCAM and cytokeratin isolation method (*79*).

Several studies have shown that CTC count is an accurate predictor of overall survival for patients with castration-resistant prostate cancer (*80, 81*). Although simply knowing the number of CTCs in a patient's circulation can be an effective indicator of treatment response, efforts are shifting to analyses of these tumor cells to further understand the mechanisms underlying tumor biology and response to therapies. Recent work has begun to analyze single CTCs, to measure the degree of AR signaling and response to hormonal therapies in patients with metastatic prostate cancer (*82*). Developments in next-generation sequencing methods and whole genome amplification (WGA) have made the genomic analysis of single cells possible (*83*). These advances are now being applied to study the genomes of individual cancer cells (*84, 85*), with the hope that this will provide a more informative picture of the tumor genome and understanding of tumor biology (*86*). This may also help obtain a clearer picture of heterogeneous tumor cell populations.

Circulating tumor DNA (ctDNA)

Over the past ten years, the presence of circulating tumor DNA (ctDNA) has increasingly become recognized as a valuable and useful blood biomarker for studying solid tumors. The presence of tumor nucleic acids in the bloodstream is thought to be due to apoptosis or necrosis of cancer cells in the tumor microenvironment, which are then phagocytosed by macrophages and their contents digested and released. The size of this DNA can vary from small fragments of about 100 base pairs (bp) up to large multi-kilobase sized fragments (*87*). In advanced stage disease, disseminated tumor cells in circulation may also contribute to the release of ctDNA. One of the benefits of ctDNA over isolation of CTCs for genomic analysis, is that this does not require the physical separation of the presumed tumor cell from the many different types of normal cells in the circulation. Assays to analyze circulating tumor DNA are beginning to be used to determine the genetic makeup of tumors, and measure response or resistance to therapy. Such alterations that can be measured include, gene amplification or loss of heterozygosity (LOH), and mutation of either tumor-suppressor genes or oncogenes (**Figure 24**) (*63, 88, 89*).

In a recent study on the prognostic value of circulating tumor DNA in patients with metastatic breast cancer, ctDNA content was compared to other more standard measures such as CTC number or cancer antigen 15-3 (CA 15-3) assays. They found that ctDNA content showed a greater dynamic range and correlated with changes in tumor burden better than the standard measures, and was also the earliest measure of response to therapy in more than 50% of patients (*90*).
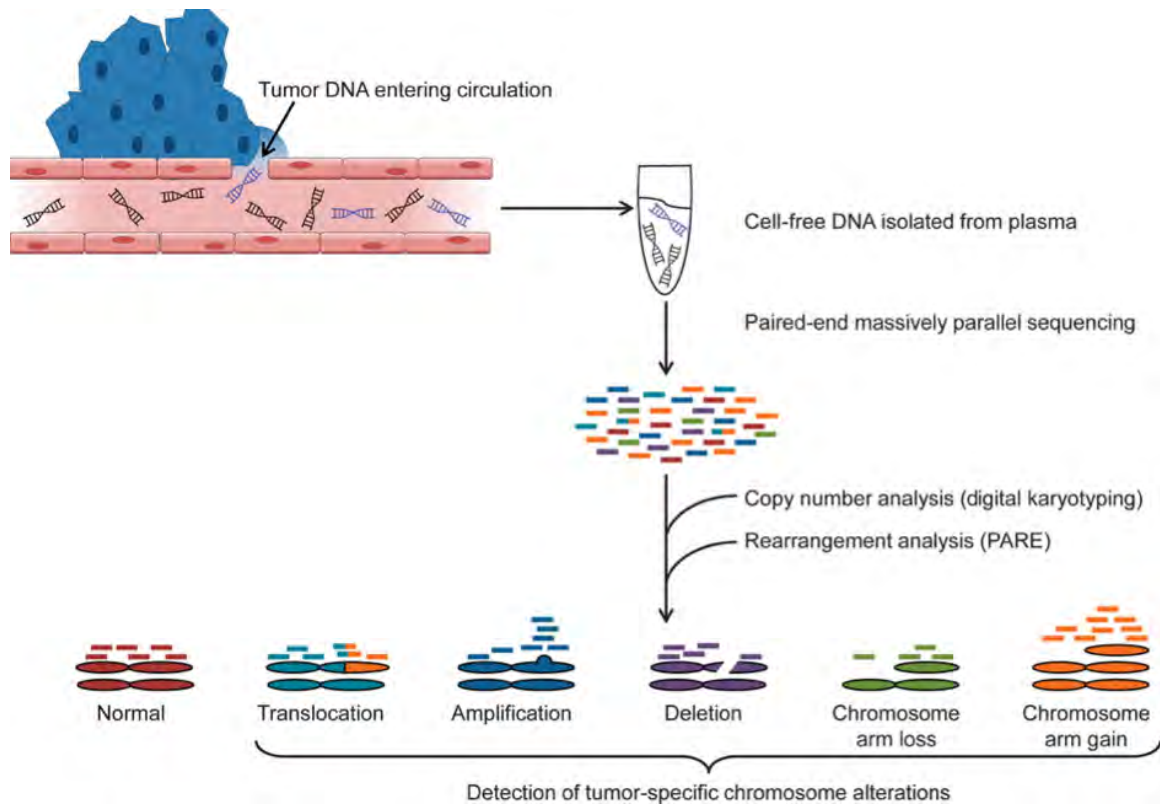
Figure 24. Schematic of analyses to detect chromosomal alterations in plasma

The method uses next-generation paired-end sequencing of cell-free DNA isolated from plasma to identify chromosomal alterations characteristic of tumor DNA. Such alterations include copy number changes (gains and losses of chromosome arms) as well as rearrangements resulting from translocations, amplifications, or deletions. (*63*)

From Science Translational Medicine 2012 Nov 28;4(162):162ra154. Reprinted with permission from AAAS.

113

BEAMing

One method we are working on utilizing for detection of AR F876L mutations in patient plasma samples is the BEAMing (Beads, Emulsion, Amplification, and Magnetics) assay developed by Dressman et al (*91, 92*). In this assay, a single DNA molecule is bound to a magnetic bead and undergoes a rolling PCR amplification to create thousands of copies of that DNA bound to the same bead. Mutant variation and frequency can be assessed using different fluorescently labeled probes that recognize and bind to these short amplicons, and then flow cytometry analysis (**Figure 25**). This method has been used recently to detect rare mutants in DNA from patient plasma samples (*62, 88*).
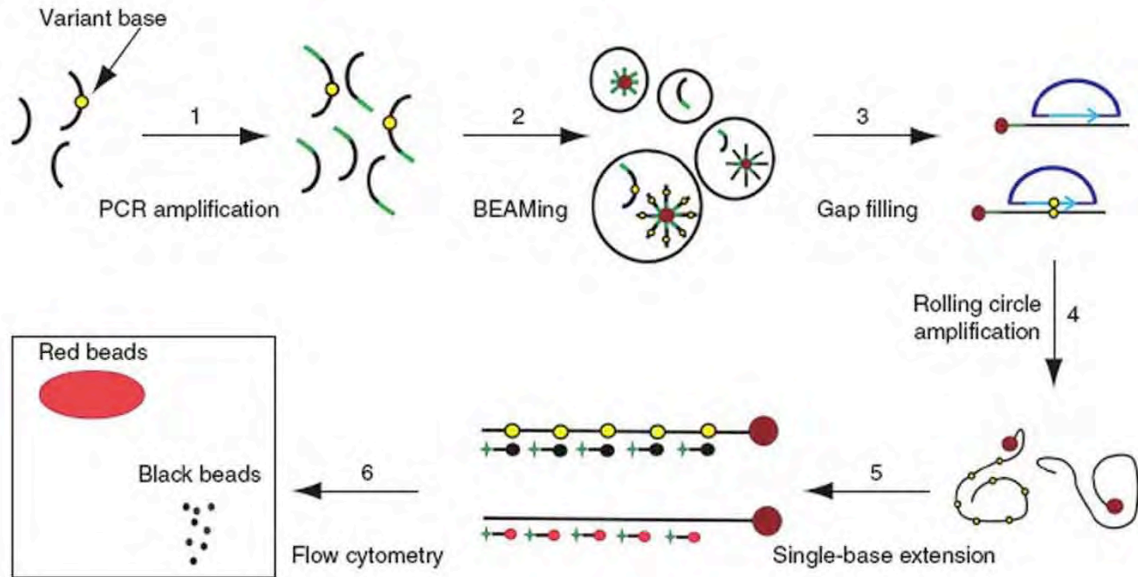
Figure 25. Schematic of the BEAMing procedure

DNA samples are amplified by PCR (step 1), then water-in-oil emulsions are formed in which single DNA molecules within each aqueous compartment are amplified and bound to beads (brown circles). In step 3, a circularizable probe is hybridized to sequences on the beads. A 1–20-bp gap is filled in by a polymerase and then the ends are ligated. In step 4, sequences to be queried on the beads are amplified through rolling circle amplification (RCA, and fluorescently labeled dideoxynucleotide terminators (red and black circles) are used to distinguish beads containing sequences that diverge at positions of interest (step 5). Finally, beads are analyzed by flow cytometry (step 6).

http://www.nature.com/nmeth/journal/v3/n2/full/nmeth850.html

115

One concern with the BEAMing method of mutation detection is that the probes are designed to bind to specific nucleotide changes. For a mutation like F876L, 3 distinct probes would be needed to detect each of the 3 possible nucleotide changes that result in this amino acid change. As our studies of additional Phe 876 mutants showed (**Figure Supplement 10**), other amino acid changes also alter the pharmacology of enzalutamide and ARN-509, and all of these mutations need to be considered when examining patient samples (**Figure 26**). For this reason, we believe next generation sequencing is the best approach to identifying AR alterations at Phe 876 that confer drug resistance in patient samples.

Figure 26. Single nucleotide changes that result in amino acid changes at F876

Three distinct single nucleotide changes result in the F876L mutation, and other amino acid substitutions that result from single nucleotide changes also confer agonism on enzalutamide and ARN-509 (see **Figure Supplement 10**).

Recent work has shown that whole-genome analysis of circulating tumor-free DNA is possible using massively parallel sequencing, and alterations detected include chromosomal copy number changes and rearrangements, including oncogene amplifications or loss of tumor suppressor genes (*63, 93*). Although next-generation DNA sequencing technology has transformed the amount of sequencing data that can be amassed, it has the drawback of high error rates which can be very problematic when sequencing heterogeneous cell populations or looking for potentially rare mutations. For this reason several groups have recently undertaken the task of optimizing sequencing approaches that can increase the sensitivity and accuracy of next-generation sequencing platforms (*94, 95*). One of these approaches is called the Safe-Sequencing System ("Safe-SeqS") and requires assignment of a unique identifier (UID) to each template molecule, amplification of each UID tagged template to create UID families, followed by redundant sequencing (**Figure 27A**). A mutation is only considered real ("supermutant") if ≥95% of amplicons in the same UID family contain the identical mutation (*95*). Comparison of conventional deep sequencing to this Safe-SeqS protocol illustrates the consistency of the higher frequency mutations between the 2 methods as well as the reduced frequency of mutations called by Safe-SeqS, suggesting that many of the mutations identified by conventional sequencing are likely to represent sequencing errors (**Figure 27B**).
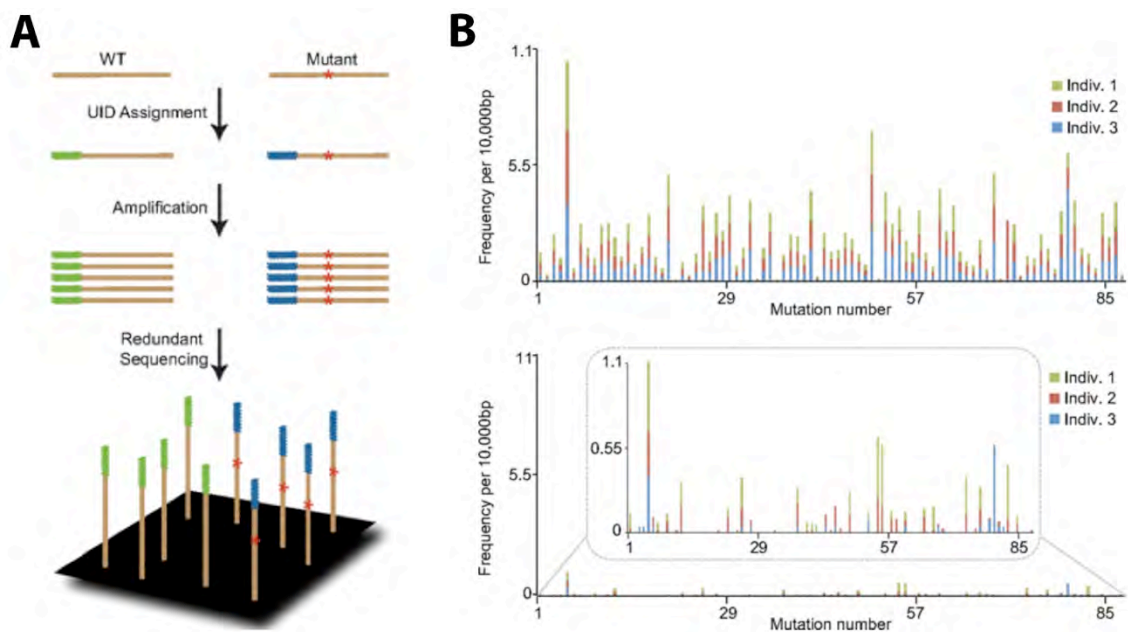
Figure 27. Outline of the Safe-SeqS method and comparison to conventional deep sequencing

(**A**) Essential elements of Safe-SeqS. In the first step, each fragment to be analyzed is assigned a unique identification (UID) DNA sequence (green or blue bars). In the second step, the uniquely tagged fragments are amplified, producing UID families, each member of which has the same UID. A supermutant is defined as a UID family in which ≥95% of family members have the same mutation. (**B**) Single-base substitutions identified by conventional and Safe-SeqS analysis. The exogenous UID strategy was used to produce PCR fragments from the *CTNNB1* gene of three normal, unrelated individuals. These fragments were sequenced on an Illumina GA IIx instrument and analyzed in the conventional manner (*top*) or with Safe-SeqS (*bottom*). Safe-SeqS results are displayed on the same scale as conventional analysis for direct comparison; the *Inset* is a magnified view. Note that most of the variants identified by conventional analysis are likely to represent sequencing errors, as indicated by their high frequency relative to Safe-SeqS and their consistency among unrelated samples. (*95*)

Proc Natl Acad Sci US A. 2011 Jun 7;108(23):9530-5.

118

Preliminary Patient Data

In collaboration with Dr. Bert Vogelstein's group, using the Safe-SeqS method described above, we have begun to analyze ctDNA isolated from plasma of CRPC patients who relapsed on either enzalutamide or ARN-509 therapy, for the presence of our novel AR F876L mutation. We have evidence of the occurrence of F876L mutation in one patient who relapsed on ARN-509 therapy (**Figure 28**). A plasma sample taken before he began treatment indicated only wild-type AR. The patient responded to ARN-509 for nearly two years, at which point his PSA level began to steadily rise. He was taken off of ARN-509 and his PSA level briefly flat-lined, possibly indicative of AWS (antiandrogen withdrawal syndrome). Plasma taken from this time point showed the emergence of AR F876L mutation. The patient was subsequently put on Zytiga (abiraterone acetate) and both his PSA level and CTC count dropped.

		Date	Mutation	Mutant / WT
★	PLS 1	06/14/10	No mutation observed	0 / 37844
★	PLS 2	07/18/12	AR F876L	956 / 4533
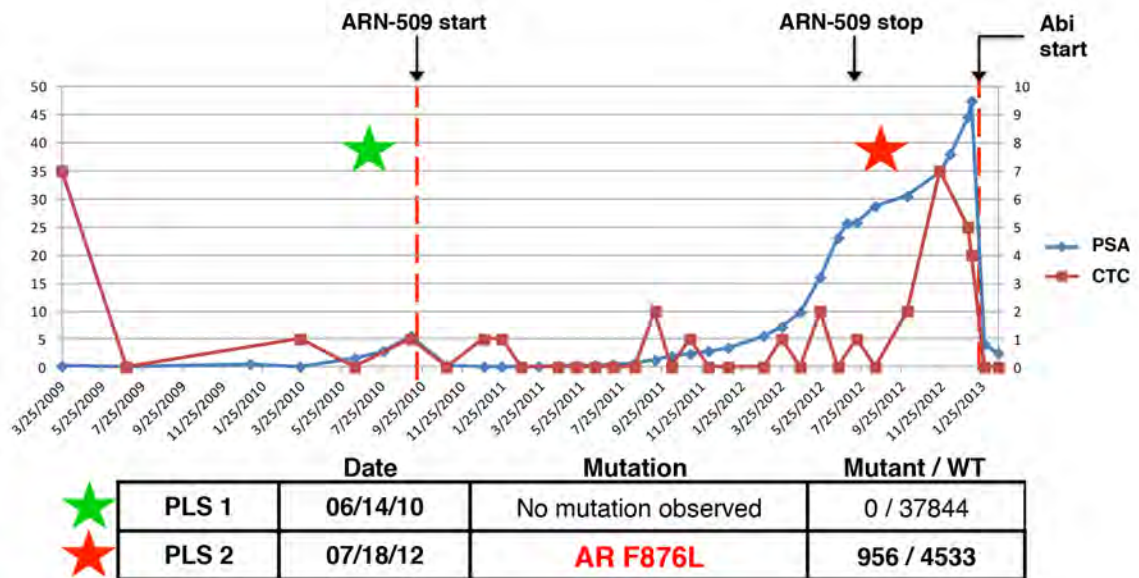
Figure 28. AR F876L mutation emerges in a patient treated with ARN-509

Before ARN-509 treatment, the patient was wild-type at Phe876, but upon relapse, sequencing revealed the presence of AR F876L mutation in ~21% of reads.

Conclusions

Testing of additional AR mutations found in drug-resistant xenograft tumors did not reveal any new mutations that conferred resistance to enzalutamide or ARN-509. Though we may not have screened to saturation, the emergence of F876L from two additional independent systems (LNCaP/AR xenografts and CWR22Pc cells) suggests that this may be the dominant AR mutation that will occur in patients. Our preliminary patient data, showing that this mutation emerged in a patient who relapsed on ARN-509 therapy provides support for the clinical relevance of this mutation. With the Safe-SeqS assay validated for this region of AR, we are currently analyzing more plasma samples from patients who have relapsed on either enzalutamide or ARN-509 therapy to determine the frequency of this mutation in patients with acquired resistance.

Bibliography

1.   K. Lassi, N. A. Dawson, Update on castrate-resistant prostate cancer: 2010. *Curr Opin Oncol* **22**, 263 (May, 2010).
2.   C. Huggins, C. V. Hodges, Studies on prostatic cancer. I. The effect of castration, of estrogen and androgen injection on serum phosphatases in metastatic carcinoma of the prostate. *CA Cancer J Clin* **22**, 232 (Jul-Aug, 1972).
3.   W. J. Catalona, Management of cancer of the prostate. *N Engl J Med* **331**, 996 (Oct 13, 1994).
4.   H. I. Scher, C. L. Sawyers, Biology of progressive, castration-resistant prostate cancer: directed therapies targeting the androgen-receptor signaling axis. *J Clin Oncol* **23**, 8253 (Nov 10, 2005).
5.   H. I. Scher *et al.*, Increased survival with enzalutamide in prostate cancer after chemotherapy. *N Engl J Med* **367**, 1187 (Sep 27, 2012).
6.   H. V. Heemers, D. J. Tindall, Androgen receptor (AR) coregulators: a diversity of functions converging on and regulating the AR transcriptional complex. *Endocr Rev* **28**, 778 (Dec, 2007).
7.   T. M. Penning, New frontiers in androgen biosynthesis and metabolism. *Curr Opin Endocrinol Diabetes Obes* **17**, 233 (Jun, 2010).
8.   E. P. Gelmann, Molecular biology of the androgen receptor. *J Clin Oncol* **20**, 3001 (Jul 1, 2002).
9.   B. He, J. A. Kemppainen, E. M. Wilson, FXXLF and WXXLF sequences mediate the NH2-terminal interaction with the ligand binding domain of the androgen receptor. *J Biol Chem* **275**, 22986 (Jul 28, 2000).
10.   F. Schaufele *et al.*, The structural basis of androgen receptor activation: intramolecular and intermolecular amino-carboxy interactions. *Proc Natl Acad Sci U S A* **102**, 9802 (Jul 12, 2005).
11.   R. Chmelar, G. Buchanan, E. F. Need, W. Tilley, N. M. Greenberg, Androgen receptor coregulators and their involvement in the development and progression of prostate cancer. *Int J Cancer* **120**, 719 (Feb 15, 2007).
12.   F. Claessens *et al.*, Diverse roles of androgen receptor (AR) domains in AR-mediated signaling. *Nucl Recept Signal* **6**, e008 (2008).
13.   M. J. Linja, T. Visakorpi, Alterations of androgen receptor in prostate cancer. *J Steroid Biochem Mol Biol* **92**, 255 (Nov, 2004).
14.   I. A. Hughes *et al.*, Androgen insensitivity syndrome. *Lancet* **380**, 1419 (Oct 20, 2012).
15.   P. Ferro, M. G. Catalano, R. Dell'Eva, N. Fortunati, U. Pfeffer, The androgen receptor CAG repeat: a modifier of carcinogenesis? *Mol Cell Endocrinol* **193**, 109 (Jul 31, 2002).
16.   C. E. Bohl, Z. Wu, D. D. Miller, C. E. Bell, J. T. Dalton, Crystal structure of the T877A human androgen receptor ligand-binding domain complexed to cyproterone acetate provides insight for ligand-induced conformational changes and structure-based drug design. *J Biol Chem* **282**, 13648 (May 4, 2007).

17.   C. E. Bohl, D. D. Miller, J. Chen, C. E. Bell, J. T. Dalton, Structural basis for accommodation of nonsteroidal ligands in the androgen receptor. *J Biol Chem* **280**, 37747 (Nov 11, 2005).

18.   C. E. Bohl, W. Gao, D. D. Miller, C. E. Bell, J. T. Dalton, Structural basis for antagonism and resistance of bicalutamide in prostate cancer. *Proc Natl Acad Sci U S A* **102**, 6201 (Apr 26, 2005).

19.   A. K. Shiau *et al.*, The structural basis of estrogen receptor/coactivator recognition and the antagonism of this interaction by tamoxifen. *Cell* **95**, 927 (Dec 23, 1998).

20.   M. E. Grossmann, H. Huang, D. J. Tindall, Androgen receptor signaling in androgen-refractory prostate cancer. *J Natl Cancer Inst* **93**, 1687 (Nov 21, 2001).

21.   M. T. Fleming, M. J. Morris, G. Heller, H. I. Scher, Post-therapy changes in PSA as an outcome measure in prostate cancer clinical trials. *Nat Clin Pract Oncol* **3**, 658 (Dec, 2006).

22.   S. I. Dickinson, Premalignant and malignant prostate lesions: pathologic review. *Cancer Control* **17**, 214 (Oct, 2010).

23.   J. I. Epstein, An update of the Gleason grading system. *J Urol* **183**, 433 (Feb, 2010).

24.   Y. Chen, N. J. Clegg, H. I. Scher, Anti-androgens and androgen-depleting therapies in prostate cancer: new agents for an established target. *Lancet Oncol* **10**, 981 (Oct, 2009).

25.   Y. Chen, C. L. Sawyers, H. I. Scher, Targeting the androgen receptor pathway in prostate cancer. *Curr Opin Pharmacol* **8**, 440 (Aug, 2008).

26.   M. S. Glickman, C. L. Sawyers, Converting cancer therapies into cures: lessons from infectious diseases. *Cell* **148**, 1089 (Mar 16, 2012).

27.   M. E. Gorre *et al.*, Clinical resistance to STI-571 cancer therapy caused by BCR-ABL gene mutation or amplification. *Science* **293**, 876 (Aug 3, 2001).

28.   M. C. Heinrich *et al.*, Kinase mutations and imatinib response in patients with metastatic gastrointestinal stromal tumor. *J Clin Oncol* **21**, 4342 (Dec 1, 2003).

29.   C. M. Emery *et al.*, MEK1 mutations confer resistance to MEK and B-RAF inhibition. *Proc Natl Acad Sci U S A* **106**, 20411 (Dec 1, 2009).

30.   S. Kobayashi *et al.*, EGFR mutation and resistance of non-small-cell lung cancer to gefitinib. *N Engl J Med* **352**, 786 (Feb 24, 2005).

31.   J. A. Engelman *et al.*, MET amplification leads to gefitinib resistance in lung cancer by activating ERBB3 signaling. *Science* **316**, 1039 (May 18, 2007).

32.   R. Nazarian *et al.*, Melanomas acquire resistance to B-RAF(V600E) inhibition by RTK or N-RAS upregulation. *Nature* **468**, 973 (Dec 16, 2010).

33.   T. Visakorpi *et al.*, In vivo amplification of the androgen receptor gene and progression of human prostate cancer. *Nat Genet* **9**, 401 (Apr, 1995).

34.   M. J. Linja *et al.*, Amplification and overexpression of androgen receptor gene in hormone-refractory prostate cancer. *Cancer Res* **61**, 3550 (May 1, 2001).

35.   C. D. Chen *et al.*, Molecular determinants of resistance to antiandrogen therapy. *Nat Med* **10**, 33 (Jan, 2004).

36.   J. P. Bergerat, J. Ceraline, Pleiotropic functional properties of androgen receptor mutants in prostate cancer. *Hum Mutat* **30**, 145 (Feb, 2009).

37.   H. Beltran *et al.*, Targeted Next-generation Sequencing of Advanced Prostate Cancer Identifies Potential Therapeutic Targets and Disease Heterogeneity. *Eur Urol*, (Sep 5, 2012).
38.   T. Hara *et al.*, Novel mutations of androgen receptor: a possible mechanism of bicalutamide withdrawal syndrome. *Cancer Res* **63**, 149 (Jan 1, 2003).
39.   J. Veldscholte *et al.*, A mutation in the ligand binding domain of the androgen receptor of human LNCaP cells affects steroid binding characteristics and response to anti-androgens. *Biochem Biophys Res Commun* **173**, 534 (Dec 14, 1990).
40.   J. A. Locke *et al.*, Androgen levels increase by intratumoral de novo steroidogenesis during progression of castration-resistant prostate cancer. *Cancer Res* **68**, 6407 (Aug 1, 2008).
41.   G. Attard, A. S. Belldegrun, J. S. de Bono, Selective blockade of androgenic steroid synthesis by novel lyase inhibitors as a therapeutic strategy for treating metastatic prostate cancer. *BJU Int* **96**, 1241 (Dec, 2005).
42.   G. Attard *et al.*, Selective inhibition of CYP17 with abiraterone acetate is highly active in the treatment of castration-resistant prostate cancer. *J Clin Oncol* **27**, 3742 (Aug 10, 2009).
43.   R. Hu *et al.*, Ligand-independent androgen receptor variants derived from splicing of cryptic exons signify hormone-refractory prostate cancer. *Cancer Res* **69**, 16 (Jan 1, 2009).
44.   P. A. Watson *et al.*, Constitutively active androgen receptor splice variants expressed in castration-resistant prostate cancer require full-length androgen receptor. *Proc Natl Acad Sci U S A* **107**, 16759 (Sep 28, 2010).
45.   Y. Li *et al.*, Androgen receptor splice variants mediate enzalutamide resistance in castration-resistant prostate cancer cell lines. *Cancer Res* **73**, 483 (Jan 15, 2013).
46.   C. Tran *et al.*, Development of a second-generation antiandrogen for treatment of advanced prostate cancer. *Science* **324**, 787 (May 8, 2009).
47.   D. Rathkopf, H. I. Scher, Androgen receptor antagonists in castration-resistant prostate cancer. *Cancer J* **19**, 43 (Jan, 2013).
48.   H. I. Scher *et al.*, Antitumour activity of MDV3100 in castration-resistant prostate cancer: a phase 1-2 study. *Lancet* **375**, 1437 (Apr 24, 2010).
49.   N. J. Clegg *et al.*, ARN-509: a novel antiandrogen for prostate cancer treatment. *Cancer Res* **72**, 1494 (Mar 15, 2012).
50.   M. Azam, R. R. Latek, G. Q. Daley, Mechanisms of autoinhibition and STI-571/imatinib resistance revealed by mutagenesis of BCR-ABL. *Cell* **112**, 831 (Mar 21, 2003).
51.   M. R. Burgess, B. J. Skaggs, N. P. Shah, F. Y. Lee, C. L. Sawyers, Comparative analysis of two clinically active BCR-ABL kinase inhibitors reveals the role of conformation-specific binding in resistance. *Proc Natl Acad Sci U S A* **102**, 3395 (Mar 1, 2005).
52.   N. P. Shah *et al.*, Sequential ABL kinase inhibitor therapy selects for compound drug-resistant BCR-ABL mutations with altered oncogenic potency. *The Journal of clinical investigation* **117**, 2562 (Sep, 2007).

53. S. Chapel-Fernandes *et al.*, Use of the PSA enhancer core element to modulate the expression of prostate- and non-prostate-specific basal promoters in a lentiviral vector context. *Cancer Gene Ther* **13**, 919 (Oct, 2006).

54. H. I. Scher *et al.*, Increased Survival with Enzalutamide in Prostate Cancer after Chemotherapy. *N Engl J Med*, (Aug 15, 2012).

55. K. Haapala *et al.*, Androgen receptor alterations in prostate cancer relapsed during a combined androgen blockade by orchiectomy and bicalutamide. *Lab Invest* **81**, 1647 (Dec, 2001).

56. M. S. Ozers *et al.*, The androgen receptor T877A mutant recruits LXXLL and FXXLF peptides differently than wild-type androgen receptor in a time-resolved fluorescence resonance energy transfer assay. *Biochemistry* **46**, 683 (Jan 23, 2007).

57. M. Karplus, J. A. McCammon, Molecular dynamics simulations of biomolecules. *Nat Struct Biol* **9**, 646 (Sep, 2002).

58. W. L. Jorgensen, The many roles of computation in drug discovery. *Science* **303**, 1813 (Mar 19, 2004).

59. M. E. Jung *et al.*, Structure-activity relationship for thiohydantoin androgen receptor antagonists for castration-resistant prostate cancer (CRPC). *J Med Chem* **53**, 2779 (Apr 8, 2010).

60. N. P. Shah *et al.*, Overriding imatinib resistance with a novel ABL kinase inhibitor. *Science* **305**, 399 (Jul 16, 2004).

61. B. Benhamou *et al.*, A single amino acid that determines the sensitivity of progesterone receptors to RU486. *Science* **255**, 206 (Jan 10, 1992).

62. F. Diehl *et al.*, Analysis of mutations in DNA isolated from plasma and stool of colorectal cancer patients. *Gastroenterology* **135**, 489 (Aug, 2008).

63. R. J. Leary *et al.*, Detection of chromosomal alterations in the circulation of cancer patients with whole-genome sequencing. *Sci Transl Med* **4**, 162ra154 (Nov 28, 2012).

64. A. Dagvadorj *et al.*, Androgen-regulated and highly tumorigenic human prostate cancer cell line established from a transplantable primary CWR22 tumor. *Clin Cancer Res* **14**, 6062 (Oct 1, 2008).

65. H. Li, R. Durbin, Fast and accurate short read alignment with Burrows-Wheeler transform. *Bioinformatics* **25**, 1754 (Jul 15, 2009).

66. H. Li *et al.*, The Sequence Alignment/Map format and SAMtools. *Bioinformatics* **25**, 2078 (Aug 15, 2009).

67. C. Trapnell, L. Pachter, S. L. Salzberg, TopHat: discovering splice junctions with RNA-Seq. *Bioinformatics* **25**, 1105 (May 1, 2009).

68. D. C. Koboldt *et al.*, VarScan 2: somatic mutation and copy number alteration discovery in cancer by exome sequencing. *Genome Res* **22**, 568 (Mar, 2012).

69. M. J. Frisch *et al.*, *Gaussian 03, Revision C.02*. (Gaussian, Inc.) (Wallingford, CT, 2004).

70. C. I. Bayly, P. Cieplak, W. D. Cornell, P. A. Kollman, A Well-Behaved Electrostatic Potential Based Method Using Charge Restraints for Deriving Atomic Charges - the Resp Model. *J Phys Chem-Us* **97**, 10269 (Oct 7, 1993).

71. W. D. Cornell, P. Cieplak, C. I. Bayly, P. A. Kollman, Application of Resp Charges to Calculate Conformational Energies, Hydrogen-Bond Energies, and Free-Energies of Solvation. *J Am Chem Soc* **115**, 9620 (Oct 20, 1993).
72. F. A. Momany, R. Rone, Validation of the General-Purpose Quanta(R)3.2/Charmm(R) Force-Field. *J Comput Chem* **13**, 888 (Sep, 1992).
73. B. R. Brooks *et al.*, CHARMM: the biomolecular simulation program. *J Comput Chem* **30**, 1545 (Jul 30, 2009).
74. B. R. Brooks *et al.*, Charmm - a Program for Macromolecular Energy, Minimization, and Dynamics Calculations. *J Comput Chem* **4**, 187 (1983).
75. A. T. Brunger, M. Karplus, Polar Hydrogen Positions in Proteins - Empirical Energy Placement and Neutron-Diffraction Comparison. *Proteins* **4**, 148 (1988).
76. E. F. Pettersen *et al.*, UCSF Chimera--a visualization system for exploratory research and analysis. *J Comput Chem* **25**, 1605 (Oct, 2004).
77. B. Gottlieb, L. K. Beitel, A. Nadarajah, M. Paliouras, M. Trifiro, The androgen receptor gene mutations database: 2012 update. *Hum Mutat* **33**, 887 (May, 2012).
78. D. Schilling *et al.*, Isolated, disseminated and circulating tumour cells in prostate cancer. *Nat Rev Urol*, (Jul 10, 2012).
79. K. Pantel, C. Alix-Panabieres, Circulating tumour cells in cancer patients: challenges and perspectives. *Trends in molecular medicine* **16**, 398 (Sep, 2010).
80. J. S. de Bono *et al.*, Circulating tumor cells predict survival benefit from treatment in metastatic castration-resistant prostate cancer. *Clin Cancer Res* **14**, 6302 (Oct 1, 2008).
81. D. C. Danila *et al.*, Circulating tumor cell number and prognosis in progressive castration-resistant prostate cancer. *Clin Cancer Res* **13**, 7053 (Dec 1, 2007).
82. D. T. Miyamoto *et al.*, Androgen receptor signaling in circulating tumor cells as a marker of hormonally responsive prostate cancer. *Cancer Discov* **2**, 995 (Nov, 2012).
83. T. Baslan *et al.*, Genome-wide copy number analysis of single cells. *Nat Protoc* **7**, 1024 (Jun, 2012).
84. N. Navin *et al.*, Tumour evolution inferred by single-cell sequencing. *Nature* **472**, 90 (Apr 7, 2011).
85. C. Zong, S. Lu, A. R. Chapman, X. S. Xie, Genome-wide detection of single-nucleotide and copy-number variations of a single human cell. *Science* **338**, 1622 (Dec 21, 2012).
86. N. Navin, J. Hicks, Future medical applications of single-cell sequencing in cancer. *Genome medicine* **3**, 31 (2011).
87. H. Schwarzenbach, D. S. Hoon, K. Pantel, Cell-free nucleic acids as biomarkers in cancer patients. *Nat Rev Cancer* **11**, 426 (Jun, 2011).
88. F. Diehl *et al.*, Detection and quantification of mutations in the plasma of patients with colorectal tumors. *Proc Natl Acad Sci U S A* **102**, 16368 (Nov 8, 2005).
89. L. A. Diaz, Jr. *et al.*, The molecular evolution of acquired resistance to targeted EGFR blockade in colorectal cancers. *Nature* **486**, 537 (Jun 28, 2012).
90. S. J. Dawson *et al.*, Analysis of circulating tumor DNA to monitor metastatic breast cancer. *N Engl J Med* **368**, 1199 (Mar 28, 2013).

91. D. Dressman, H. Yan, G. Traverso, K. W. Kinzler, B. Vogelstein, Transforming single DNA molecules into fluorescent magnetic particles for detection and enumeration of genetic variations. *Proc Natl Acad Sci U S A* **100**, 8817 (Jul 22, 2003).

92. M. Li, F. Diehl, D. Dressman, B. Vogelstein, K. W. Kinzler, BEAMing up for detection and quantification of rare sequence variants. *Nat Methods* **3**, 95 (Feb, 2006).

93. R. J. Leary *et al.*, Development of personalized tumor biomarkers using massively parallel sequencing. *Sci Transl Med* **2**, 20ra14 (Feb 24, 2010).

94. M. W. Schmitt *et al.*, Detection of ultra-rare mutations by next-generation sequencing. *Proc Natl Acad Sci U S A* **109**, 14508 (Sep 4, 2012).

95. I. Kinde, J. Wu, N. Papadopoulos, K. W. Kinzler, B. Vogelstein, Detection and quantification of rare mutations with massively parallel sequencing. *Proc Natl Acad Sci U S A* **108**, 9530 (Jun 7, 2011).